DEVELOPMENT OF IMPROVED METHODS FOR WATERSHED-SCALE TOPOGRAPHIC ANALYSIS AND HYDROLOGIC MODELING

A Dissertation
Submitted to the Graduate Faculty
of the
North Dakota State University
of Agriculture and Applied Science

By

Ning Wang

In Partial Fulfillment of the Requirements
for the Degree of
DOCTOR OF PHILOSOPHY

Major Department:
Civil and Environmental Engineering

June 2020

Fargo, North Dakota

North Dakota State University
Graduate School

Title

DEVELOPMENT OF IMPROVED METHODS FOR WATERSHED-SCALE TOPOGRAPHIC ANALYSIS AND HYDROLOGIC MODELING

By

Ning Wang

The Supervisory Committee certifies that this ***disquisition*** complies with North Dakota State University's regulations and meets the accepted standards for the degree of

DOCTOR OF PHILOSOPHY

SUPERVISORY COMMITTEE:

Xuefeng Chu

Chair

Stephanie Day

Xiaodong Zhang

Xiangfa Wu

Approved:

July 09, 2020 — Date

David Steward — Department Chair

ABSTRACT

Surface depressions are one of the significant topographic characteristics in depression-dominated areas and can retain runoff and break the hydrologic continuity in watersheds. In traditional semi-distributed models, the entire area of a watershed is assumed to be well connected to its associated outlet and depressions are often lumped as a single depth to control runoff water release. Consequently, hydrologic processes related to depressions cannot be directly simulated. The overall goal of this dissertation research is to analyze and quantify the topographic characteristics of surface depressions and their impacts on hydrologic processes in depression-dominated areas. The specific objectives of this research are: (1) to improve watershed delineation to further reveal the topographic characteristics and hydrologic connectivity within watersheds, (2) to analyze the impact of depressions on runoff processes during rainfall events and the mechanism of water release from depressions, and (3) to analyze the functionalities of depressions in continuous simulation of hydrologic processes and connectivity. A new algorithm was developed for hydrologic unit delineation of depressions and channels (HUD-DC), in which a unique method was proposed to identify depression- and channel-associated hydrologic units and their connections. The HUD-DC delineation results highlighted the significance of depressions and the complex connectivity in depression-dominated areas. Additionally, the delineation under different filling conditions provided helpful guidance for the identification of filling thresholds to remove artifacts in digital elevation models. To achieve the second objective, a depression-oriented, event-based hydrologic model (HYDROL-D) was developed with considering separate modeling for depressional and non-depressional areas, and hierarchical control thresholds for water release from depressions. The HYDROL-D modeling results for a watershed in North Dakota revealed the intrinsic threshold

behavior of surface runoff over the watershed and the effectiveness of the hierarchical control thresholds. A depression-oriented hydrologic model with accounting for dynamic hydrologic connectivity (HYDROL-DC) was further developed to continuously track runoff unit by unit. The application of HYDROL-DC in a depression-dominated watershed showed that depressions had not only retention but also acceleration capabilities in surface runoff generation. Additionally, the spatial distribution of depressions exhibited dynamic influences on hydrologic connectivity and the related threshold behavior of runoff processes.

ACKNOWLEDGEMENTS

First of all, I would like to express my sincere gratitude to my adviser, Dr. Xuefeng Chu, for giving me inestimable support and guidance not only in academic research but also in paper writing. Dr. Chu's extensive professional knowledge and rigorous academic attitude have benefited me greatly during my study at NDSU, and this wealth will also benefit me for my future life.

Second, I would also like to sincerely thank my other committee members, Dr. Stephanie Day, Dr. Xiaodong Zhang, and Dr. Xiangfa Wu for their precious time and suggestion. The successful completion of this paper is also inseparable from their great help and support. I am also delighted to thank my group members, Mohsen Tahmasebi Nasab, Kendall Morgan Grimm, Lan Zeng, Hadi Bazrkar, and Xingwei Liu. Thanks for their cooperation and contribution to group research, making our study more interesting.

Third, I sincerely thank the financial support from the National Science Foundation Established Program to Stimulate Competitive Research (NSF EPSCoR, Grant No. IIA-1355466), the North Dakota Water Resources Research Institute (NDWRRI), and the Department of Civil and Environmental Engineering, which allows me to complete my Ph.D. research and participate in academic conferences.

Finally, I would like to extend my special gratitude to my parents and parents-in-law for their unconditional understanding and support. I want to dedicate my gratitude to my wife Kangxin Sun. Without her sacrifice and support, I would not successfully finish my doctoral study. Thank her love, accompany, and encouragement in the past years.

TABLE OF CONTENTS

LIST OF TABLES

LIST OF FIGURES

1. GENERAL INTRODUCTION

1.1. Background

With the development of computer technology in recent decades, watershed modeling has become an efficient way to understand water movement in watersheds and provide essential guidance for water resources management, water quality and other related issues (Borah and Bera 2004; Arabi et al. 2006; Daniel et al., 2011; Chourushi et al., 2019). Moreover, various surface delineation algorithms have been developed to extract topographic characteristics (e.g., drainage network, slope, watershed boundary) from digital elevation models (DEMs) for watershed modeling (DeVantier and Feldman 1993; Sui and Maggio 1999; Verma et al., 2017). The emergence of watershed models and surface delineation algorithms significantly promotes the efficiency of hydrologic research and enhances our understanding of hydrologic processes. However, all algorithms or models have their applicable areas (Daniel et al., 2010), and thus diverse models and algorithms are required for different purposes.

For a landform that is lower than its surrounding area, an individual surface depression can capture and retain water on the land surface. Considering the relationships between depressions, the behaviors of depressions can be generalized as filling, spilling, merging, and splitting (Chu et al., 2013a; Yang and Chu 2015), and surface depressions in a depression-dominated area can generate a hierarchical drainage network that significantly influences hydrologic processes such as runoff generation, flow direction, flow accumulation and infiltration (Darboux et al., 2002; Darboux and Huang 2005; Martin et al., 2008; Rossi and Ares, 2012; Tahmasebi Nasab et al., 2017a; Wang et al., 2019). Additionally, the irregular distribution of depressions increases the complexity of surface connectivity and leads to a challenge in analyzing the hydrologic processes on land surfaces (Yang et al. 2010; Chi et al., 2012; Golden

et al. 2014; Grimm and Chu 2018). Since hydrologic processes are the bases of the transport of pollutants (Parajuli and Ouyang 2013), depressions also influence soil erosion and the transport of sediments, nutrients, and other contaminants (Hansen et al., 1999; Chu et al., 2013b).

Traditionally, depressions, their spatial distributions, and their connectivity are oversimplified in surface delineation and hydrologic modeling at watershed scales (Wang et al., 2019; Wang and Chu 2020). Although many studies have been conducted to analyze the influences of depressions on surface delineation and hydrologic modeling in recent years (e.g., Helming et al., 1998; Govers et al., 2000; Chu et al., 2010; Tahmasebi Nasab et al., 2017b; Grimm and Chu 2020), our understanding of the topography and hydrologic processes associated with depressions is still limited. Therefore, more efforts are required to improve surface delineation and hydrologic simulation in depression-dominated areas. The following sections (i.e., Sections 1.2 and 1.3) provide detailed literature reviews of the related studies, current research gaps, and the significance of this dissertation research in analyzing and quantifying the impacts of depressions on topographic characteristics and hydrologic processes.

1.2. Watershed Delineation with Considering Complex Topography

Watershed delineation provides topographic parameters needed for hydrologic modeling (Luo et al., 2011; Bhatt et al., 2014; Wang and Chu 2020). The traditional delineation algorithms generally implement the following steps: (1) removal of depressions, (2) determination of flow directions, (3) calculation of flow accumulations, (4) identification of drainage networks, and (5) determination of watershed boundary. A watershed can be further divided into a set of subbasins based on the user-defined subbasin outlets. For example, Martz and Garbrecht (1993) developed a digital elevation drainage network model (DEDNM) to determine drainage networks and topographic parameters based on raster-based DEMs. Furthermore, an upgraded program of

DEDNM, TOPAZ (Topographic Parameterization), was developed by Garbrecht and Martz (2000) and further incorporated into the Watershed Modeling System (WMS 2015). Instead of using raster-based DEMs, Jones et al. (1990) proposed an algorithm to search the drainage network and watershed boundary by tracking the path of steepest descent based on a triangulated irregular network (TIN).

Marks et al. (1984) developed the first algorithm to eliminate depressions and create depressionless watersheds. In the algorithm, all single-cell depressions were identified and filled first, and then large closed depressions which had flat bottoms were found and filled. However, the algorithm tended to generate overestimated depression areas and inappropriate pour points (Wang and Liu 2006). Martz and Jong (1998) modified the method by considering more complex depression conditions, including closed depressions and flat areas. Another filling algorithm proposed by Jenson and Domingue (1988) has been integrated into ArcGIS as a “Fill” tool and has been widely used. Although the validity and accuracy of this algorithm have been proven, its efficiency can be low because all depressions are gradually filled in the algorithm. Planchon and Darboux (2002) proposed a new algorithm to enhance the efficiency of filling depressions. Unlike the algorithm proposed by Jenson and Domingue (1988), the new algorithm inundated cells on a surface with a water layer and then removed excess water from the filled cells to identify fully-filled depressions. Moreover, Wang and Liu (2006) utilized a novel least-cost algorithm to identify and fill depressions, and Xu et al. (2007) proposed another efficient algorithm by classifying cells in a DEM based on a quantile classification method and scanning the cells whose elevations needed to be raised, instead of all cells. The above removal methods were developed based on the filling process of depressions. Some other removal methods also

were proposed by breaching depressions or combining the filling and breaching methods (e.g., Rieger 1993; Rieger 1998; Martz and Garbrecht 1999; Soille 2004).

The calculation of flow directions is the base of the determination of flow accumulations, drainage network, and watershed boundary. O'Callaghan and Mark (1984) proposed the D8 method to calculate flow directions based on DEMs. In their method, it is assumed that each DEM cell only drains water to one of its eight neighboring cells with the steepest descent. This assumption simplified the calculation of flow directions, but also limited the accuracy of the D8 method (Moore and Grayson 1991; Costa-Cabral and Burges 1994; Rahman et al., 2010). Some methods were proposed to improve the D8 method (e.g., Costa-Cabral and Burges 1994; Tarboton 1997; Orlandini et al., 2003; Seibert and McGlynn 2007). Although the D8 method has the above limitation, it is still widely used in many tools (e.g., Arc Hydro). Once the flow directions of all DEM cells are determined, the flow accumulations of the cells and the drainage network can be calculated accordingly, and the watershed boundary can be found by searching the contributing cells of the watershed outlet (Martz and Garbrecht 1993).

Because of the removal of depressions, the internal connections of a watershed delineated by the above algorithms are well developed. In reality, an individual depression consists of a ponding area and its associated threshold(s) (Chu et al., 2013a; Chu 2017). Additionally, following a filling process, depressions sharing the same thresholds can merge and generate a higher-level depression until all highest-level depressions are generated. Therefore, depressions in a watershed can generate a hierarchal system that increases the topographic complexity of the watershed, and the existence of depressions influences flow directions and accumulations. The topographic characteristics and hydrologic connectivity calculated by the traditional algorithms cannot reveal the real conditions in depression-dominated areas. Since surface delineation is a

pre-procedure of hydrologic modeling, the delineation results are critical to precisely depict the topographic characteristics and hydrologic processes within depression-dominated areas.

In recent years, some new algorithms have been proposed to handle watershed delineation in depression-dominated areas by considering the intrinsic characteristics of depressions in watersheds. In general, the algorithms can be classified into two categories: (1) algorithms that focus on the highest-level depressions (e.g., Maidment 2002; Temme et al., 2006; Arnold 2010); and (2) algorithms that center on the depressions at all hierarchical levels (e.g., Chu 2010; Tahmasebi Nasab et al., 2017b). The algorithms in the first category are generally for large-scale surfaces (e.g., watersheds) without considering the lower-level depressions. By doing so, these algorithms can capture the major topographic characteristics and the connectivity on surfaces and meanwhile guarantee their efficiency in delineation. The major functions of these algorithms are to determine the highest-level depressions and their contributing areas. However, channels and the connections between depressions and channels are ignored in these algorithms (Wang and Chu 2020). Compared with the algorithms in the first category, the algorithms in the second category can identify all-level depressions, their hierarchical relationships and connections, and their contributing areas (Chu 2010; Tahmasebi Nasab et al., 2017b; Wang and Chu 2020). Moreover, the algorithm proposed by Tahmasebi Nasab et al. (2017b) can identify channels, their contributing areas, and the connectivity between channels and depressions. Even though these algorithms can provide more topographic details than the algorithms in the first category in surface delineation, they are usually used for relatively small-scale surfaces.

Compared with the traditional delineation algorithms, the algorithms in the above two categories have obvious advantages in extracting topographic characteristics for depression-

dominated areas. However, there are still some room for improvement. For example, current algorithms in the first category cannot get enough topographic information, while the algorithms in the second category require intensive computation. Therefore, a possible research topic is to develop a new algorithm that can get sufficient topographic information at a watershed scale without a significant compromise of its efficiency.

1.3. Hydrologic Modeling and Process Analysis in Depression-dominated Areas

Different watershed-scale hydrologic models have been developed to address various water-related issues. For example, Schuol et al. (2008) estimated available freshwater in West Africa by using the Soil and Water Assessment Tool (SWAT). Fassieh and Zaki (2014) developed a watershed model to simulate the response of water level in the Toshka Depression for different scenarios. Göppert et al. (1998) developed a model to forecast floods in the Lenne River catchment in Germany and provided management strategies. Additionally, there are many other models that simulated dynamic hydrologic processes with changes in climate, land use, and pollution (e.g., Breuer et al. 2009; Ficklin et al. 2009; Lai et al. 2011).

The hydrologic processes related to depressions are oversimplified in most models by lumping all depressions in each subbasin and assuming that there is no water released from the lumped depression to its associated subbasin outlet until it is fully filled. Moreover, based on the contributing area of the lumped depression, those models can be further classified into two categories: (1) models in which the entire subbasin is assumed to contribute runoff water to the lumped depression and (2) models in which only part of a subbasin is assumed to drain runoff water to the lumped depression. HEC-HMS is a semi-distributed hydrologic model that belongs to the first category. In HEC-HMS, the soil conservation service curve number (SCS-CN) method and a soil moisture accounting (SMA) method are used to calculate surface runoff in the

event and continuous simulations, respectively (USACE and HEC 2016). The maximum depression storage of each subbasin is lumped in the initial abstraction of the SCS-CN method or is considered as an empirical tank that needs to be filled in the SMA method. Since it is assumed that the entire subbasin contributes water to the lumped depression, no surface runoff is generated until the lumped depression is fully filled. In reality, even in a subbasin of a depression-dominated watershed, a certain area can be directly connected to the subbasin outlet (Wang et al., 2019; Wang and Chu 2020). Therefore, the application of HEC-HMS in depression-dominated areas can cause misleading simulation results.

In the second category, the Precipitation-Runoff Modeling System (PRMS) is a physical-based modeling system designed to simulate surface runoff with considering complex environmental conditions (Markstrom et al., 2015). In PRMS, a watershed can be divided into different hydrologic response units (HRUs), and depressions in each "land HRU" are lumped together. Users can specify the percentage of each "land HRU" that contributes water to its associated lumped depression and the percentages of the open part (with water release) and close part (no water release) of the lumped depression. Vining (2002) utilized the PRMS for hydrologic simulation in a depression-dominated subbasin of the Devils Lake watershed. Hay et al. (2018) applied the PRMS to simulate the depression storage variations of a watershed within the prairie pothole region (PPR) of North Dakota. SWAT is another widely used hydrologic model that belongs to the second category. In SWAT, a watershed is delineated into a number of subbasins and three functions are provided to simulate ponded water in each subbasin, including the pothole function, the wetland function, and the lake function (Gassman et al., 2007). Similar to the PRMS, depressions of a subbasin are lumped together in SWAT, and a user-specified parameter is utilized to control water release from the lumped depression (Neitsch et al., 2011).

However, in SWAT, it is assumed that the entire lumped depression in a subbasin contributes water to the subbasin outlet when it is fully filled. Even though specifying the contributing areas for lumped depressions can improve the hydrologic simulation in depression-dominated areas, the depression functions used in the models in the second category are still very simple. For example, limited parameters, which need to be calibrated, are used to depict the characteristics of depressions, and only a single threshold is used to control water release from the lumped depression of a subbasin.

To improve the performance of existing models in depression-dominated areas, Wang et al. (2008) proposed a hydrologic equivalent wetland (HEW) concept to consider the properties of depressions and incorporated this concept into SWAT for hydrologic simulation of a watershed in the Red River basin. Tahmasebi Nasab et al. (2017a) coupled a puddle delineation (PD) algorithm (Chu 2010) with SWAT to analyze the influence of depressions on the hydrologic processes in a depression-dominated watershed in the PPR. In that study, the depression characteristics (e.g., storage and contributing area) were accurately calculated by the PD algorithm and further used in SWAT for depression-controlled hydrologic modeling. Mekonnen et al. (2016) developed a modified SWAT model, the SWAT-Probability Distribution Landscape Distribution (SWAT-PDLD) model, which incorporated surface depression heterogeneity in SWAT modeling by using a probability distribution function. Grimm and Chu (2020) proposed a depression threshold control proxy (DTCP) to enhance the performance of HEC-HMS in the hydrologic simulation for depression-dominated areas. Because of the storage-discharge function in DTCP, the modified HEC-HMS successfully simulated the discharge and the variation of the contributing area of a watershed in the PPR.

The above models are semi-distributed models that handle depressions in lumped ways. Therefore, these models cannot provide detailed variations of the ponding conditions of all individual depressions and their connections in depression-dominated areas. In recent years, the impacts of the dynamic hydrologic connectivity caused by depressions have been highlighted in many studies. For example, Leibowitz and Vining (2003) observed and analyzed the temporal connectivity between two depressions in the PPR and discussed the potential chemical and biological consequences caused by the temporal connectivity. Phillips et al. (2011) analyzed the dynamic stream drainage network with the influences of complex landforms (e.g., lakes, exposed bedrock, and soil filled areas) and quantified the streamflow and runoff response to the network. Chu et al. (2013a) developed a fully distributed puddle to puddle (P2P) model to simulate the dynamic filling-spilling-merging-splitting processes of all depressions, surface runoff routing, and infiltration in depression-dominated areas. Moreover, the P2P model was utilized in analyzing the influences of microtopography on structural and functional hydrologic connectivity (e.g., Yang and Chu 2013; Grimm and Chu 2018). Even though P2P has superior capability in tracking the variation of hydrologic processes and connectivity related to depressions, it requires intensive computation resources, especially for large-scale surfaces.

Both existing semi-distributed and fully distributed models have their advantages and disadvantages. An interesting research question is: how to incorporate some essential processes simulated by the fully distributed models into semi-distributed models for large-scale watershed modeling?

1.4. Dissertation Objectives

As aforementioned, surface depressions are one of the significant topographic characteristics in depression-dominated areas. However, existing surface delineation algorithms

and hydrologic models have their limitations in addressing watershed-scale hydrologic problems related to depressions. This dissertation research focuses on development of some improved methods to analyze and quantify the impacts of surface depressions on topographic characteristics and watershed-scale hydrologic processes. The specific objectives of this research are to:

- Improve watershed delineation to further reveal the topographic characteristics and hydrologic connectivity within watersheds.
- Analyze the impact of surface depressions on runoff processes during rainfall events and the mechanism of water release from depressions.
- Analyze the watershed-scale functionalities of depressions in continuous simulation of hydrologic processes and connectivity.

1.5. Organization of the Dissertation

This dissertation consists of five chapters, including a general introduction (Chapter 1), three main research topics (Chapters 2 - 4), and an overall conclusion (Chapter 5). Chapter 1 shows the background, literature review, current problems, and the objectives of this dissertation research. Chapter 2 introduces a new algorithm for hydrologic unit delineation of depressions and channels. In this algorithm, unique procedures are proposed to efficiently identify depression and channel hydrologic units and their connections. The algorithm has been applied to a watershed in North Dakota and one paper has been published in Water (Wang and Chu 2020). Chapter 3 focuses on the development and application of a depression-oriented hydrologic model that considers separate modeling for different components of subbasins (e.g., depressional and non-depressional areas) and hierarchical control thresholds for water release from depressions. Based on the materials in Chapter 3, a paper has been published in the Journal of Hydrologic

Engineering (Wang et al. 2019). Chapter 4 describes a novel depression-oriented hydrologic model for continuous simulation of the dynamic hydrologic processes and connectivity within subbasins by tracking runoff between puddle-based units, off-stream channel-based units and on-stream channel-based units within each subbasin. The model has been applied to a watershed in the PPR to investigate the functionalities of depressions in runoff routing and hydrologic connectivity modeling, and one paper related to this model is in preparation. Chapter 5 summarizes all major findings and contributions from this dissertation research.

1.6. References

Arabi, M., Govindaraju, R., Sophocleous, M., Koelliker, J., 2006. Use of distributed models for watershed management: case studies. Watershed models. Boca Raton, FL: Taylor and Francis.

Arnold, N., 2010. A new approach for dealing with depressions in digital elevation models when calculating flow accumulation values. Prog. Phys. Geogr., 34, 781-809.

Bhatt, G., Kumar, M., Duffy, C. J., 2014. A tightly coupled GIS and distributed hydrologic modeling framework. Environ. Modell. Softw., 62, 70-84.

Borah, D. K., Bera, M., 2004. Watershed-scale hydrologic and nonpoint-source pollution models: Review of applications. Trans. ASABE., 47(3), 789.

Breuer, L., Huisman, J., Willems, P., Bormann, H., Bronstert, A., Croke, B., Frede, H.-G., Gräff, T., Hubrechts, L., Jakeman, A., 2009. Assessing the impact of land use change on hydrology by ensemble modeling (LUCHEM). I: Model intercomparison with current land use. Adv. Water Resour., 32(2), 129-146.

Chi, Y., Yang, J., Bogart, D., Chu. X., 2012. Fractal analysis of surface microtopography and its application in understanding hydrologic processes. Trans. ASABE. 55(5), 1781-1792.

Chourushi, S., Lodha, P. P., Prakash, I., 2019. A Critical Review of Hydrological Modeling Practices for Flood Management. Pramana Res. J., 9(3).

Chu, X., Zhang, J., Chi, Y., Yang, J., 2010. An improved method for watershed delineation and computation of surface depression storage. In Watershed Management 2010: Innovations in Watershed Management Under Land Use and Climate Change, Proc. of the 2010 Watershed Management Conf., 1113-1122. K. W. Potter and D. K. Frevert, eds. Reston, Va.: ASCE.

Chu, X., Yang, J., Chi, Y., Zhang, J., 2013a. Dynamic puddle delineation and modeling of puddle-to-puddle filling-spilling-merging-splitting overland flow processes. Water Resour. Res., 49(6), 3825-3829.

Chu, X., Nelis, J., Rediske, R., 2013b. Preliminary study on the effects of surface microtopography on tracer transport in a coupled overland and unsaturated flow system. J. Hydrol. Eng., 18(10), 1241-1249.

Chu, X., 2017. Delineation of pothole-dominated wetlands and modeling of their threshold behaviors. J. Hydrol. Eng., 22, D5015003.

Costa-Cabral, M. C., Burges, S. J., 1994. Digital elevation model networks (DEMON): A model of flow over hillslopes for computation of contributing and dispersal areas. Water Resour. Res., 30(6), 1681-1692.

Daniel, E. B., Camp, J. V., LeBoeuf, E. J., Penrod, J. R., Abkowitz, M. D., Dobbins, J. P., 2010. Watershed Modeling Using GIS Technology: A Critical Review. J. Spatial Hydrol., 10(2).

Daniel, E. B., Camp, J. V., LeBoeuf, E. J., Penrod, J. R., Dobbins, J. P., Abkowitz, M. D., 2011. Watershed modeling and its applications: A state-of-the-art review. The Open Hydrol. J., 5(1).

Darboux, F., Davy, P., Gascuel-Odoux, C., Huang, C., 2002. Evolution of soil surface roughness and flowpath connectivity in overland flow experiments. Catena, 46(2-3), 125-139.

Darboux, F., Huang, C., 2005. Does soil roughness increase or decrease water and particletransfer? Soil Sci. Soc. America J., 69(3), 748-756.

DeVantier, B. A., Feldman, A. D., 1993. Review of GIS applications in hydrologic modeling. J. Water Res. Plan. Man., 119(2), 246-261.

Fassieh, K. M., Zaki, M. A., 2014. A Water Management Model for Toshka Depression. J. Appl. Math., 2014.

Ficklin, D. L., Luo, Y., Luedeling, E., Zhang, M., 2009. Climate change sensitivity assessment of a highly agricultural watershed using SWAT. J. Hydrol., 374(1), 16-29.

Garbrecht, J., Martz, L.W., 2000. An automated digital landscape analysis tool for topographic evaluation, drainage identification, Watershed Segmentation and Subcatchment Parameterization: TOPAZ User Manual. USDA, Agricultural Research Service, Grazinglands Research Laboratory, El Reno, USA.

Gassman, P. W., Reyes, M. R., Green, C. H., Arnold, J. G., 2007. The soil and water assessment tool: historical development, applications, and future research directions. Trans. ASABE, 50(4), 1211-1250.

Golden, H. E., Lane, C. R., Amatya, D. M., Bandilla, K. W., Kiperwas, H. R., Knightes, C. D., Ssegane, H., 2014. Hydrologic connectivity between geographically isolated wetlands

and surface water systems: a review of select modeling methods. Environ. Modell. Softw., 53, 190-206.

Göppert, H., Ihringer, J., Plate, E., Morgenschweis, G., 1998. Flood forecast model for improved reservoir management in the Lenne River catchment, Germany. Hydrol. Sci. J., 43(2), 215-242.

Govers, G., Takken, I., Helming, K., 2000. Soil roughness and overland flow. Agronomie, 20(2), 131-146.

Grimm, K., Chu, X., 2018. Modeling of spatiotemporal variations in runoff contribution areas and analysis of hydrologic connectivity. Land Degrad.Dev., 29(8), 2629-2643.

Grimm, K., Chu, X., 2020. Depression threshold control proxy to improve HEC-HMS modeling of depression-dominated watersheds. Hydrol. Sci. J., 65(2), 200-211.

Hansen, B., Schjønning, P., Sibbesen, E., 1999. Roughness indices for estimation of depression storage capacity of tilled soil surfaces. Soil Till. Res., 52(1-2), 103-111.

Hay, L., Norton, P., Viger, R., Markstrom, S., Regan, R. S., Vanderhoof, M., 2018. Modelling surface-water depression storage in a Prairie Pothole Region. Hydrol. Process., 32(4), 462-479.

Helming, K., Römkens, M. J. M., Prasad, S. N., 1998. Surface roughness related processes of runoff and soil loss: a flume study. Soil Sci. Soc. America J., 62, 243-250.

Jenson, S. K., Domingue, J. O., 1988. Extracting topographic structure from digital elevation data for geographic information system analysis. Photogramm. Eng. Rem. S., 54(11), 1593-1600.

Jones, N. L., Wright, S. G., Maidment, D. R., 1990. Watershed delineation with triangle-based terrain models. J. Hydraul. Eng., 116(10), 1232-1251.

Lai, Y., Yang, C., Hsieh, C., Wu, C., Kao, C., 2011. Evaluation of non-point source pollution and river water quality using a multimedia two-model system. J. Hydrol., 409(3), 583-595.

Leibowitz, S. G., Vining, K. C., 2003. Temporal connectivity in a prairie pothole complex. Wetlands, 23(1), 13-25.

Luo, Y., Su, B., Yuan, J., Li, H., Zhang, Q., 2011. GIS techniques for watershed delineation of SWAT model in plain polders. Procedia Environ. S., 10, 2050-2057.

Marks, D., Dozier, J., Frew, J., 1984. Automated basin delineation from digital elevation data. Geo-Processing, 2, 299-311.

Martz, L. W., Jong, E.D., 1988. CATCH: A FORTRAN program for measuring catchment area from digital elevation models. Comput. Geosci., 14(5), 627-640.

Martz, L. W., Garbrecht, J., 1993. Automated extraction of drainage network and watershed data from digital elevation models 1. JAWRA J. Am. Water Resour. As., 29(6), 901-908.

Martz, L. W., Garbrecht, J., 1999. An outlet breaching algorithm for the treatment of closed depressions in a raster DEM. Comput. Geosci., 25(7), 835-844.

Martin, Y., Valeo, C., Tait, M., 2008. Centimetre-scale digital representations of terrain and impacts on depression storage and runoff. Catena, 75, 223-233.

Maidment, D.R., 2002. ArcHydro: GIS for Water Resour; ESRI Press: Redlands, CA, USA.

Markstrom, S. L., Regan, R. S., Hay, L. E., Viger, R. J., Webb, R. M., Payn, R. A., LaFontaine, J. H., 2015. PRMS-IV, the precipitation-runoff modeling system, version 4. US Geological Survey Techniques and Methods (6-B7).

Mekonnen, B. A., K. A. Mazurek, G. Putz., 2016. Incorporating landscape depression heterogeneity into the Soil and Water Assessment Tool (SWAT) using a probability distribution. Hydrol. Process., 30 (13), 2373-2389.

Moore ID, Grayson RB, 1991. Terrain-based catchment partitioning and runoff prediction using vector elevation data. Water Resour. Res., 27(6), 1177-1191.

Neitsch, S. L., Arnold, J. G., Kiniry, J. R., Williams, J. R., 2011. Soil and water assessment tool theoretical documentation version 2009. Texas Water Resources Institute.

O'Callaghan, J. F., Mark, D. M., 1984. The extraction of drainage networks from digital elevation data. Comput. Vis. Graph Image Process, 28(3), 323-344.

Orlandini S., Moretti G., Franchini M., Aldighieri B., Testa B., 2003. Path-based methods for the determination of nondispersive drainage directions in grid-based digital elevation models". Water Resour. Res. 39(6), 1144.

Parajuli, P. B., Ouyang, Y., 2013. Watershed-scale hydrological modeling methods and applications. Current perspectives in contaminant hydrology and water resources sustainability, 57-80.

Phillips, R. W., Spence, C., Pomeroy, J. W., 2011. Connectivity and runoff dynamics in heterogeneous basins. Hydrol. Process., 25(19), 3061-3075.

Planchon, O., Darboux, F., 2002. A fast, simple and versatile algorithm to fill the depressions of digital elevation models. Catena, 46(2-3), 159-176.

Rahman, M. M., Arya, D. S., Goel, N. K., 2010. Limitation of 90 m SRTM DEM in drainage network delineation using D8 method-a case study in flat terrain of Bangladesh. Applied Geomatics, 2(2), 49-58.

Rieger, W., 1993. Automated river line and catchment area extraction from DEM data. ISPRS Archives, 29, 642.

Rieger, W., 1998. A phenomenon-based approach to upslope contributing area and depressions in DEMs. Hydrol. Process., 12(6), 857–872.

Rossi, M. J., Ares, J. O., 2012. Depression storage and infiltration effects on overland flow depth-velocity-friction at desert conditions: field plot results and model. Hydrol., Earth Syst., Sci., 16, 3293-3307.

Schuol, J., Abbaspour, K. C., Srinivasan, R., Yang, H., 2008. Estimation of freshwater availability in the West African sub-continent using the SWAT hydrologic model. J. Hydrol., 352(1), 30-49.

Seibert J., McGlynn B.L., 2007. A new triangular multiple flow direction algorithm for computing upslope areas from gridded digital elevation models. Water Resour. Res. 43: W04501.

Soille, P., 2004. Optimal removal of spurious pits in grid digital elevation models. Water Resour. Res., 40(12). W12509.

Sui, D. Z., Maggio, R. C., 1999. Integrating GIS with hydrological modeling: practices, problems, and prospects. Comput. Environ. Urban, 23(1), 33-51.

Tahmasebi Nasab, M., Singh, V., Chu, X., 2017a. SWAT Modeling for Depression-Dominated Areas: How Do Depressions Manipulate Hydrologic Modeling? Water 9(1), 58.

Tahmasebi Nasab, M., Zhang, J., Chu, X., 2017b. A new depression-dominated delineation (D-cubed) method for improved watershed modeling. Hydrol. Process., 31(19), 3364-3378.

Tarboton D.G., 1997. A new method for the determination of flow directions and upslope areas in grid digital elevation models. Water Resour. Res., 33(2), 309–319.

USACE, HEC (Hydrologic Engineering Center). 2016. Hydrologic modeling system HEC-HMS, user's manual, version 4.2. Davis, CA: USACE-HEC.

Verma, S., Verma, R. K., Mishra, S. K., Singh, A., Jayaraj, G. K., 2017. A revisit of NRCS-CN inspired models coupled with RS and GIS for runoff estimation. Hydrol. Sci. J., 62(12), 1891-1930.

Vining, K. C., 2002. Simulation of streamflow and wetland storage, Starkweather Coulee subbasin, North Dakota, water years 1981-98 (No. 2002-4113).

Wang, L., Liu, H., 2006. An efficient method for identifying and filling surface depressions in digital elevation models for hydrologic analysis and modelling. Int. J. Geog. Inf. Sci., 20(2), 193-213.

Wang, X., Yang, W., Melesse, A. M., 2008. Using hydrologic equivalent wetland concept within SWAT to estimate streamflow in watersheds with numerous wetlands. Trans. ASABE 51(1), 55-72.

Wang, N., Zhang, X., Chu, X., 2019. New model for simulating hydrologic processes under influence of surface depressions. J. Hydrol. Eng., 24(5), 04019008.

Wang, N., Chu, X., 2020. A new algorithm for delineation of surface depressions and channels. Water, 12(1), 7.

WMS., 2015. WMS User Manual 10.1. Brigham Young Univ., Environmental Modeling Research Laboratory, Provo, Utah.

Xu, J., Zhang, W., Liu, C., 2007. A novel method for filling the depressions in massive DEM data. In Geoscience and Remote Sensing Symposium, 2007. IGARSS 2007. IEEE International (pp. 4080-4083). IEEE.

Yang, J., Chu X., 2013. Quantification of the spatio-temporal variations in hydrologic connectivity of small-scale topographic surfaces under various rainfall conditions. J. Hydrol., 505, 65-77.

Yang, J., Chu, X., 2015. A new modeling approach for simulating microtopography-dominated, discontinuous overland flow on infiltrating surfaces. Adv. Water Resour. 78 (4): 80-93.

Yang, W., Wang, X., Liu, Y., Gabor, S., Boychuk, L., Badiou, P., 2010. Simulated environmental effects of wetland restoration scenarios in a typical Canadian prairie watershed. Wetl. Ecol. Manag., 18(3), 269-279.

2. A NEW ALGORITHM FOR DELINEATION OF SURFACE DEPRESSIONS AND CHANNELS

2.1. Abstract

Topographic delineation is critical to watershed hydrologic modeling, which may significantly influence the accuracy of model simulations. In most traditional delineation methods, however, surface depressions are fully filled and hence watershed-scale hydrologic modeling is based on depressionless topography. In reality, dynamic filling and spilling of depressions affect hydrologic connectivity and surface runoff processes especially in depression-dominated areas. Thus, accounting for the internal hydrologic connectivity within a watershed is crucial to such hydrologic simulations. The objective of this study is to improve watershed delineation to further reveal such complex hydrologic connectivity. To achieve this objective, a new algorithm, HUD-DC, is developed for delineation of hydrologic units (HUs) associated with depressions and channels. Unlike the traditional delineation methods, HUD-DC considers both filled and unfilled conditions to identify depressions and their overflow thresholds, as well as all channels. Furthermore, HUs, which include puddle-based units and channel-based units, are identified based on depressions and channels, and the detailed connectivity between the HUs is determined. A watershed in North Dakota was selected for testing HUD-DC, and Arc Hydro was also utilized to compare with HUD-DC in depression-oriented delineation. The results highlighted the significance of depressions and the complexity of hydrologic connectivity. In addition, HUD-DC was utilized to evaluate the variations in topographic characteristics under different filling conditions, which provided helpful guidance for identification of filling thresholds to effectively remove artifacts in digital elevation models.

2.2. Introduction

Surface depressions are one of the dominant topographic characteristics for many landscapes. For example, the Prairie Pothole Region (PPR) in North America is unique due to its numerous depressions. It can be a challenge to model hydrologic processes in such depression-dominated areas (Vanderhoof et al. 2016; Hay et al. 2018). As a pre-processing procedure of hydrologic modeling, surface delineation is essential and critical to reveal hydrologic connectivity across a land surface. Many methods have been developed for surface delineation based on digital elevation models (DEMs) (e.g., O'Callaghan and Mark 1984; Jenson and Domingue 1988; Garbrecht and Martz 1997; Martínez-Casasnovas and Stuiver 1998; Jasiewicz and Metz 2011). In traditional delineation methods, however, depressions in a watershed (including artifact depressions) are commonly removed by implementing filling and/or breaching approaches (McCormack et al. 1993; Rieger 1993; Garbrecht and Martz 1997; Martz and Garbrecht 1998; Soille 2004; Arnold 2010; Shaw et al., 2013; Huang and Lee 2015). That is, it is assumed in these methods that the entire watershed contributes surface runoff to its associated outlet. This assumption can be appropriate for watersheds with fewer depressions, but not for depression-dominated areas like PPR. In reality, depressions have threshold controls on the hydrologic connectivity of a watershed (Chu et al., 2013; Chu 2017; Wang et al., 2019), and only a portion of the watershed contributes surface runoff to the outlet in most rainfall-runoff events. In recent years, various studies, which focused on investigating hydrologic connectivity and the related impacts on hydrologic processes, highlighted the significance of depressions (McCauley and Anteau 2014; Tahmasebi Nasab et al., 2017a; Grimm and Chu 2018). Therefore, new watershed delineation methodologies are needed to capture the detailed connectivity between depressions and reveal the real hydrologic processes.

Generally, a typical depression consists of a ponding area and at least one threshold (i.e., pour point). Depressions in an area exhibit a hierarchical characteristic. Following a filling process, the depressions that share the same threshold can merge into a larger, higher-level depression (Chu et al., 2013; Chu 2017). Such a merging process continues until all highest-level depressions are generated. In the existing delineation methods, some algorithms focus on delineation of highest-level depressions only, while others center on characterizing all level depressions. For example, Temme et al. (2006) developed an algorithm to search DEM cells for identification of the highest-level depressions and the algorithm was further incorporated into a geomorphological model, LAPSUS, to investigate the dynamic landscape evolution. Arc Hydro is an ArcGIS-based tool that handles data pre-processing for hydrologic modeling (Maidment 2002). Different from the method by Temme et al. (2006), in Arc Hydro all highest-level depressions are identified based on the differences between the fully-filled DEM and the original DEM. Consequently, it cannot provide hydrologic connectivity between depressions. In addition, both methods do not consider channels in their surface delineation. Chu et al. (2010) developed a puddle delineation (PD) algorithm to identify depressions at all different levels, and their associated thresholds and puddle-based units (PBUs). The PD algorithm was further used to provide depression information for hydrologic modeling to analyze the influence of depressions on hydrologic processes across various spatial scales (Chu et al., 2013; Yang and Chu 2015; Wang et al., 2019). Tahmasebi Nasab et al. (2017b) improved the PD algorithm by considering channels and developed a depression-dominated delineation (D-cubed) algorithm. In addition to depressions at different levels, the D-cubed algorithm further identifies PBUs and channel-based units (CBUs) based on the highest-level depressions and channels. The PD and D-cubed algorithms are mainly used for delineation of smaller scale surfaces.

The objective of this study is to reveal the internal hydrologic connectivity within watersheds. To achieve this objective, a new algorithm, HUD-DC, is developed for delineation of hydrologic units (HUs) associated with depressions and channels at a watershed scale. The performance of HUD-DC is evaluated by comparing it with Arc Hydro in an application to the Upper Pipestem Creek watershed in North Dakota. In addition, the original DEM is pre-filled with a series of incremental water depths to analyze the variations in topographic characteristics under different filling conditions and determine the filling threshold, which can be used to control or eliminate artifacts in DEMs.

2.3. Materials and Methods

2.3.1. Development of HUD-DC

HUD-DC implements ArcGIS-based surface delineation to reveal the hydrologic connectivity at a watershed scale by identifying a series of HUs including PBUs and CBUs, and provides topographic information related to depressions and channels for hydrologic modeling in depression-dominated watersheds. Following Chu et al. (2010) and Tahmasebi Nasab et al. (2017b), a PBU consists of a highest-level depression and its contributing area, while a CBU includes a channel segment and its contributing area. Moreover, one highest-level depression may have a number of embedded lower-level depressions. Since a PBU does not contribute water to its downstream HU(s) (PBU or CBU) until the highest-level depression of the PBU is fully filled and the focus of HUD-DC is on the surface delineation at a watershed scale, the dynamic merging and splitting of lower-level depressions within a PBU are not taken into account in HUD-DC. Compared with Arc Hydro, HUD-DC considers both depressions and channels when identifying contributing areas, and provides the detailed connectivity between HUs. Similar to the D-cubed algorithm, HUD-DC delineates a surface into numerous HUs

(PBUs and CBUs) and determines their relationships and connectivity. However, instead of searching for depressions at all levels, HUD-DC only identifies the highest-level depressions, and new approaches are used in HUD-DC for watershed-scale surface delineation. To illustrate the methodology of HUD-DC, an artificial surface with 10x10 DEM grids (Figure 2.1a) was used in this study. Figures 2.1b and 2.1c respectively show the fully-filled DEM and the flow directions under a fully-filled condition, both of which are utilized as input data of HUD-DC. The fully-filled DEM was created by using the ArcGIS filling function, while the flow directions were determined by using the methods developed by Tarboton et al. (1991) and Jenson and Domingue (1988). HUD-DC consists of two major modules, depression identification module and channel and HU identification module. Their procedures are detailed in the following sections.

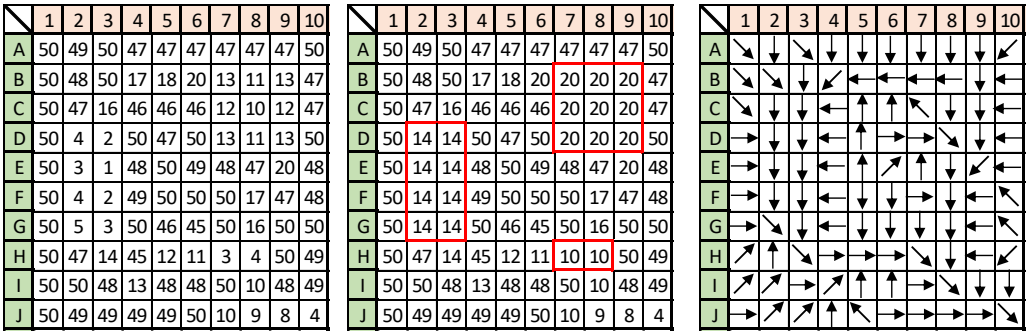

Figure 2.1. Input data of HUD-DC: (a) original DEM; (b) fully-filled DEM; and (c) flow directions under the fully-filled condition.

2.3.1.1. Identification of depressions

Figure 2.2 shows the flowchart of the depression identification module. The identification of depressions includes four major steps: (1) identification of the filled cells; (2) searching for possible depression cells; (3) elimination of 'fault' depression cells; and (4) identification of 'real' depression cells.

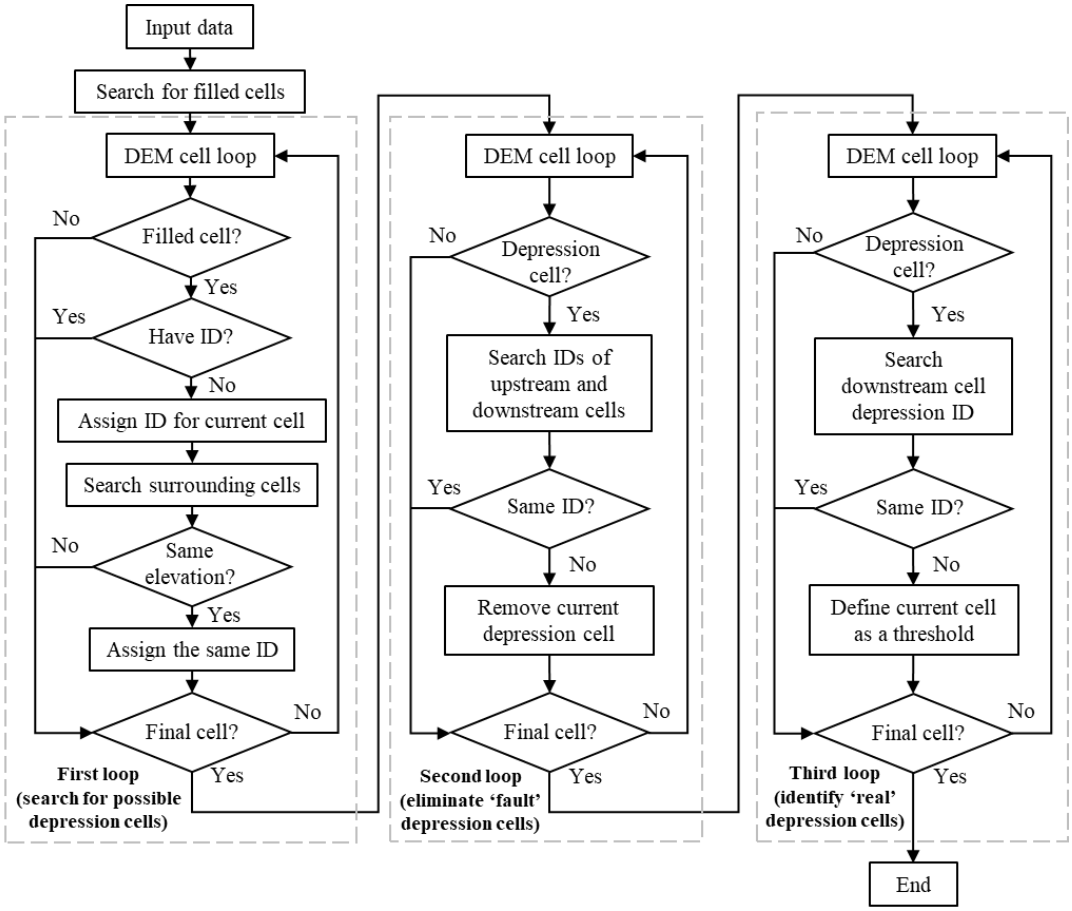

Figure 2.2. Flowchart of the depression identification module.

Figure 2.3 shows the detailed depression delineation processes for an artificial surface. In this module, a searching process is implemented for all filled DEM cells by comparing the elevation differences between the original DEM and the fully-filled DEM (Figures 2.2 and 2.3a). Each highest-level depression includes filled cells in an area and its associated threshold(s). Thus, after the filled cells are found, three cell loops are carried out to identify the overflow thresholds related to the filled cells. The first cell loop (Figure 2.2) is executed to find all possible depression cells and assign IDs to them based on the fully-filled DEM (Figure 2.3b). In this loop, if one cell is a filled cell without ID, a new ID is generated and assigned to it and the same ID is given to its surrounding cells with an identical elevation. This loop continues until all possible depression cells are located. Since the first cell loop is only based on the elevations of

the cells in a fully-filled condition, some possible depression cells have the same elevation but no hydrologic connectivity with 'real' depression cells. For example, the elevation of cell J7 in Figure 2.3b equals 10, which is the same as the elevation of other cells in depression P3. However, cell J7 receives runoff from cell J6 and discharges to cell J8, while cell I8 receives the runoff generated from cells H7 and H8 and then transmits runoff to cell G9 (Figure 2.1c). Therefore, cell J7 is a 'fault' depression cell that has no hydrologic connectivity with other 'real' depression cells in P3.

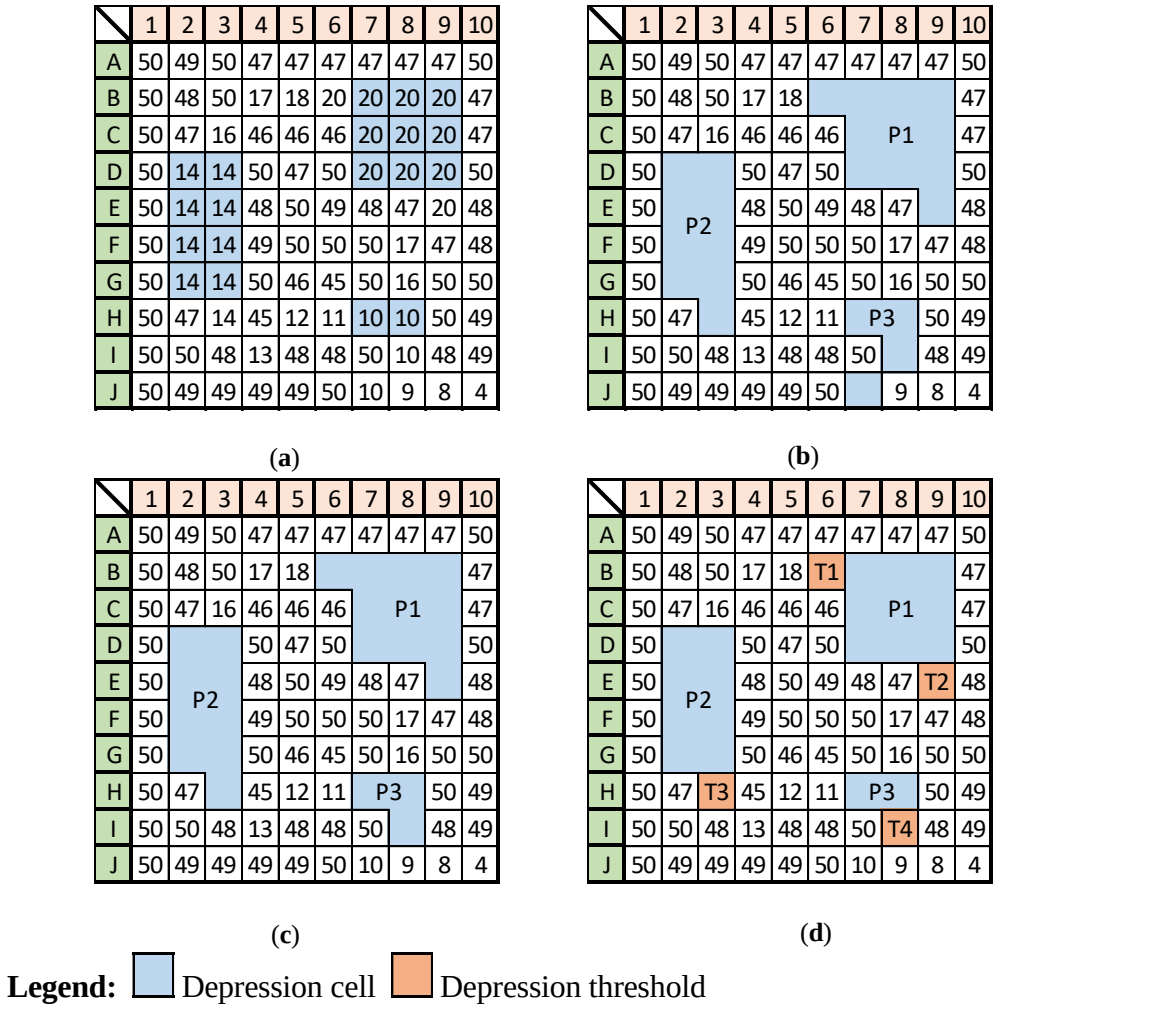

Figure 2.3. Schematic diagrams for depression identification: (a) identification of the filled cells; (b) searching for possible depression cells; (c) elimination of 'fault' depression cells; and (d) identification of 'real' depression cells.

The second cell loop (Figure 2.2) is designed to remove the 'fault' cells like J7 (Figure 2.3c). In this loop, both the upstream and downstream cells of each possible depression cell are located based on the flow directions. If neither upstream cell nor downstream cell belong to the same depression with the possible depression cell, it is defined as a 'fault' depression cell and removed from its associated depression. After all 'real' depression cells are confirmed, the third cell loop (Figure 2.2) is initiated to find the thresholds of depressions and assign IDs to them. If a cell is a depression cell and its downstream cell is not a depression cell, it is defined as the threshold of its associated depression. Particularly, a depression may contain multiple thresholds. For example, both threshold T1 and threshold T2 in Figure 2.3d belong to depression P1 (a two-threshold depression), while thresholds T3 and T4 respectively are the thresholds of their associated depressions P2 and P3 (two single-threshold depressions).

2.3.1.2. Identification of channels and hydrologic units

The channel and HU identification module is executed to identify channels, PBUs, CBUs, and the connectivity between HUs. The method proposed by Jenson and Domingue (1988) is used in this module to find channels in the fully-filled condition, depending on a user-defined flow accumulation threshold and the flow directions (Figure 2.4). Figure 2.5a shows channel cells for the artificial surface (Figure 2.1a) when the flow accumulation threshold is set to 5. Note that the channel cells within depressions are removed by overlaying the channels and depressions (Figure 2.4), and the IDs of remaining channel cells are determined by using the 'Stream Link' function in ArcGIS. Figure 2.5b shows the cells identified for four channels. To identify PBUs and CBUs, it is required to find the 'outlets' of depressions and channels, which are depression thresholds and channel ending points. Since all depression thresholds have been found in the depression identification module, only channel ending points are searched by using

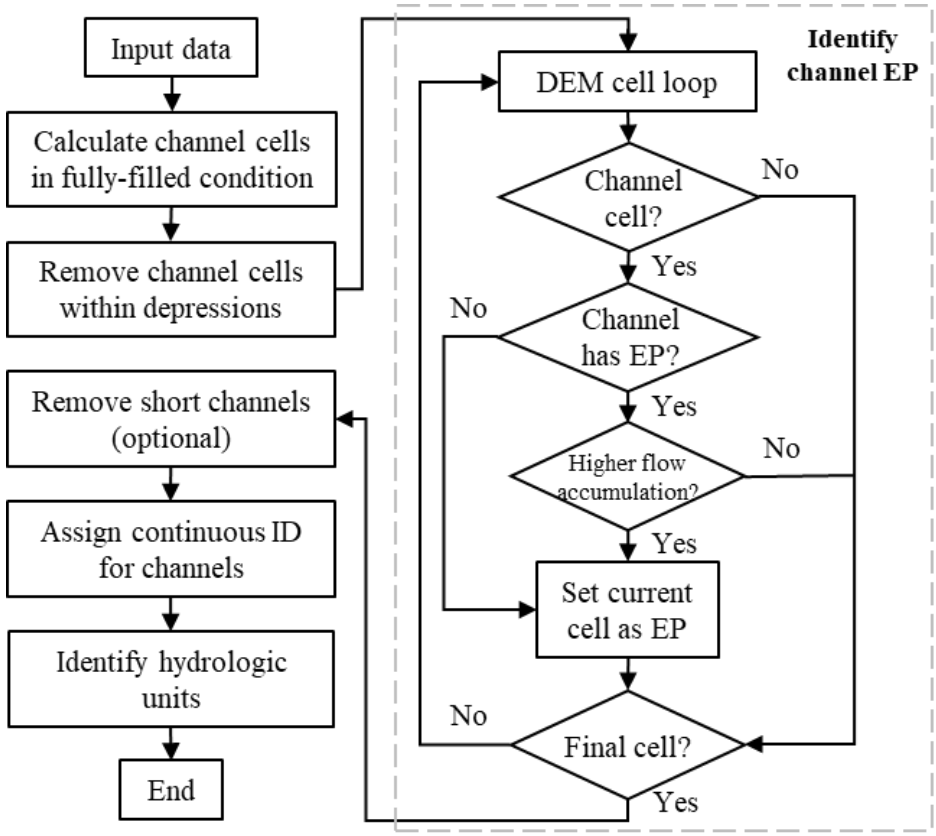

Figure 2.4. Flowchart of the channel and HU identification module (EP: Ending point of a channel).

a cell loop after the identification of channel cells within depressions (Figure 2.4). If a cell belongs to one channel and this channel does not have an ending point, the cell is defined as the channel ending point. On the other hand, if the cell belongs to one channel that already has an ending point, the flow accumulation of the cell and the current ending point are compared and the cell with a higher flow accumulation is set as the new channel ending point. This loop continues until all channel cells are searched and identified. Following this cell loop, the ending points of the four channels are identified (i.e., O1 - O4 in Figure 2.5c). Since HUD-DC focuses on the watershed-scale surface delineation, an optional procedure can be executed to eliminate short channels based on a user-defined channel length threshold (Figure 2.4). The criteria to delete a channel are: (1) the length of a channel is shorter than the user-defined length threshold,

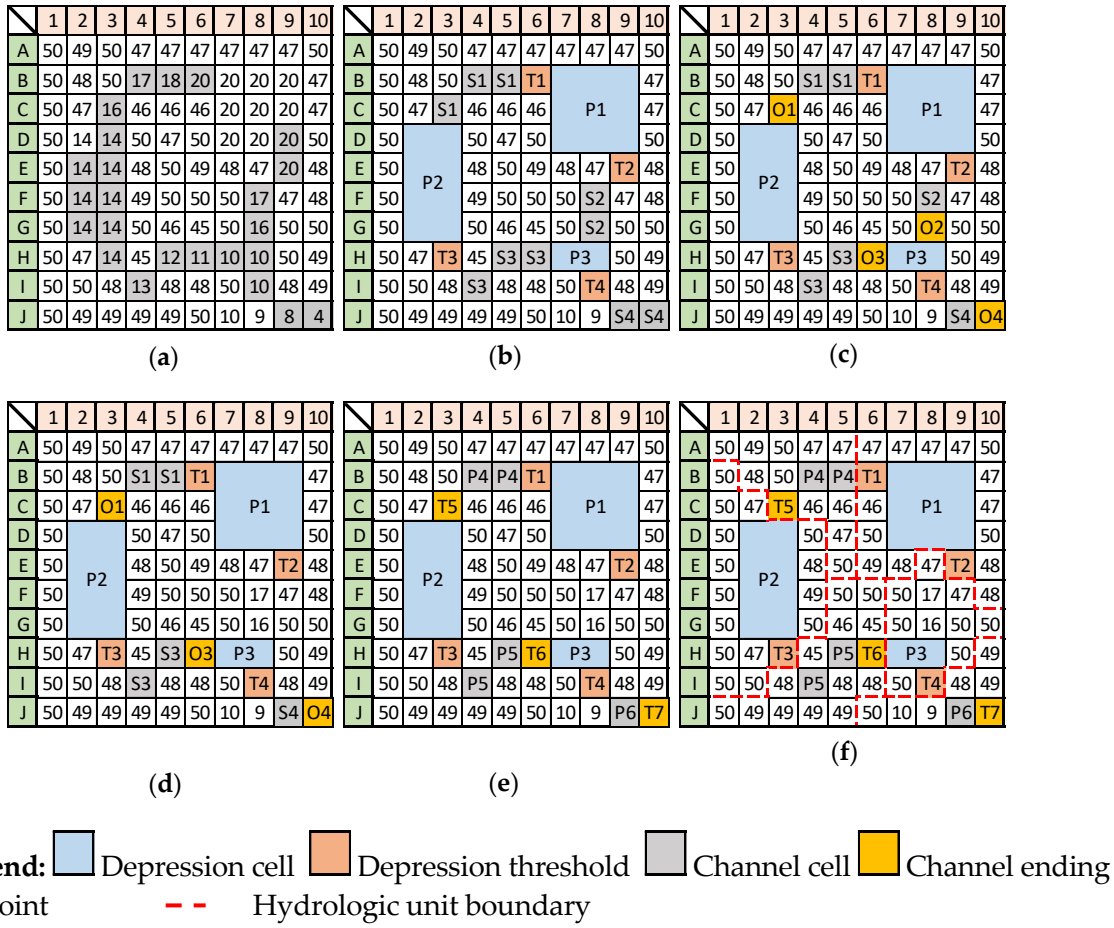

Figure 2.5. Schematic diagrams for delineation of channels and hydrologic units: (a) searching for channel cells, (b) overlay of channel cells and depression cells, (c) identification of channel ending points, (d) elimination of short channels, (e) assignment of continuous IDs, and (f) delineation of hydrologic unit boundaries.

and (2) the flow direction at the ending point of the channel does not point toward the outside (i.e., the ending point is an outlet). In this study, channel ending points are considered in the calculation of channel lengths. For example, the length of channel S2 is 2 (Figure 2.5b). If the channel length threshold is 3, S2 is removed from the channel cells, and cells F8 and G8 in channel S2 are then assigned as contributing cells of P3 (Figure 2.5d). For S4, however, although its length is the same as that of S2 (i.e., 2), it is still considered as a channel because cell J10 is the final outlet of the entire surface (Figure 2.5d). After all channel ending points are finalized, a channel loop is performed to assign continuous IDs for the channels and their ending points that

follow the IDs of the depressions and their thresholds, respectively (Figure 2.4). For example, channel S1 and channel ending point O1 are changed to P4 and T5, respectively (Figure 2.5e). The delineation of HUs is the final key procedure in the channel and HU identification module. HUD-DC employs the 'Watershed' function in ArcGIS to handle the delineation of HUs by considering the depression thresholds and the channel ending points as pour points (Figures 2.4 and 2.5f). The IDs of the identified depressions and HUs are assigned to their associated HUs.

2.3.2. Study Area and Testing of HUD-DC

In this study, the Upper Pipestem Creek watershed in North Dakota (Figure 2.6) was selected to test the performance of HUD-DC in surface delineation. As the contributing area of the USGS 06469400 Pipestem creek gauge station (47°10'03" N, 98°58'07" W), the study area covers an area of 1668.12 km^2, including parts of four counties in North Dakota (i.e., Wells, Foster, Kidder, and Stutsman counties) (Figure 2.6). Based on the 2011 NLCD (National Land Cover Database), the study area is mainly covered by cultivated crops (42.89%), herbaceous (26.01%), and pasture (14.81%). Moreover, the open water and emergent herbaceous wetlands account for 6.28% and 5.89%, respectively.

Since numerous depressions are scattered across the study area, analyzing depressions and their connectivity is critical to modeling of hydrologic processes in this watershed. An original 30-m DEM of the watershed was downloaded from the USGS National Map Viewer (https://viewer.nationalmap.gov/advanced-viewer/) and used as the input data of HUD-DC for surface delineation. Arc Hydro was also applied to the study area and compared with HUD-DC in delineation of depressions. In addition, the similarities and differences between the two methods were analyzed according to the surface delineation results and the underlying

methodologies. Based on the delineation results of HUD-DC, topographic characteristics of the study area were analyzed to highlight the significance of depressions.

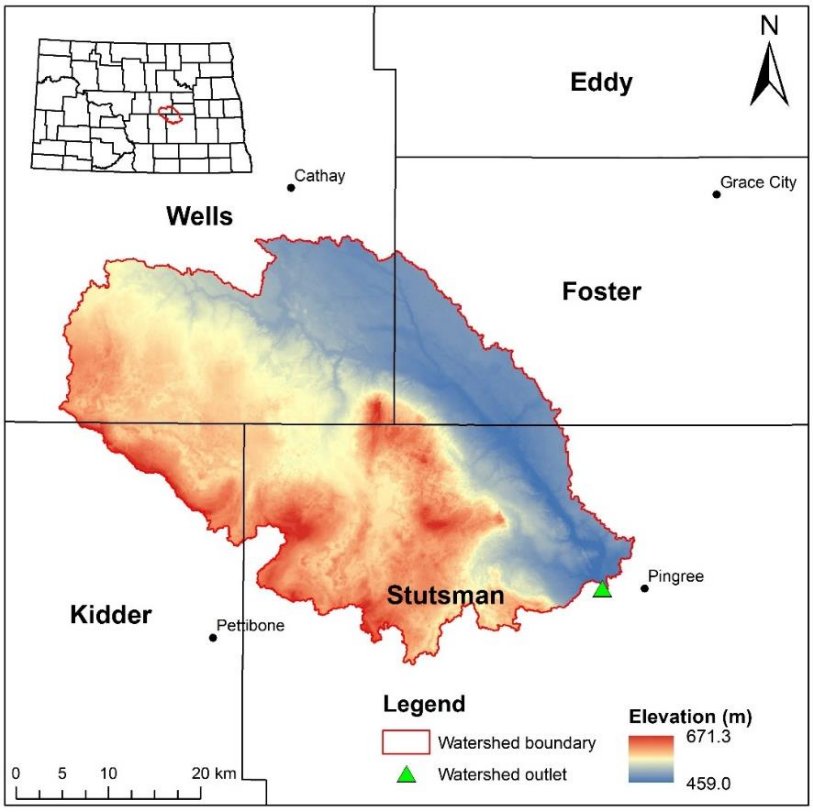

Figure 2.6. Geographical location of the Upper Pipestem Creek watershed.

The existence of artifacts in DEM is a critical issue in depression identification. Numerous insignificant depressions can be generated from the original DEM (Liu et al., 2017). In this study, the original DEM was pre-filled. Specifically, a series of incremental water depths were applied to fill depressions, and meanwhile the variations in topographic characteristics (e.g., MDS, MPA, and number of depressions) with the filling depths were analyzed, from which a filling threshold was identified to ensure that the artifacts were effectively removed without significantly changing the topographic characteristics and hydrologic connectivity of the study area.

2.4. Results and Discussions

2.4.1. Watershed Delineation and Topographic Analysis

Figures 2.7a and 2.7b respectively show the surface delineation results from Arc Hydro and HUD-DC based on the original DEM of the Upper Pipestem Creek watershed. For Arc Hydro, because channels were not considered in the 'Depression Evaluation' tool, only depressions and their associated contributing areas (CAs) were identified for the watershed (Figure 2.7a). Compared with Arc Hydro, HUD-DC extracted the channel drainage network of the watershed from the DEM (Figure 2.7b), identified CAs for all depressions and channels, and calculated the connectivity between HUs.

It can be observed from the delineation results that depressions dominate the study area, and they divide the entire watershed into numerous relatively independent HUs, which causes hydrologic disconnectivity. The depressions delineated by both methods have a similar distribution: numerous small depressions are scattered across the watershed, and large depressions are mainly located in the southwest of the study area (Figure 2.7). The channels identified by HUD-DC are mainly located in the middle of the watershed, forming a drainage network that connect different depressions. Specifically, 17,827 depressions were identified by HUD-DC. The MDS and MPA of the entire watershed are 404.33×10^6 m^3 and 292.04 km^2, respectively (Table 2.1). Note that the numbers of depressions and the values of MPA from HUD-DC and Arc Hydro are different (Table 2.1). This can be attributed to the difference in the definition of depressions in both methods. In Arc Hydro, each filled area is defined as one depression, and depression thresholds are not considered. In HUD-DC, however, depression thresholds are determined for all filled areas. If two filled areas share the same thresholds, they are combined, forming one depression. Therefore, the number of depressions calculated by

HUD-DC is smaller than that from Arc Hydro. In addition, the MPA calculated by HUD-DC is the summation of all filled areas and threshold areas. Consequently, the MPA obtained by HUD-DC is larger than that by Arc Hydro.

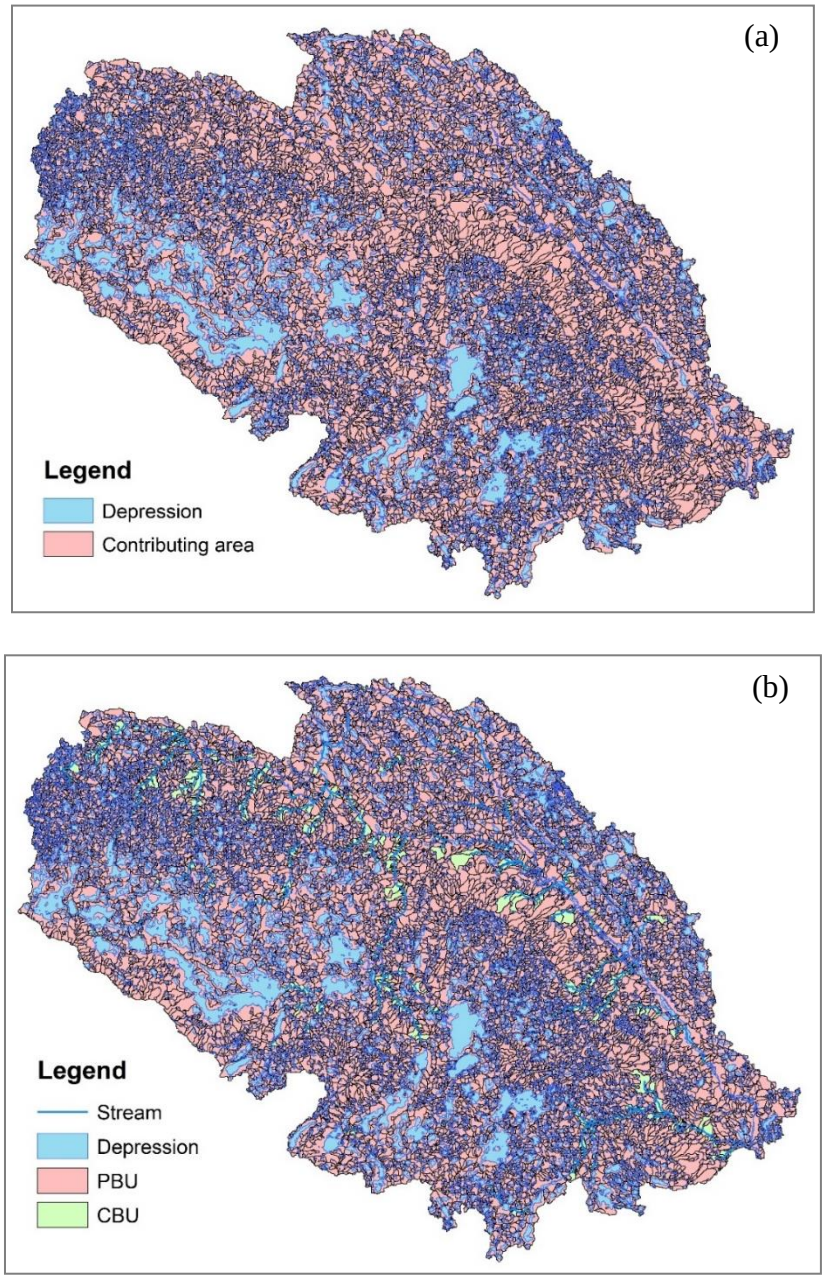

Figure 2.7. Surface delineation results of (a) Arc Hydro; and (b) HUD-DC. (PBU: puddle-based unit; CBU: channel-based unit).

Table 2.1. Comparison of the delineation results from Arc Hydro and HUD-DC.

	Number of depressions	MDS	MPA	PBU or DCA	
		(10^6 m^3)	(km^2)	(km^2)	(%)
Arc Hydro	18190	404.33	267.47	1668.12	100.00
HUD-DC	17827	404.33	292.04	1597.22	95.19

Note: MDS: maximum depression storage; MPA: maximum ponding area; PBU: puddle-based unit in HUD-DC; DCA: depression contributing area in Arc Hydro.

2.4.2. Identification of Filling Threshold for Removing Artifacts

As aforementioned, numerous small depressions, including artifacts were identified in the delineation process. To identify the filling threshold for removing those artifacts, the original DEM was pre-filled gradually with a set of incremental water depths and the variations in topographic characteristics (e.g., MDS, MPA, number of depressions) were examined under different filling conditions. Figure 2.8 shows the variations of the normalized maximum depression storage (NMDS), normalized maximum ponding area (NMPA), and normalized number of depressions (NDN) with the increase of the filling depth. The NMDS, NMPA, and NDN in a filling condition are defined as the ratios of the MDS, the MPA, and the number of depressions under such a filling condition to their corresponding values under the unfilled condition. An overall decreasing pattern can be observed for the three dimensionless topographic parameters (Figure 2.8). NDN exhibits the steepest decrease, while NMPA and NMDS decrease gradually with an increase of the filling depth (Figure 2.8). From Figure 2.8, four stages can be identified in the filling process: (1) removal of the artifacts (filling depth = 0-0.1 m), (2) filling small depressions (filling depth = 0.1-1.0 m), (3) filling medium depressions (filling depth = 1-5 m), and (4) filling large depressions (filling depth = 5-13 m). In the first stage, NMDS and NMPA decrease 0.007 and 0.178, respectively (Figure 2.8). However, NDN decrease 0.645, indicating that the depressions filled during this stage are mainly extremely small depressions

that almost have no storage capacities. Thus, these depressions can be considered as artifacts and thus 0.1 m can be used as the filling threshold to control most artifacts for this study area. During the second stage, the decreasing rates of NMPA and NDN gradually become smaller. These phenomena are due to the filling of small depressions, which are the major depressions in quantity, but have limited storages and areas in the watershed. The medium depressions are fully filled in the third stage. During this period, NMDS decrease from 0.904 to 0.298 with a relatively stable rate, but NMPA and NDN still show a decreasing trend (Figure 2.8). In general, the decreasing rates of NMPA and NMDS are higher than that of NDN, which indicates that the medium depressions have relatively larger storages and areas, but their number is limited. When the filling depth reaches 5 m, NDN equals 0.002 (Figure 2.8), implying that only a few large depressions are not fully filled in the study area at the fourth stage. Because the depressions with substantial storages and areas are fully filled, hierarchical drops of NMDS and NMPA can be observed during the filling process in this stage. According to the depression characteristics in the four stages, the small depressions and medium depressions are the dominant depressions that influence the variations of hydrologic connectivity in the study area. Additionally, since the large depressions require large amounts of runoff water to reach a fully-filled condition, they can be considered as ‘dead zone’ in the hydrologic connectivity analyses and hydrologic simulations.

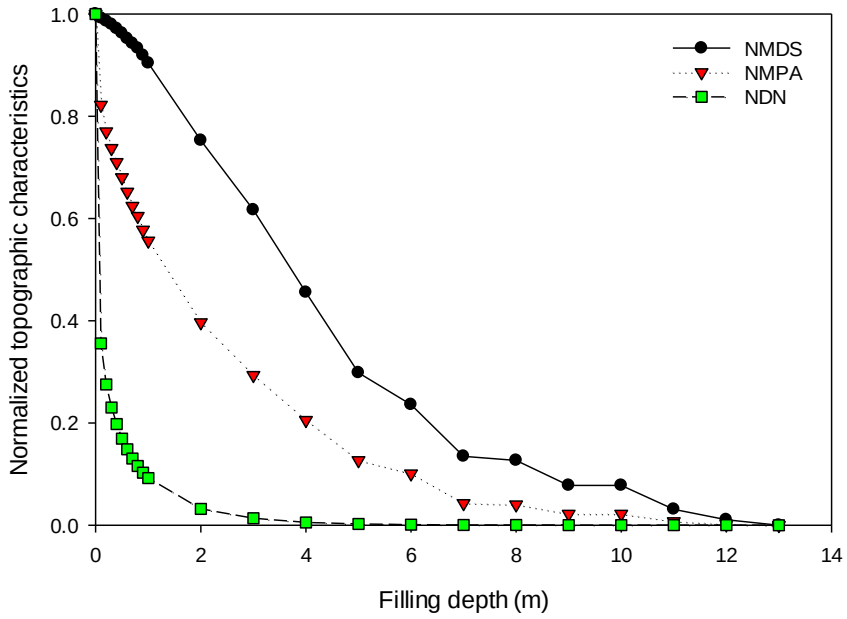

Figure 2.8. Variations of topographic characteristics with different filling depths. (NMDS: normalized maximum depression storage; NMPA: normalized maximum ponding area; NDN: normalized number of depressions).

Figure 2.9 shows the spatial distributions of depressions and HUs and the variations of hydrologic connectivity with an increase of filling depths. Compared with the unfilled condition (Figure 2.7b), when depressions were filled with a water depth of 0.1 m, more CBUs were developed in the middle of the watershed, but the hydrologic connectivity was still not well developed due to the existence of small depressions (Figure 2.9a). In this condition, the percentages of PBUs and CBUs for the entire area were 86.90% and 13.10% (Table 2.2), respectively, indicating that depressions still dominated the study area. When filling depth reached 1 m, both PBUs and CBUs accounted for almost half of the total watershed area (Table 2.2) and a relatively complete channel network emerged in the northeast of the watershed (Figure 2.9b). However, because two large PBUs (i.e., the PBUs in the rectangle areas in Figure. 2.9b) broke the connectivity between CBUs, the CA of the watershed outlet was still limited. This phenomenon highlights the important impact of the distribution of depressions on hydrologic

connectivity. When depressions were filled by a 5-m depth, CBUs dominated the study area and accounted for 90.30% of the entire watershed area. Figure 2.9c illustrates that almost the entire watershed has a well-developed connection to its associated outlet, except for several PBUs in the southwest and south of the watershed.

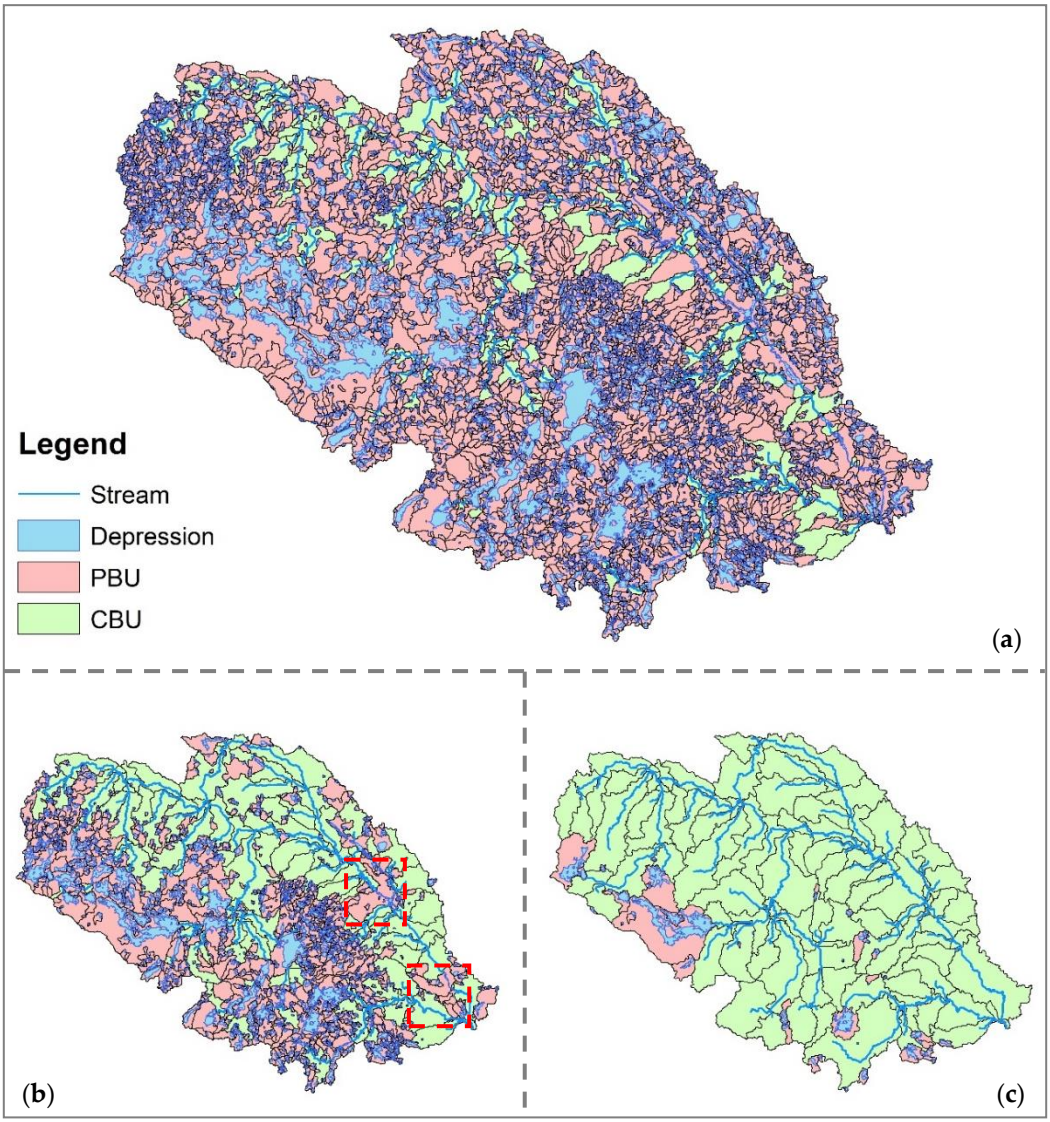

Figure 2.9. Spatial distributions of depressions and hydrologic units with the original DEM filled by a depth of (a) 0.1 m; (b) 1 m; and (c) 5 m. (PBU: puddle-based unit; CBU: channel-based unit; rectangle frames: PBUs that break the connectivity of CBUs).

Table 2.2. Topographic characteristics of the Upper Pipestem Creek watershed with the original DEM filled by a depth of 0.1 m, 1.0 m, and 5.0 m.

Filling depth	**MDS**	**MPA**	**PBU**		**CBU**	
(m)	(10^6 m^3)	(km^2)	(km^2)	(%)	(km^2)	(%)
0.1	401.19	240.09	1449.51	86.90	218.61	13.10
1.0	365.55	162.47	912.26	54.69	755.86	45.31
5.0	120.56	36.97	161.82	9.70	1506.30	90.30

Note: MDS: maximum depression storage; MPA: maximum ponding area; PBU: puddle-based unit; CBU: channel-based unit

2.5. Conclusions

In this study, HUD-DC was developed to investigate hydrologic connectivity in depression dominated areas (e.g., PPR) and provide detailed topographic characteristics for hydrologic models. To test the performance of HUD-DC in surface delineation, it was applied to the Upper Pipestem Creek watershed in North Dakota and compared with the 'Depression Evaluation' function in Arc Hydro. The topographic characteristics of the study area under the unfilled condition were analyzed. Particularly, HUD-DC was utilized to evaluate the changes in topographic features under different filling conditions, which enabled to identify the filling threshold to effectively remove artifacts in the DEM.

In the comparison with Arc Hydro, HUD-DC yielded similar results, demonstrating its accuracy in surface delineation and identification of depressions. The differences between the two methods were mainly associated with the definition of depressions and the depression searching procedure. Numerous depressions were scattered across the study area and the percentage of PBUs was 95.19%, which emphasized the significance of depressions in hydrologic connectivity in this depression-dominated watershed. In the analyses of topographic characteristics for various filling depths, four filling stages were identified based on the variation

trends of NMDS, NMPA, and NDN, and dynamic variations of hydrologic connectivity in the study area were observed. For the selected watershed, a depth of 0.1 m was selected as the filling threshold that can be used to control or remove most artifacts in the DEM. Although HUD-DC has been successfully applied to the Upper Pipestem Creek watershed for surface delineation, more tests would be helpful to improve its efficiency and demonstrate its applicability especially for large-scale watersheds.

2.6. References

Arnold, N., 2010. A new approach for dealing with depressions in digital elevation models when calculating flow accumulation values. Prog. Phys. Geogr., 34, 781-809.

Chu, X., Zhang, J., Chi, Y., Yang, J., 2010. An improved method for watershed delineation and computation of surface depression storage. In Watershed Management 2010: Innovations in Watershed Management Under Land Use and Climate Change, Proc. of the 2010 Watershed Management Conf., 1113-1122. K. W. Potter and D. K. Frevert, eds. Reston, Va.: ASCE.

Chu, X., Yang, J., Chi, Y., Zhang, J., 2013. Dynamic puddle delineation and modeling of puddle-to-puddle filling-spilling-merging-splitting overland flow processes. Water Resour. Res., 49, 3825-3829.

Chu, X., 2017. Delineation of pothole-dominated wetlands and modeling of their threshold behaviors. J. Hydrol. Eng., 22(1), 1-11, D5015003.

Garbrecht, J., Martz, L. W, 1997. TOPAZ: An Automated Digital Landscape Analysis Tool for Topographic Evaluation, Drainage Identification, Watershed Segmentation and Subcatchment Parameterization: TOPAZ User Manual, Grazinglands Research Laboratory, USDA Agricultural Research Services, El Reno, OK, USA.

Grimm, K., Chu, X, 2018. Modeling of spatiotemporal variations in runoff contribution areas and analysis of hydrologic connectivity. Land Degrad. Dev., 29, 2629-2643.

Hay, L., Norton, P., Viger, R., Markstrom, S., Regan, R. S., Vanderhoof, M, 2018. Modeling surface-water depression storage in a Prairie Depression Region. Hydrol. Processes, 32, 462-479.

Huang, P. C., Lee, K. T, 2015. A simple depression-filling method for raster and irregular elevation datasets. J. Earth Syst. Sci., 124, 1653-1665.

Jasiewicz, J., Metz, M, 2011. A new GRASS GIS toolkit for Hortonian analysis of drainage networks. Comput. Geosci., 37, 1162-1173.

Jenson, S. K., Domingue, J. O, 1988. Extracting topographic structure from digital elevation data for geographic information system analysis. Photogramm. Eng. Remote Sensing, 54, 1593-1600.

Liu, X., Wang, N., Shao, J., Chu, X, 2017. An automated processing algorithm for flat areas resulting from DEM filling and interpolation. ISPRS Int. J. Geo-Inf., 6, 376.

Maidment, D.R, 2002. ArcHydro: GIS for Water Resources. ESRI Press, Redlands, CA, USA.

Martínez-Casasnovas, J. A., Stuiver, H. J, 1998. Automated delineation of drainage networks and elementary catchments from digital elevation models. Int. J. Appl. Earth Obs. Geoinf., 3, 198-208.

Martz, L. W., Garbrecht, J, 1998. The treatment of flat areas and depressions in automated drainage analysis of raster digital elevation models. Hydrol. Processes, 12, 843-855.

McCauley, L. A., Anteau, M. J., 2014. Generating nested wetland catchments with readily-available digital elevation data may improve evaluations of land-use change on wetlands. Wetlands, 34, 1123-1132.

McCormack, J. E., Gahegan, M. N., Roberts, S. A., Hogg, J., Hoyle, B. S, 1993. Feature-based derivation of drainage networks. Int. J. Geogr. Inf. Sci., 7, 263-279.

O'Callaghan, J. F., Mark, D. M, 1984. The extraction of drainage networks from digital elevation data. Comput.Gr.Image Process., 28, 323-344.

Rieger, W, 1993. Automated river line and catchment area extraction from dem data. Int. Arch. Photogramm. Remote Sens., 29, 642-642.

Shaw, D. A., Pietroniro, A., Martz, L. W, 2013. Topographic analysis for the prairie pothole region of Western Canada. Hydrol. Processes, 27, 3105-3114.

Soille, P, 2004. Optimal removal of spurious pits in grid digital elevation models. Water Resour. Res., 40, W12509.

Tarboton, D. G., Bras, R. L., Rodriguez-Iturbe, I, 1991. On the extraction of channel networks from digital elevation data. Hydrol. Processes, 5, 81-100.

Tahmasebi Nasab, M., Singh, V., Chu, X, 2017a. SWAT modeling for depression-dominated areas: how do depressions manipulate hydrologic modeling? Water, 9, 58.

Tahmasebi Nasab, M., Zhang, J., Chu, X, 2017b. A new depression-dominated delineation (D-cubed) method for improved watershed modeling. Hydrol. Processes, 31, 3364-3378.

Temme, A. J., Schoorl, J. M., Veldkamp, A, 2006. Algorithm for dealing with depressions in dynamic landscape evolution models. Comput. Geosci., 32, 452-461.

Vanderhoof, M. K., Alexander, L. C., Todd, M. J, 2016. Temporal and spatial patterns of wetland extent influence variability of surface water connectivity in the Prairie Pothole Region, United States. Landsc. Ecol., 31, 805-824.

Wang, N., Zhang, X., Chu, X, 2019. New model for simulating hydrologic processes under influence of surface depressions. J. Hydrol. Eng., 24(5), 1-13, 04019008.

Yang, J., Chu, X, 2015. A new modeling approach for simulating microtopography-dominated, discontinuous overland flow on infiltrating surfaces. Adv. Water Resour., 78, 80-93.

3. SIMULATION OF HYDROLOGIC PROCESSES UNDER INFLUENCE OF SURFACE DEPRESSIONS

3.1. Abstract

Surface depressions significantly influence hydrologic processes. In traditional semi-distributed models, however, the entire area is connected to the outlet of a watershed and surface depressions are often lumped as a single depth to control runoff water release. As a result, hydrologic processes related to topographic characteristics of depressions cannot be directly simulated. The objective of this study is to quantify the impact of depressions on rainfall-runoff processes and the mechanism of dynamic water release from depressions. To achieve this objective, a new semi-distributed depression-oriented hydrologic model (HYDROL-D) is developed. Unlike the traditional methods, a unique modeling framework is proposed in HYDROL-D to facilitate separate modeling for the depressional area (DA) and non-depressional area (NDA) of each subbasin. A DA is further divided into time-varying contributing area (CA) and ponding area (PA). A depression-dominated delineation (D-cubed) algorithm is utilized to provide specific characteristics of surface depressions (e.g., maximum depression storage and maximum ponding area at various depression levels for all subbasins), which are processed to define the characteristic areas (i.e., NDA, DA, CA, and PA), varying functions of CA and PA, and the hierarchical control thresholds for water release in HYDROL-D. The model was applied to a site in North Dakota, compared with the widely-used hydrologic modeling system Hydrologic Engineering Center, Hydrologic Modeling System (HEC-HMS), and calibrated using the observed data. The results demonstrated that because of the discontinuity caused by depressions, only a small portion of the study area contributed water directly to the outlet. The new modeling framework was able to effectively account for the dynamic processes associated

with surface depressions. In addition, compared with the single threshold, multiple hierarchical control thresholds showed a better ability to reveal the mechanism of dynamic water release from depressions.

3.2. Introduction

Surface depressions are an important characteristic of topography that influences surface runoff generation, flow directions, and other hydrologic processes (Darboux et al., 2002). Digital elevation models (DEMs) have been widely used for determination of flow directions and accumulations, and delineation of watershed boundaries. However, traditionally, pre-processing of an original DEM is often performed to fill all depressions and create a depressionless and hydrologically well-connected watershed (e.g., Martz and Garbrecht, 1993). In the traditional hydrologic modeling methods, depression storage is generally included in initial abstractions or treated as a lumped depth, and the entire watershed area contributes runoff to this lumped depression storage (depth). Thus, new modeling approaches are required to explicitly account for surface depressions and their hierarchical and dynamic roles in surface runoff.

To simulate hydrologic processes under the influence of depressions, different studies have been conducted. For example, Kreymborg and Forman (2001) developed the pothole-river networked watershed model (PRINET) for hydrologic simulation in depression-dominated areas. A watershed was delineated by using ArcGIS and the Geospatial Hydrologic Modeling Extension (HEC-GeoHMS). Depressions in a subbasin were categorized as on-river or off-river lumped depressions. In a subbasin, surface runoff first drained to the off-river depression, and then to the on-river depression after the off-river depression was fully filled. Amoah et al. (2013) developed a lumped depressional storage capacity model and coupled it with DRAINMOD

(Skaggs et al., 2012) for watershed hydrologic modeling. In the lumped model, depression storage was determined by the difference between the original and fully-filled DEMs.

In most existing modeling studies, surface depression storage is conceptualized as a single depth (threshold) to control water release from depressions, and the entire area of a basin drains water to its associated outlet. Therefore, they cannot reveal the real dynamic hydrologic processes in a depression-dominated area. The Soil and Water Assessment Tool (SWAT) has been widely used for hydrologic modeling (Gassman et al., 2007). The pothole function in SWAT facilities simulation of the effects of potholes/depressions based on the user-specified area within a hydrologic response unit that drains water to the associated depressions (Neitsch et al., 2011). Tahmasebi Nasab et al. (2017a) coupled the puddle delineation (PD) algorithm (Chu et al., 2010) with SWAT to analyze the influence of depressions on hydrologic modeling in a depression-dominated watershed in the Prairie Pothole Region (PPR). Based on the DEM data, the PD program provided accurate depression storage and contributing area, which were further used in the pothole function in SWAT for depression-controlled hydrologic modeling. The model also used the maximum depression storage to control water release from depressions. In addition, the wetland function in SWAT also can be used to simulate the impact of depressions on hydrologic processes. Almendinger et al. (2014) utilized ArcGIS to identify the depression area and volume for two watersheds, and imported these data into the pothole and wetland tools of SWAT to quantify the impact of depressions on surface runoff and sediment delivery. Even though SWAT allows users to specify the percentage of an area that contributes water directly to its associated outlet, only one or two thresholds can be used to control water release (e.g., one threshold in the pothole function and two thresholds in the wetland function), and the

relationship of ponding area and depression storage is oversimplified (e.g., the shape of a pothole is defined as a cone in the pothole function).

Hay et al. (2018) applied the Precipitation-Runoff Modeling System (PRMS), a physical-process hydrologic modeling system (Markstrom et al. 2015), to simulate depression storage in the Upper Pipestem Creek watershed within the PPR of North Dakota. In their modeling, the watershed was delineated into a set of hydrologic response units, in each of which depressions were lumped and simulated with a single threshold to control water release. Chu et al. (2013) and Yang and Chu (2015) developed a physically-based, puddle-to-puddle (P2P) modeling system to simulate the P2P filling-spilling-merging-splitting processes. The P2P modeling system incorporates the PD algorithm to quantify depressions and their hierarchical relationships, and has been tested for laboratory-scale, field-scale, and watershed-scale land surfaces (Chu et al., 2010; Chu et al., 2013; Chu, 2017). Similarly, Shaw et al. (2013) proposed a conceptual model to simulate filling and spilling processes of depressions, and applied it to quantify dynamic contributing areas and depression storages in two small basins. Mekonnen et al. (2016) modified SWAT and developed the SWAT-Probability Distribution Landscape Distribution (SWAT-PDLD) model, which incorporated surface depression heterogeneity, in a lumped manner, in SWAT modeling by using a probability distribution function to account for the depressional effect and simulate water release from surface depressions. Tahmasebi Nasab et al. (2017b) improved the PD algorithm by developing the depression-dominated delineation (D-cubed) algorithm. In the new D-cubed algorithm, a surface is divided into a series of puddle-based units (PBUs) and channel-based units (CBUs), which form a hierarchical drainage system.

The objective of this study is to analyze the impact of depressions on rainfall-runoff processes and the mechanism of water release from depressions. A new depression-oriented

hydrologic model (HYDROL-D) is developed for simulating rainfall-runoff processes under the influence of surface depressions by incorporating a unique modeling framework with threshold control of ponded water release. The D-cubed algorithm is utilized to characterize surface depressions and the resulting topographic properties are further incorporated into hydrologic modeling. To demonstrate the performance of HYDROL-D and highlight its unique features in the simulation of hydrologic processes under influence of surface depressions, it is compared with the widely-used, semi-distributed HEC-HMS (USACE, 2016), which is based on a depressionless DEM created by the "fill sinks" pre-processing (different from HYDROL-D) and a subbasin-level modeling framework (similar to HYDROL-D). Furthermore, HYDROL-D is applied to a depression-dominated watershed in North Dakota.

3.3. Materials and Methods

3.3.1. Introduction to WMS and HEC-HMS

The Watershed Modeling System (WMS) is a comprehensive software package for watershed hydrologic and hydraulic modeling and analysis. It includes many widely-used models such as HEC-HMS, HEC-1, TR-20, TR-55, and National Flood Frequency Model (NFF) for hydrologic modeling. WMS also provides the ability to download various geographic information system (GIS) data and perform automatic watershed delineation. In addition, WMS incorporates many tools to calculate hydrologic parameters such as curve numbers (CNs), time of concentration, and storage coefficient. HEC-HMS (USACE, 2016) is a semi-distributed, subbasin-based modeling system for precipitation-runoff simulation. It incorporates a variety of loss, transform, baseflow, and flow routing methods. Since the release of the initial version of HEC-HMS, more functions and methods have been included in the latest HEC-HMS, which can be used for both event and continuous hydrologic modeling. In this study, WMS was utilized for

DEM-based watershed delineation and calculation of hydrologic parameters, while HEC-HMS was primarily used for comparison with the new HYDROL-D model.

3.3.2. Characterization of Surface Depressions

The D-cubed algorithm (Chu et al., 2010; Tahmasebi Nasab et al., 2017b) was utilized to identify depressions (including their centers and overflow thresholds) at different levels and compute depression characteristics for all identified depressions. First, the D-cubed program identifies puddle centers based on the DEM of a basin. Then, it searches for the corresponding puddle cells. Specifically, for each puddle center, its eight neighbor cells are added to a searching list, from which the cell with the lowest elevation is added to the puddle. The searching list is continuously updated by adding more puddle cells until an overflow threshold cell is identified. In this way, the algorithm delineates all first-level puddles. If two first-level puddles share a common threshold, they merge, forming a second-level puddle. The merging process continues until the highest-level puddles are identified. After puddle delineation, the D-cubed program defines PBUs and CBUs, and determines basin/subbasin boundaries. It provides the details on the puddles in each PBU, such as their maximum depression storages (MDSs) and maximum ponding areas (MPAs) at various levels, as well as the relationships of the PBUs and their puddles.

3.3.3. New HYDROL-D Model

HYDROL-D is a watershed-scale, semi-distributed rainfall-runoff model with a special capability of simulating the impact of surface depressions on hydrologic processes for a rainfall event. The Soil Conservation Service (SCS) curve-number method is employed to simulate surface runoff and infiltration; either SCS or Clark unit hydrograph (UH) technique can be utilized to transform rainfall excess into direct runoff at subbasin outlets; the recession method is

used to simulate baseflow; and the lag method is used for channel routing. Unlike other traditional models, HYDROL-D is featured with a unique modeling framework to facilitate the simulation of the influence of surface depressions (Figure 3.1).

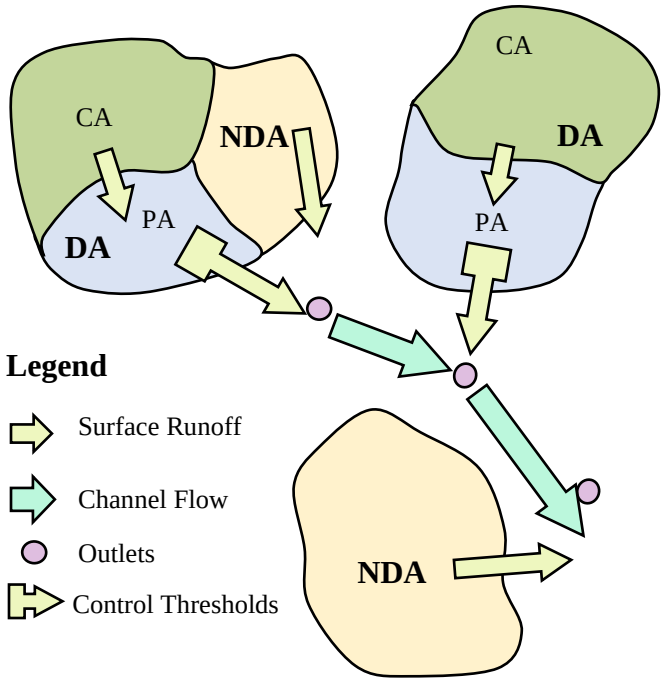

Figure 3.1. HYDROL-D modeling framework (NDA = non-depressional area; DA = depressional area; CA = contributing area; and PA = ponding area).

In HYDROL-D, a watershed is divided into many subbasins, and each subbasin is further divided into a non-depressional area (NDA) and a depressional area (DA). The DA and NDA represent, respectively, the total areas of the PBUs and CBUs in a subbasin. A DA includes two distinct sub-areas: contributing area (CA) and ponding area (PA) (Figure 3.1). Rainfall is the only water input of an NDA and a CA, while water inputs of a PA include rainfall and surface runoff from its corresponding CA. An NDA is subject to infiltration and makes runoff contribution directly to its associated subbasin outlet. In addition to infiltration, a CA drains surface runoff into its connected PA. The PA releases water to its associated subbasin outlet,

depending on its control thresholds. For event modeling, infiltration in a PA and evapotranspiration in all areas are not simulated in HYDROL-D. After flow routing for all subbasins, HYDROL-D implements channel routing and then determines the discharge for all outlets (Figure 3.1).

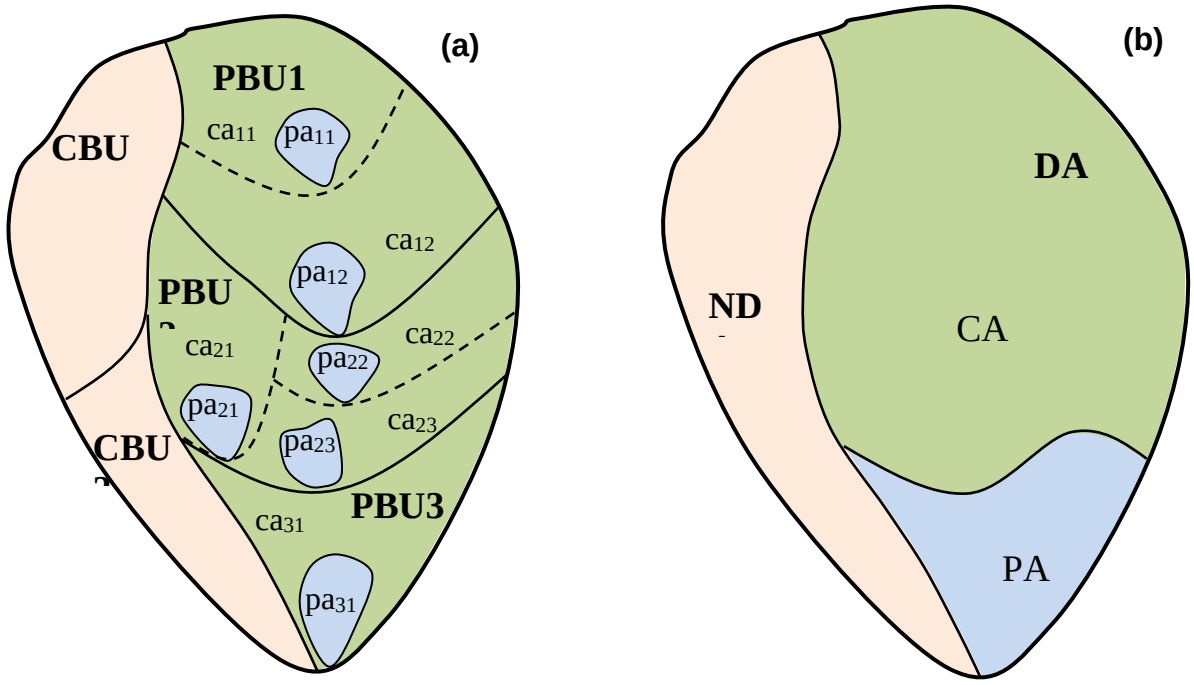

Figure 3.2. Conceptualization of a hypothetical subbasin at a ponding condition: (a) delineated subbasin by the D-cubed algorithm, (b) conceptualized subbasin (PBU = puddle-based unit; CBU = channel-based unit; NDA = non-depressional area in a subbasin; DA = depressional area in a subbasin; CA = contributing area in a subbasin; PA = ponding area in a subbasin; ca = contributing area in a PBU; and pa = ponding area in a PBU).

Figure 3.2 shows the methodology to generate the lumped feature areas (i.e., NDA, DA, CA, and PA) for a hypothetical subbasin. The subbasin was divided into two CBUs and three PBUs (Figure 3.2a). All CBUs and PBUs are lumped as an NDA and a DA, respectively (Figure 3.2b). The areas of the NDA and DA are respectively given by:

$$NDA = \sum_{i=1}^{n} CBU_i \tag{3.1}$$

$$DA = \sum_{j=1}^{m} PBU_j \tag{3.2}$$

where *NDA* is the non-depressional area in the subbasin, *DA* is the depressional area in the subbasin, CBU_i is channel-based unit *i*, PBU_j is puddle-based unit *j*, *n* is the number of CBUs, and *m* is the number of PBUs.

Note that the PA and CA of the DA are respectively the lumped areas of all ponding areas and contributing areas in the DA, which vary depending on the ponding conditions. Figure 3.2 only shows one ponding condition between the initial empty condition (i.e., no ponded water) and the fully-filled condition, and does not reflect the variability of the CA and PA. As shown in Figure 3.2, there are three PBUs (PBU1, PBU2, and PBU3), and they have different numbers of ponding areas and contributing areas. There are two ponding areas (pa_{11} and pa_{12}) in PBU1, three ponding areas (pa_{21}, pa_{22} and pa_{23}) in PBU2, and one ponding area (pa_{31}) in PBU3. The CA and PA in Figure 3.2b are the summations of all contributing areas and ponding areas in all PBUs in Figure 3.2a, respectively. The CA and PA of a subbasin at a ponding condition can be respectively expressed as:

$$CA = \sum_{i=1}^{n} \sum_{j=1}^{m_i} ca_{ij} = DA - PA \tag{3.3}$$

$$PA = \sum_{i=1}^{n} \sum_{j=1}^{m_i} pa_{ij} = DA - CA \tag{3.4}$$

where *CA* is the contributing area at a ponding condition in the subbasin, *PA* is the ponding area at a ponding condition in the subbasin, ca_{ij} is the contributing area of puddle *j* under a ponding condition in PBU *i*, pa_{ij} is the ponding area of puddle *j* at a ponding condition in PBU *i*, *n* is the number of PBUs, and m_i is the number of puddles in PBU *i*.

It is assumed in HYDROL-D that a PBU drains water to its associated subbasin outlet when its highest-level puddle is fully filled, and the same level puddles in a subbasin are fully filled at the same time. A control threshold (CT) is defined as the ponding condition of a subbasin when one or more PBUs are fully filled. A subbasin has at least one CT. PBUs may

have different numbers of puddle levels. In this study, the number of CTs in a subbasin is defined as the number of puddle levels of the PBU that has the highest puddle level. Figure 3.3 schematically shows the methodology used in HYDROL-D to define the hierarchical CTs of a hypothetical subbasin which consists of three PBUs. There are three, two, and one puddle levels in PBU1, PBU2, and PBU3, respectively (Plot 1 in each of Figures 3.3a-3.3c). Therefore, this hypothetical subbasin has three CTs. In Figure 3.3a, all the 1st level puddles are fully filled in each PBU, but only in PBU3 the highest-level puddle is fully filled. This ponding condition (Plot 2 in Figure 3.3a) is defined as control threshold 1 (CT1). In Figure 3.3b, the 1st level puddle in PBU3 and all the 2nd level puddles in PBU1 and PBU2 are fully filled. That is, the highest-level puddles in PBU2 and PBU3 are fully filled. This ponding condition (Plot 2 in Figure 3.3b) is defined as CT2. Similarly, CT3 is defined as the ponding condition which is shown in the Plot 2 of Figure 3.3c. TDS, TCA, and TPA are depression storage (DS), CA, and PA of a subbasin at a specific CT. The DS of a subbasin under a ponding condition can be calculated by:

$$DS = \sum_{i=1}^{n} \sum_{j=1}^{m_i} ds_{ij} \tag{3.5}$$

where *DS* is the depression storage at a ponding condition in the subbasin, ds_{ij} is the depression storage of puddle *j* at a ponding condition in PBU *i*, *n* is the number of PBUs, and m_i is the number of puddles in PBU *i*.

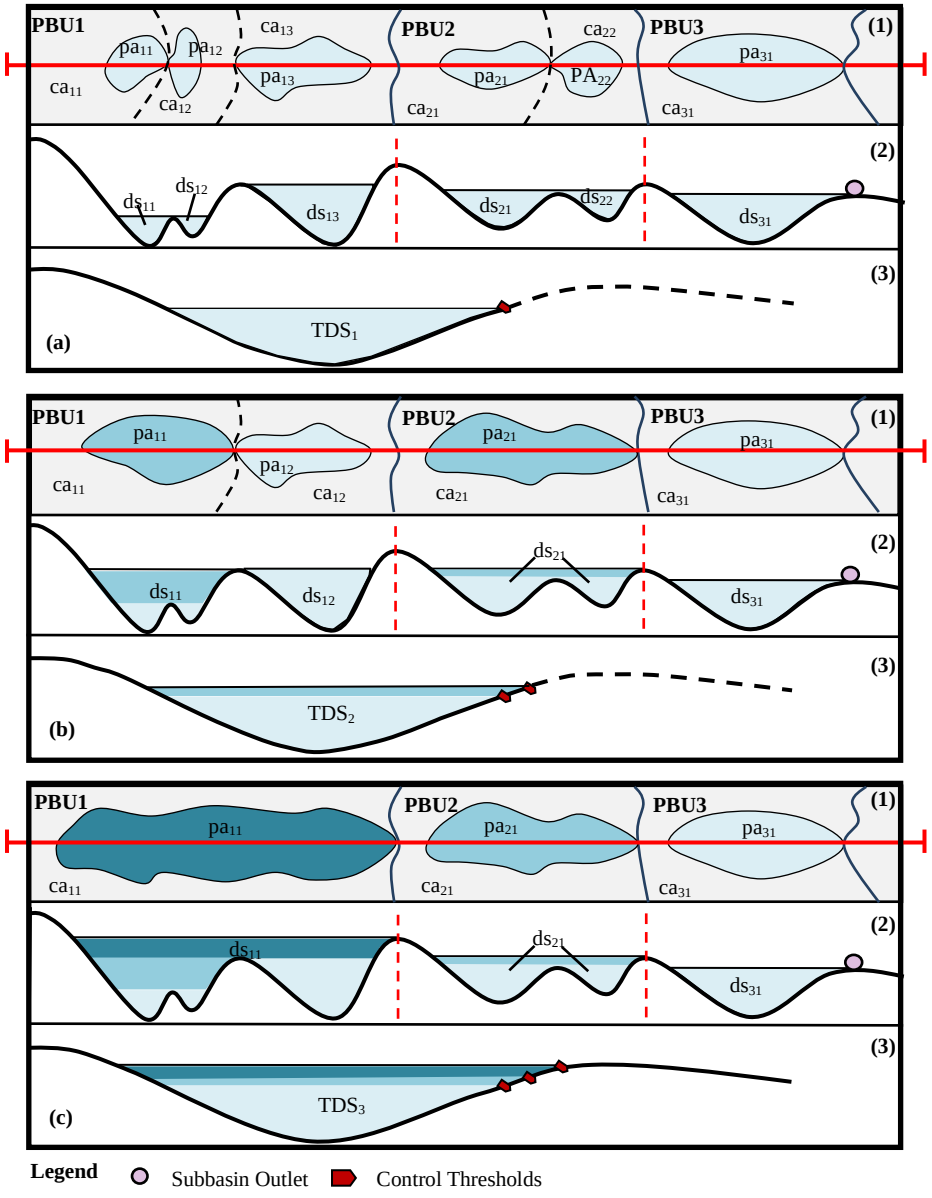

Figure 3.3. Methodology to define the control thresholds for a hypothetical subbasin: (a) Control threshold 1; (b) Control threshold 2; and (c) Control threshold 3. TDS = total depression storage in a subbasin at a CT; and ds = depression storage of a puddle in a PBU.

The amount of water released under different ponding conditions are determined based on the areas of the portions of the CA and PA that contribute water to their associated subbasin outlet at a ponding condition, which are respectively defined as active contributing area (ACA) and active ponding area (APA). In addition, the remaining portions of the CA and PA are respectively defined as inactive contributing area (ICA) and inactive ponding area (IPA). The

runoff water generated in the ACA and APA of a subbasin drains to the subbasin outlet, while the runoff water generated in the ICA and IPA fills depressions to increase the DS. Similarly, the active ponding area, active contributing area, inactive ponding area, and inactive contributing area in a PBU can be defined as apa, aca, ipa, and ica, respectively. The ACA, APA, ICA, and IPA in a subbasin at a ponding condition can be expressed as:

$$ACA = \sum_{i=1}^{n} \sum_{j=1}^{m_i} aca_{ij} \tag{3.6}$$

$$APA = \sum_{i=1}^{n} \sum_{j=1}^{m_i} apa_{ij} \tag{3.7}$$

$$ICA = CA - ACA \tag{3.8}$$

$$IPA = PA - APA \tag{3.9}$$

where *ACA* is the active contributing area in a subbasin at a ponding condition, *APA* is the active ponding area in a subbasin at a ponding condition, *ICA* is the inactive contributing area in a subbasin at a ponding condition, *IPA* is the inactive ponding area in a subbasin at a ponding condition, aca_{ij} is the active contributing area of puddle *j* in PBU *i* at a ponding condition, apa_{ij} is the active ponding area of puddle *j* in PBU *i* at a ponding condition, *n* is the number of PBUs, and m_i is the number of the highest-level puddles in PUB *i*.

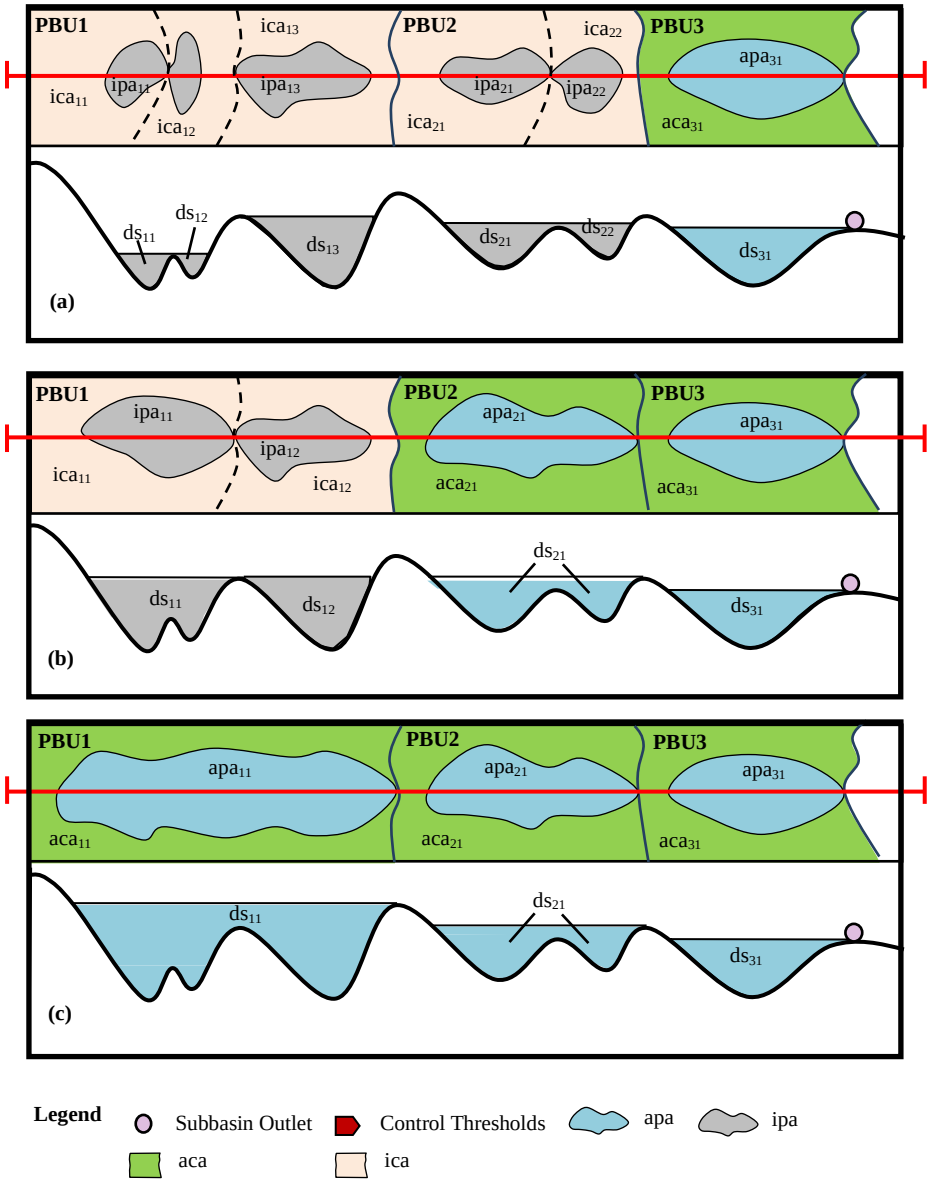

Figure 3.4. Methodology to define the areas of the portions of CA and PA that contribute water to their associated subbasin outlet for a hypothetical subbasin at control thresholds: (a) Control threshold 1; (b) Control threshold 2; and (c) Control threshold 3. aca = active contributing area of a puddle in a PBU; apa = active ponding area of a puddle in a PBU; ipa = inactive ponding area of a puddle in a PBU; and ica = inactive contributing area of a puddle in a PBU.

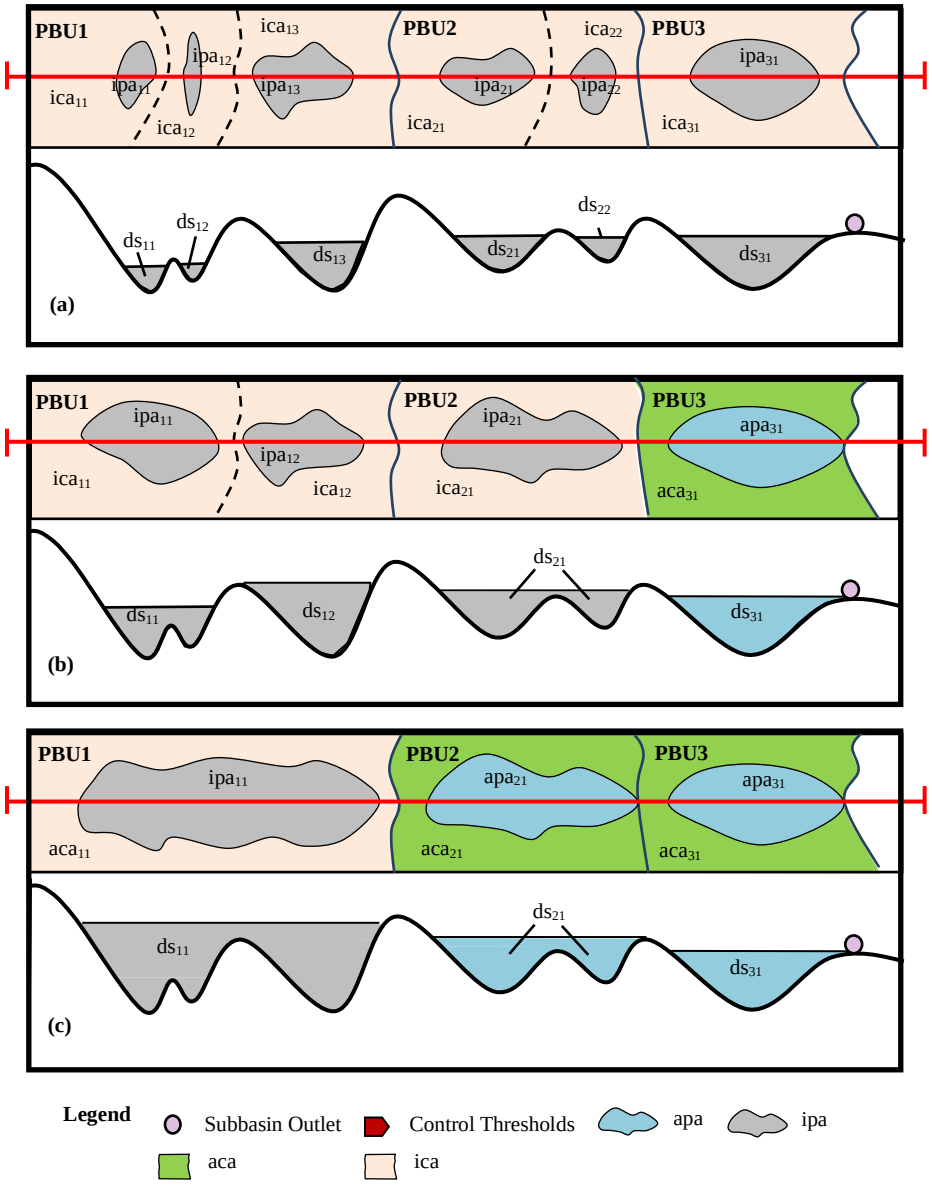

Figure 3.5. Ponding conditions between two control thresholds for a hypothetical subbasin: (a) ponding condition between an initial empty condition and CT1; (b) ponding condition between CT1 and CT2; and (c) ponding condition between CT2 and CT3.

The same subbasin used in Figure 3.3 is utilized in Figure 3.4 to schematically show how to determine the ACAs, APAs, ICAs, and IPAs at three CTs. For CT1, only the puddle in PBU3 is fully filled, and aca_{31} and apa_{31} drain water to their associated outlet (ACA = aca_{31}, APA = apa_{31}, Figure 3.4a). The ICA and IPA at CT1 can be calculated by Equations 3.8 and 3.9. The runoff water generated in PBU3 flows to the subbasin outlet at CT1. However, because the

highest-level puddles in PBU1 and PBU2 are not fully filled at CT1 (Figure 3.4a), the runoff water generated in PBU1 and PBU2 is still used to increase the DS (i.e., at the filling stage). The puddles in PBU2 and PBU3 are fully filled at CT2. Thus, aca_{21}, apa_{21}, aca_{31}, and aca_{31} contribute water to the subbasin outlet (ACA = aca_{21} + aca_{31}, APA = apa_{21} + apa_{31}, Figure 4b). The runoff water generated in PBU1 is used to increase the DS, instead of flowing to the subbasin outlet. Eventually, all puddles in all PBUs are fully filled at CT3, and the entire subbasin drains water to the subbasin outlet at CT3 (Figure 3.4c).

Note that Figure 3.4 only shows how to define the ACAs, APAs, ICAs, and IPAs in a subbasin at various CTs. Figure 3.5 displays the methodology used to define these parameters between two CTs. Between two CTs, the ACA and APA are constant, and are the same as their values at the preceding CT. The ICA and IPA given by Equations 3.8 and 3.9 are variable. Figure 3.5a shows a ponding condition between the initial empty condition and CT1. In this ponding condition, all puddles in all PBUs are not fully filled, the APA and ACA of the subbasin are zero (Figure 3.5a). The areas in the DA are IPA and ICA (i.e., IPA = PA, ICA = CA). The runoff water generated in the IPA and ICA is used to increase the DS. The PA increases with an increase in the DS. The variations of the DS and PA are based on a linear relationship between the TDSs and TPAs of the initial empty condition and CT1. Between CT1 and CT2 (Figure 3.5b), the APA and ACA are the same as their values at CT1 (Figure 3.4a). However, the IPA and ICA are different because of the varying PA. When the ponding condition is between CT2 and CT3 (Figure 3.5c), the APA and ACA are the same as their values at CT2 (Figure 3.4b). The IPA and ICA keep changing until the ponding condition reaches CT3. Given DS, the PA can be expressed as:

$$PA = (DA - TDS_i) \times \frac{TPA_j - TPA_i}{TDS_j - TDS_i} + TPA_i \quad (3.10)$$

where *PA* is the ponding area at a ponding condition in a subbasin, *DS* is the depression storage at a ponding condition in a subbasin, TPA_i is the ponding area at preceding CT *i*, TPA_j is the ponding area at following CT *j*, TDS_i is the depression storage at preceding CT *i*, and TDS_j is the depression storage at following CT *j*.

HYDROL-D consists of two nested loops: subbasin loop and time loop (Figure 3.6). The time loop is nested in the subbasin loop. That is, the time loop is performed for each subbasin. Surface runoff and infiltration in the NDA and DA of a subbasin are simulated for all time steps. Then, the DS and ponding condition are determined based on the simulated surface runoff in the DA. If the DS is smaller than the TDS at the 1st CT (TDS_1 in Figure 3.6), there is no outflow from the DA to its associated subbasin outlet. If the DS is greater than the TDS at the highest CT (TDS_h in Figure 3.6), all surface runoff generated in the DA flows to the subbasin outlet, and the DS equals the TDS_h. Otherwise, the quantity of the released water and the new DS are calculated. Then, based on the new DS, new CA and PA are determined (Figure 3.6). By combining the surface runoff from NDA and DA, the total discharge at a subbasin outlet at the current time step is obtained. After simulating the total discharge at the subbasin outlet for all time steps, the baseflow, water mass balance, and hydrograph of a subbasin are determined. After the simulation for all subbasins in the subbasin loop, flow routing is performed throughout the entire channelized drainage network based on the hydrographs of all subbasins (Figure 3.6). The input data of HYDROL-D include rainfall, watershed property parameters (e.g., CNs, time of concentrations, and percentages of NDAs, CAs, and PAs), baseflow parameters, lag times of all channels, depression characteristics (e.g., depression levels, DS-PA relationships), as well as the connections/relationships of all subbasins, outlets, and channels. HYDROL-D provides water

balance tables for all subbasins, hydrographs for all subbasins and outlets, as well as inflows and outflows of all channels.

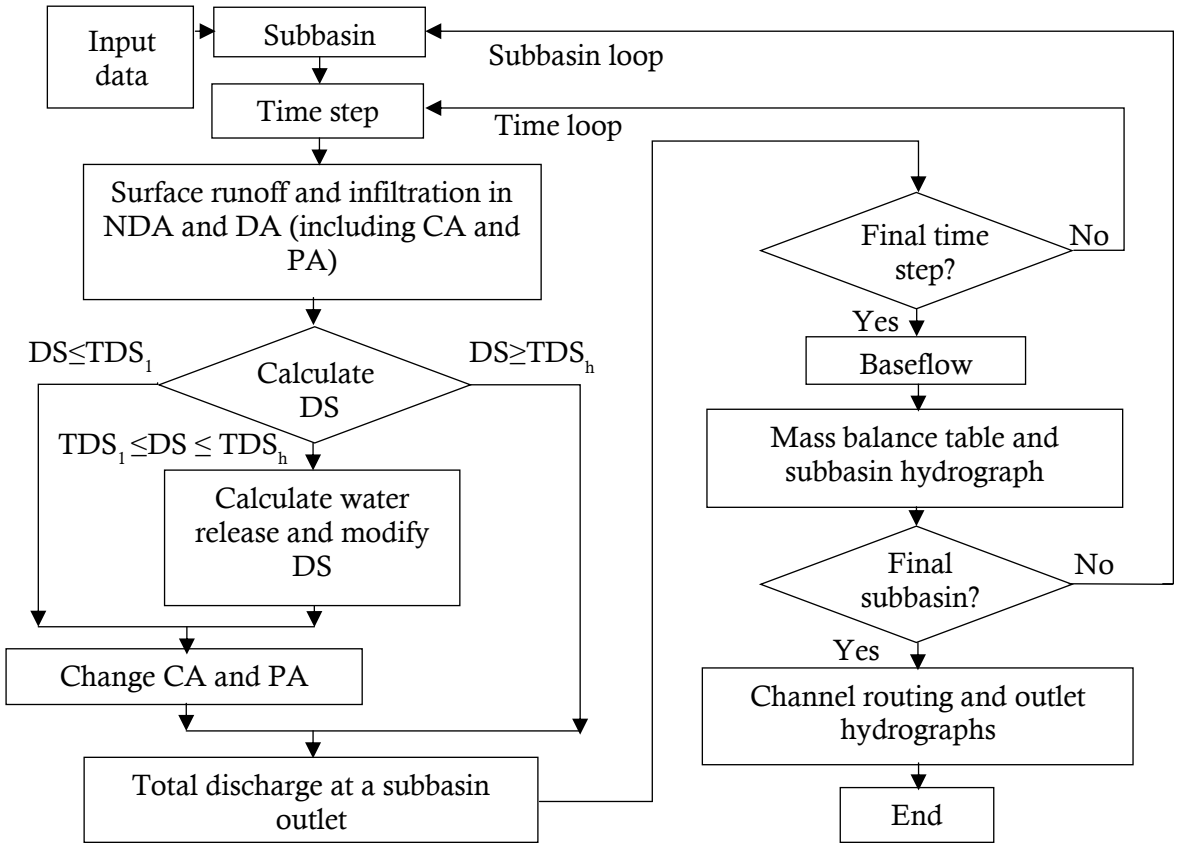

Figure. 3.6. Flowchart of HYDROL-D (NDA = non-depressional area; DA = depressional area; CA = contributing area in DA; PA = ponding area in DA; DS = depression storage; TDS1 = total depression storage at the first control threshold; and TDSh = total depression storage at the highest control threshold)

3.3.4. Study Area and Application

To test HYDROL-D and demonstrate its capability of quantifying the influence of depressions on hydrologic processes, a study site in the Middle Sheyenne River watershed in east central North Dakota was selected (Figure 3.7a). The Middle Sheyenne River watershed is part of the Red River basin and covers 5,314.9 km^2. The final outlet of the study area was located at the USGS 05057200 Baldhill Creek gaging station (latitude: 47^o 13’ 45’’ N; longitude: 98^o 07’ 28’’ W) in Barnes County. The gaging station drains an area of 1,790 km^2 (i.e., the area of the

selected watershed), with an elevation range from 402 m to 529 m. Baldhill Creek flows from northwest to southeast across the watershed.

For the comparison purpose, the same DEM, soil type, land use, and other data of the watershed were used in HEC-HMS and HYDROL-D. The 30-m DEM was downloaded from the USGS National Map Viewer (USGS 2017c). The 2011 National Land Cover Database (NLCD) land use (USGS 2017c) and State Soil Geographic Dataset (STATSGO) soil type data (USDA 2017) were used for computation of curve numbers under the average antecedent moisture condition for all subbasins. A precipitation station was set up in the east-central part of the study area (latitude: 47° 23' 24.97" N; longitude: 98° 19' 37.06" W) (Figure 3.7a) and 5-min rainfall data were recorded and utilized in this modeling study. The observed discharges at the Baldhill Creek gaging station were downloaded from the USGS National Water Information System (USGS 2017a).

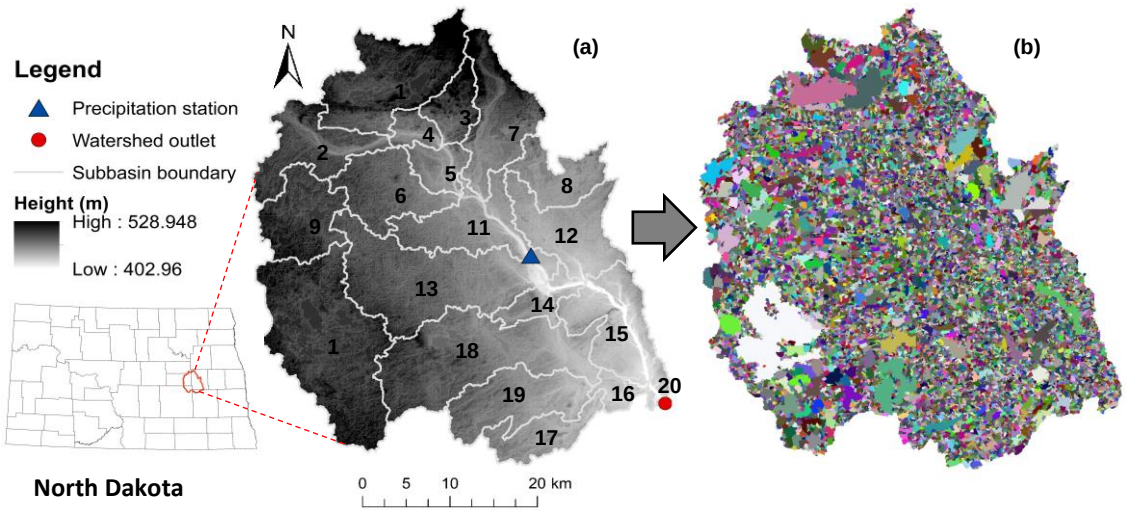

Figure 3.7. Watershed and delineation results: (a) location of the study area; and (b) delineated PUBs and CBUs.

3.3.5. Model Setup and Evaluation Methods

HYDROL-D was tested by following the procedures detailed in Figure 3.8, which included the modeling for a single subbasin under a design storm and a real application for the entire watershed under a real rainfall event. The real application involved comparisons of three models: M1 (HEC-HMS), M2 (HYDROL-D with a single CT), and M3 (HYDROL-D with multiple CTs). In this study, WMS was used to delineate subbasins and calculate hydrologic parameters (e.g., time of concentration and curve number) for both HEC-HMS and HYDROL-D models, ArcGIS and the D-cubed algorithm were used to process the GIS data, identify depressions and their contributing areas, and calculate topographic parameters. An Natural Resources Conservation Service (NRCS) 24-hr storm with a depth of 86.36 mm was used for the design storm modeling, while a real rainfall event from July 11, 2016, 18:50 to July 13, 2016, 09:40 recorded at the aforementioned precipitation station was selected for the real application. The observed discharge data for the same period were used to compare with the simulated values. The initial baseflow was determined based on the observed streamflow data.

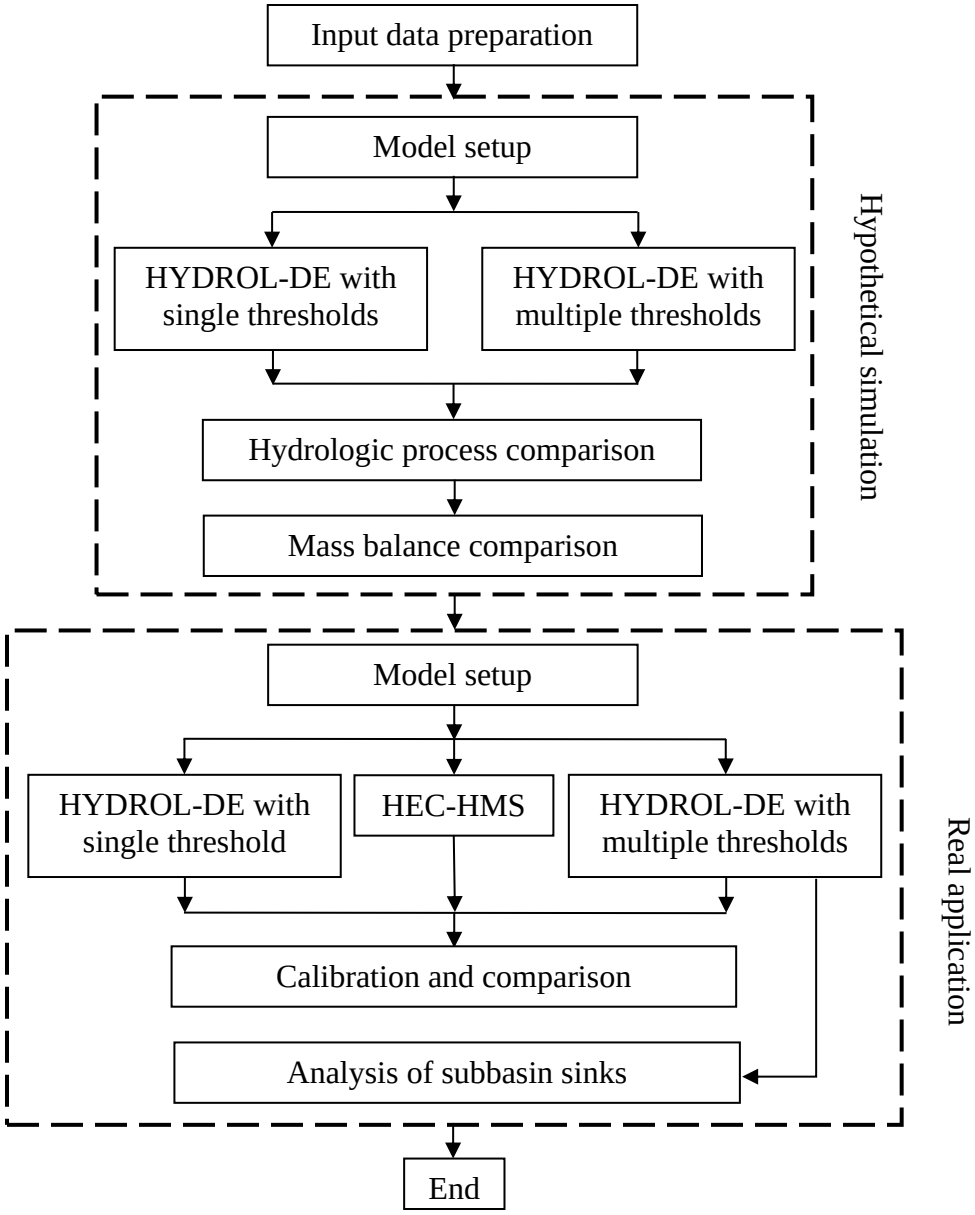

Figure 3.8. Procedures of the HYDROL-D testing.

The default initial abstraction ($I_a = 0.2S$) was used in M1 (HEC-HMS modeling). In addition, the impact of depressions was simulated by considering a non-contributing area for each subbasin. According to the USGS survey data (USGS 2017b), the contributing drainage area of the watershed is 909.09 km^2 (i.e., 50.80% of the entire drainage area of 1789.68 km^2). In this study, the fill function of ArcGIS was applied to fill the original DEM downloaded from the USGS National Map Viewer, which identified all depressions and their contributing area

(53.49% of the entire watershed) (Figure 3.9). The ArcGIS result is close to the USGS survey data. Thus, it was assumed that 46.51% of the watershed contributed runoff water to the watershed outlet in the HEC-HMS modeling (M1). The active contributing areas of all subbasins for M1 are shown in Table 3.1.

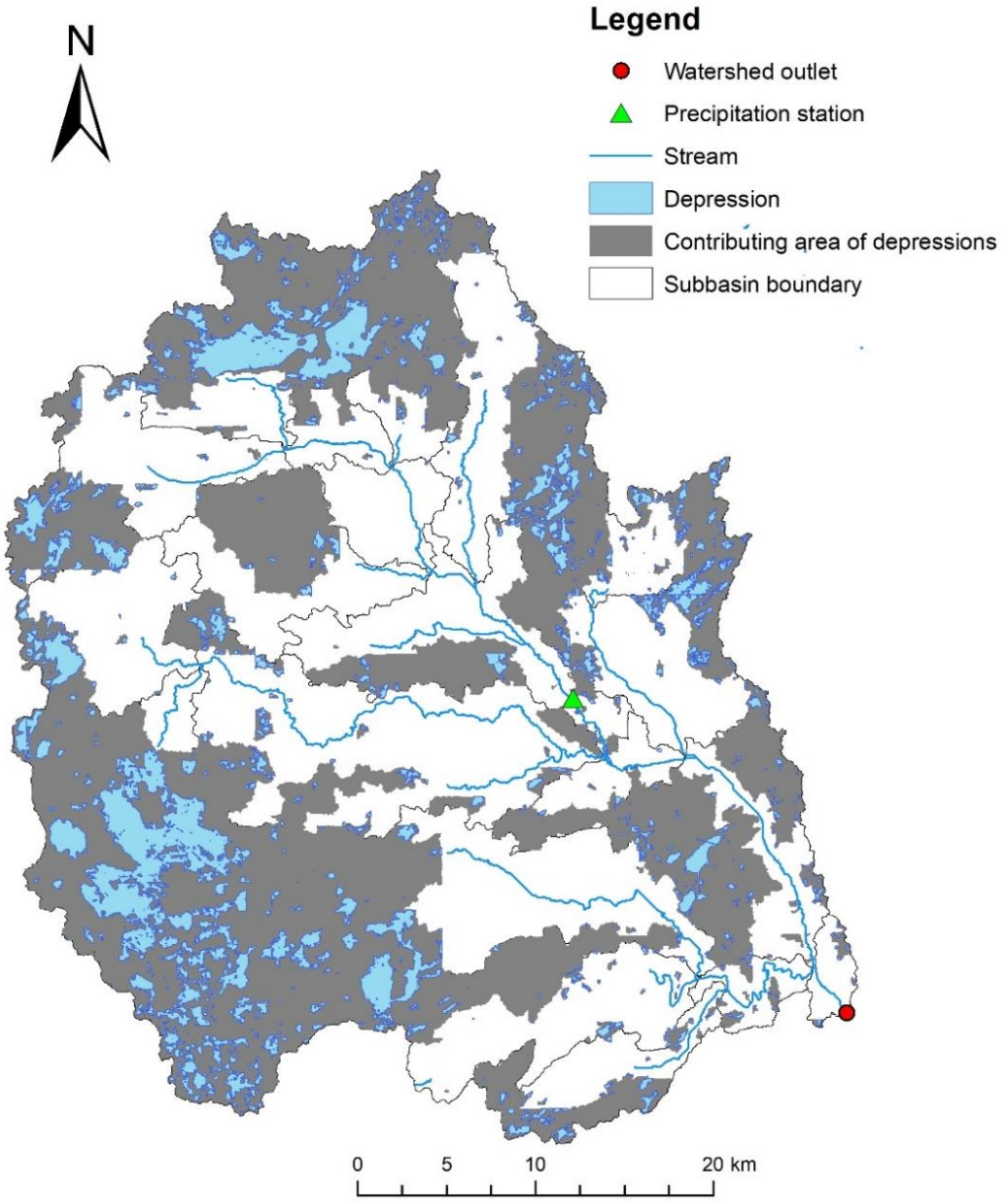

Figure 3.9. Depressions and their contributing areas in the watershed.

Table 3.1. Contributing drainage areas of all subbasins used in M1.

Subbasin	Area (km^2)	CDA (km^2)	CDA/Area (%)
1	139.63	21.44	15.35
2	84.44	53.92	63.86
3	38.37	12.44	32.43
4	21.41	16.92	79.04
5	32.43	32.33	99.71
6	82.71	41.11	49.70
7	99.37	56.63	56.98
8	55.79	17.49	31.34
9	81.22	53.39	65.73
10	224.51	11.96	5.33
11	96.02	63.38	66.00
12	90.09	48.54	53.88
13	183.39	125.14	68.24
14	32.63	18.92	57.97
15	93.88	30.82	32.82
16	19.76	14.23	72.02
17	50.33	25.60	50.85
18	190.70	85.58	44.88
19	92.38	60.29	65.26
20	11.82	10.31	87.26

Note: CDA = contributing drainage area; and M1 = HEC-HMS model.

For M2 and M3, the original unfilled DEM was used in the D-cubed algorithm to identify PBUs and CBUs. The topographic parameters from the D-cubed program included the NDA and DA of each subbasin, the TDS and TPA at different CTs, as well as ACA, APA, ICA, and IPA for each CT. The relationships between the TDSs and TPAs at all CTs were imported into the model to calculate variable CA and PA in each subbasin at all time steps. In addition, the ACAs and APAs were utilized to control water release from the associated depression storage. The single CT in M2 means that water is released from the PA of a subbasin only when the ponding condition reaches the highest CT, but the variations of CA and PA are still calculated based on the relationship between TDSs and TPAs at all CTs.

In the real application, the HYDROL-D model was calibrated by using the observed discharge data and the major calibrated parameters included the curve number and time of concentration of each subbasin. The Nash-Sutcliffe efficiency (NSE) coefficient (Nash & Sutcliffe, 1970) and the root-mean-square error (RMSE) were computed to quantify the goodness of fit. The NSE and RMSE can be respectively expressed as:

$$NSE = 1 - \frac{\sum_{i=1}^{T}(Q_{0,i} - Q_{s,i})^2}{\sum_{i=1}^{T}(Q_{0,i} - \overline{Q_0})^2} \tag{3.11}$$

$$RMSE = \sqrt{\frac{\sum_{i=1}^{T}(Q_{0,i} - Q_{s,i})^2}{T}} \tag{3.12}$$

where $Q_{o,i}$ is the observed discharge at time step i; $Q_{s,i}$ is the simulated discharge at time step i; $\overline{Q_0}$ is the mean observed discharge; and T is the total number of time steps.

3.4. Results and Discussions

3.4.1. Surface Topographic Characteristics

The selected watershed was divided into 20 subbasins, which were further divided into 6,031 PBUs and CBUs (Figure 3.7b). Table 3.2 lists the major topographic parameters of all subbasins computed by the D-cubed algorithm. The percentages of the NDAs range from 3.72% to 19.91%, indicating that only a limited area contributes surface runoff to each subbasin outlet directly. The values of TDS_h vary from 0.47×10^6 to 83.87×10^6 m^3 and the values of TPA at the highest CT (TPA_h) change from 1.21 km^2 to 89.71 km^2 (Table 3.2). Because of the high variations in topographic characteristics, there are no specific relationships between NDA, TDS_h, TPA_h, and the number of control thresholds (NCT). For example, subbasin 1 has the largest TDS_h (0.46 m), but its DA, TPA_h, and NCT are not the largest. Subbasins 8 and 10 have a similar DA (in percentage), but the NCT values for subbasins 8 and 10 are 136 and 527, respectively.

Table 3.2. Topographic parameters of all subbasins from the D-cubed algorithm.

Sub-basin	Area	NDA	NDA/ Area	DA	DA/A rea	TPA_h	TPA_h /Area	TDS_h		NCT
	(km^2)	(km^2)	(%)	(km^2)	(%)	(km^2)	(%)	(10^6 m^3)	(m)	
1	139.60	11.99	8.58	127.60	91.42	46.02	32.97	63.83	0.46	281
2	84.43	6.18	7.32	78.26	92.68	20.06	23.76	10.04	0.12	94
3	38.36	7.64	19.91	30.73	80.09	7.01	18.27	3.23	0.08	54
4	21.40	3.64	16.98	17.77	83.02	2.49	11.64	0.53	0.02	14
5	32.42	5.00	15.40	27.43	84.60	4.10	12.65	0.89	0.03	24
6	82.71	3.49	4.22	79.22	95.78	21.10	25.51	5.89	0.07	51
7	99.37	15.63	15.72	83.75	84.28	17.48	17.59	9.06	0.09	44
8	55.78	2.12	3.81	53.66	96.19	22.03	39.49	16.07	0.29	136
9	81.22	4.30	5.30	76.92	94.70	26.73	32.91	17.09	0.21	88
10	224.50	8.35	3.72	216.10	96.28	89.71	39.96	83.87	0.37	527
11	96.02	7.43	7.74	88.59	92.26	20.26	21.10	6.01	0.06	30
12	90.09	5.54	6.15	84.55	93.85	29.11	32.31	13.04	0.14	125
13	183.30	10.91	5.95	172.40	94.05	41.54	22.66	13.13	0.07	39
14	32.62	3.56	10.90	29.07	89.10	4.95	15.17	1.58	0.05	26
15	93.88	12.30	13.10	81.58	86.90	15.33	16.33	17.36	0.18	109
16	19.75	1.68	8.49	18.08	91.51	3.24	16.41	1.43	0.07	41
17	50.33	3.27	6.49	47.07	93.51	10.52	20.90	4.40	0.09	33
18	190.70	14.83	7.78	175.80	92.22	50.00	26.22	27.37	0.14	202
19	92.38	9.21	9.97	83.17	90.03	16.28	17.62	4.64	0.05	48
20	11.82	1.55	13.08	10.27	86.92	1.21	10.24	0.47	0.04	14

Note: NDA = non-depressional area; DA = depressional area; NCT = number of control thresholds; TPAh = total ponding area at the highest control threshold; and TDSh = total depression storage at the highest control threshold.

Figure 3.10 shows the relationships between the normalized ponding area (NPA), (i.e., PA/TPA_h, and the normalized depression storage (NDS), (i.e., DS/TDS_h) for all subbasins. As aforementioned, HYDROL-D utilizes these relationships to control the variations of the PA and DS in each subbasin. Although the functional relationships vary for different subbasins due to

the variations in surface topography, they follow an increasing trend. Since small depressions are filled quickly in the beginning of a simulation and some of them are combined, forming larger higher-level puddles, the PA increases faster than the DS. As more higher-level puddles are generated, and it takes much longer time to fully fill such larger puddles, the DS increases faster than the PA.

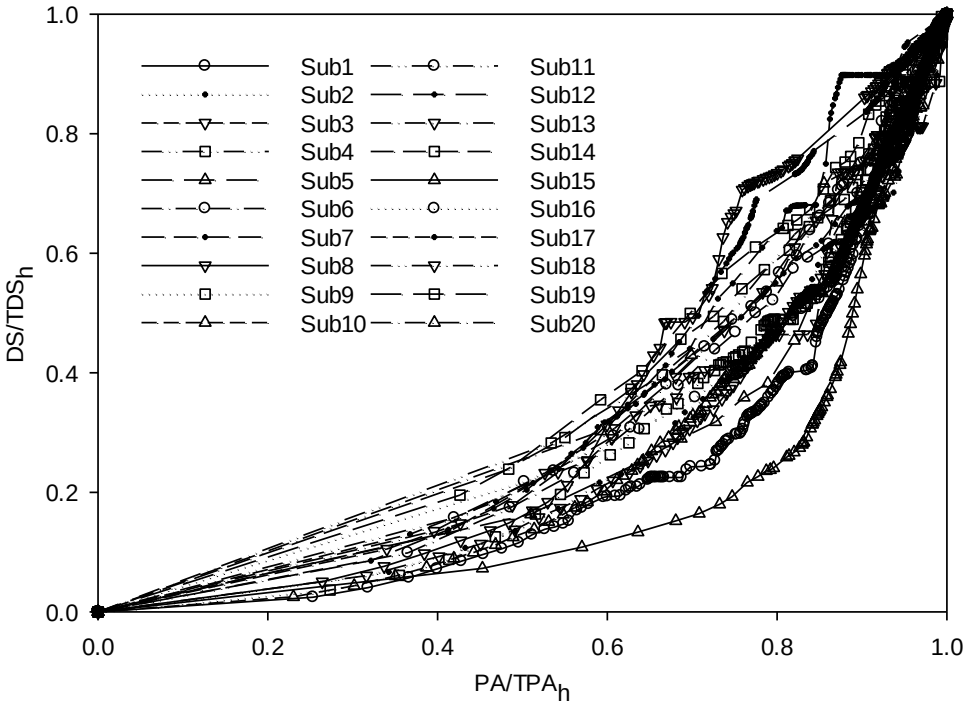

Figure 3.10. Relationships between the normalized ponding area ($PA=TPA_h$) and the normalized depression storage ($DS=TDS_h$) for all subbasins. TPA_h = total ponding area at the highest control threshold.

3.4.2. Model Testing for Design Storm: Single vs. Multiple Control Thresholds

The performance of HYDROL-D was evaluated by examining the variations in the DS and PA simulated by M2 and M3. Simulations of M2 and M3 for the selected 24-hour design storm were conducted for Subbasin 4. The water balance tables of Subbasin 4 for M2 and M3 are shown in Table 3.3. As shown in the water balance tables, infiltration accounted for almost half of the rainfall (50.73% in M2 and 50.89% in M3). Due to the use of multiple CTs in M3, more

water was released from the DA (19.09%), while the DA outflow in M2 was only 12.60%. M2 yielded a greater DA depression storage (28.72%). These results can be mainly attributed to the difference between the single and multiple CTs in M2 and M3. For the NDA, there is no difference in the water balance between M2 and M3.

Table 3.3. Water balance tables of Subbasin 4 simulated by M2 and M3 for the 24-hour design storm.

Type	Water balance term	M2		M3	
		Amount	Percentage	Amount	Percentage
		(10^5 m^3)	(%)	(10^5 m^3)	(%)
Source	Rainfall	18.49	100.00	18.49	100.00
	Total	**18.49**	**100.00**	**18.49**	**100.00**
Losses	NDA outflow	1.47	7.95	1.47	7.95
	NDA infiltration	1.67	9.03	1.67	9.03
	DA outflow	2.33	12.60	3.53	19.09
	DA infiltration	7.71	41.70	7.74	41.86
	DA depression storage	5.31	28.72	4.08	22.07
	Total	**18.49**	**100.00**	**18.49**	**100.00**

Note: NDA = non-depressional area; DA = depressional area; M2 = HYDROL-D with a single control threshold; and M3 = HYDROL-D with multiple control thresholds.

The variations in the PA and CA of a subbasin simulated by HYDROL-D influenced the modeling of hydrologic processes. Figure 3.11 shows the variations of the NPA and NDS simulated by M2 and M3 for the design storm. The squares on Figure 3.11 indicate the CTs (CT1 – CT14) for water release in HYDROL-D. Since evapotranspiration, lateral flow, and depression percolation were not considered for the PA in the event modeling, the PA increased with DS during the simulation period and reached the maximum at the final time step in both M2 (Figure 3.11a) and M3 (Figure 3.11b). Before reaching CT1 (NDS = 0.28), M2 and M3 exhibited similar

variations in NPA and NDS. Afterwards, however, the variation of the NPA with NDS simulated by M3 was smaller than that of M2, which can be attributed to the release of runoff water in M3. As a result, M2 reached the highest CT (i.e., CT = CT14) and fully-filled condition (i.e., PA = TPA_h, and DS = TDS_h) at the final time step (Figure 3.11a), but the depression filling process in M3 stopped between CT6 and CT7 (Figure 3.11b).

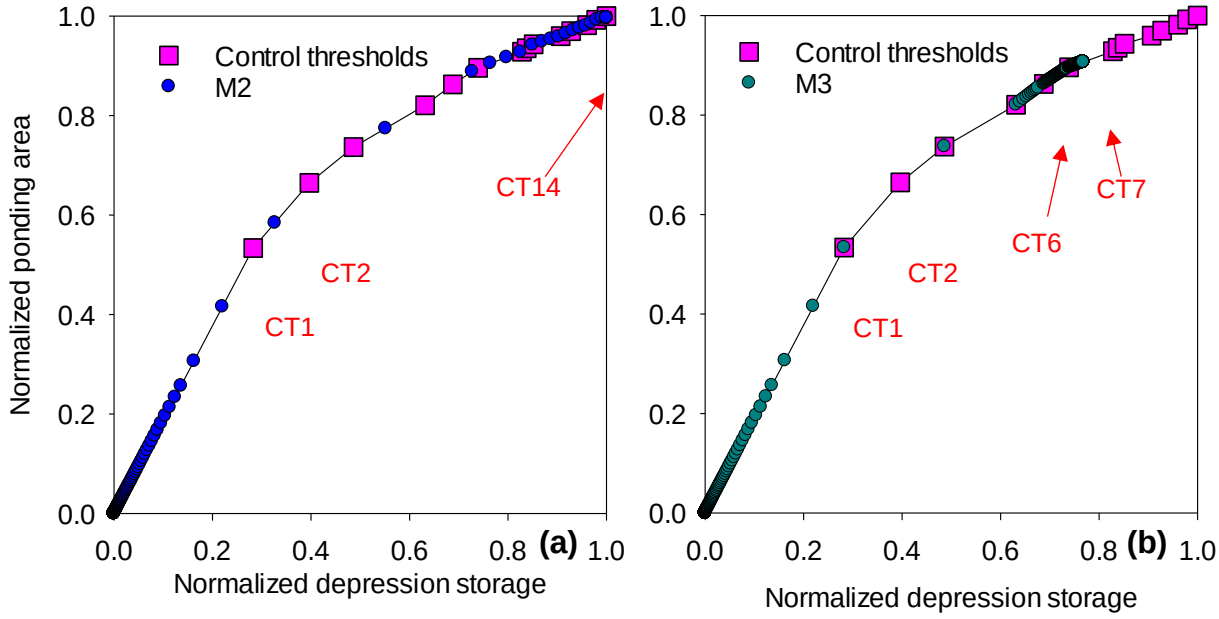

Figure 3.11. Relationships of the normalized depression storage and the normalized ponding area for Subbasin 4 simulated by M2 and M3 for the design storm: (a) M2; and (b) M3.

Figure 3.12 shows the relationships between the normalized cumulative rainfall (NCR) with other hydrologic variables of subbasin 4, including normalized cumulative NDA outflow (NCF_{NDA}), normalized cumulative DA outflow (NCF_{DA}), NDS, NPA, and normalized active drainage area (NADA). Note that the active drainage area is the sum of ACA and APA of subbasin 4. In the simulation of M2 with a single CT (Figure 3.12a), there was no outflow from the DA and no active drainage area until the lumped depression was fully filled (i.e., NCF_{DA} = 0 and NADA = 0 before NCR = 0.8). In HYDROL-D, the NDA was assumed to be well connected to its associated subbasin outlet. Hence, the NCF_{NDA} of subbasin 4 increases smoothly. The

variations of the NDS and NPA follow the curve in Figure 3.11. As shown in Figure 3.11, the PA of subbasin 4 has a faster changing rate than the DS before CT reaches the CT2 (NPA = 0.66 and NDS = 0.40 when CT = CT2). Thereafter, a reverse changing pattern of the PA and DS can be observed. The changing rate of the NPA is faster than that of the NDS when the NCR is smaller than 0.43 (i.e., NPA = 0.42 and NDS = 0.33 when NDR = 0.43) (Figure 3.12a). The NPA shows an opposite changing pattern when the NCR is greater than 0.57 (i.e., NPA = 0.58 and NDS = 0.55 when NDR = 0.57). As shown in Figure 3.12b, the NADA increases hierarchically with an increase of the normalized rainfall, which demonstrates the improved performance of M3 with multiple CTs. Once a CT is reached, a certain area in the DA releases water to its associated subbasin outlet. There is no difference in NCF_{NDA} in M2 and M3 (Figures 9a and 9b), but NCF_{DA} follows the variation of NADA. Both Figures 3.9a and 3.9b show that the changing rate of the NPA is faster than that of the NDS when the NCR is smaller than 0.43, and a reverse trend can be observed when the NCR is greater than 0.57. This is because the changing rates of NPA and NDS are controlled by the variation curves in Figure 3.10, and the number of CTs controlling water release does not influence the variation trend of the NPA and NDS.

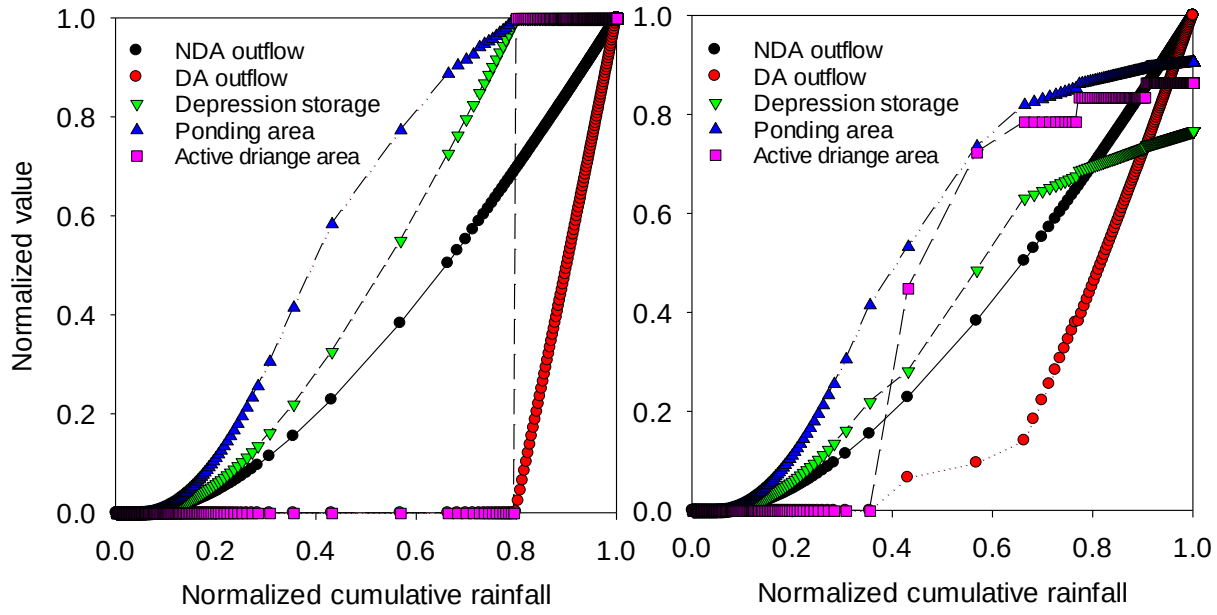

Figure 3.12. Relationships of the normalized cumulative rainfall and other normalized hydrologic variables for Subbasin 4 simulated by M2 and M3 for the design storm: (a) M2; and (b) M3.

3.4.3. Evaluation of Model Performance in Real Application

Figure 3.13 shows the comparisons of the observed and simulated hydrographs at the watershed outlet (i.e., USGS 05057200 Baldhill Creek gaging station) under the real rainfall event. The modeling results highlight the important influence of depressions on hydrologic processes in this depression-dominated area. HEC-HMS (M1) accounted for the impact of depressions by introducing the non-contributing drainage area. For the contributing drainage area, however, depressions were simply simulated by using the lumped initial abstraction, and the entire contributing drainage area was assumed to be well connected to the watershed outlet. The M1 hydrograph exhibits a quick increase in the rising limb and a fast decline in the recession limb (Figure 3.13). This study demonstrated that consideration of the non-contributing area improved the HEC-HMS modeling for depression-dominated areas. However, depending upon the actual surface topography and rainfall conditions, certain “non-contributing” drainage areas

can be potentially converted to “contributing” areas. Such dynamic changes were not considered in the current study.

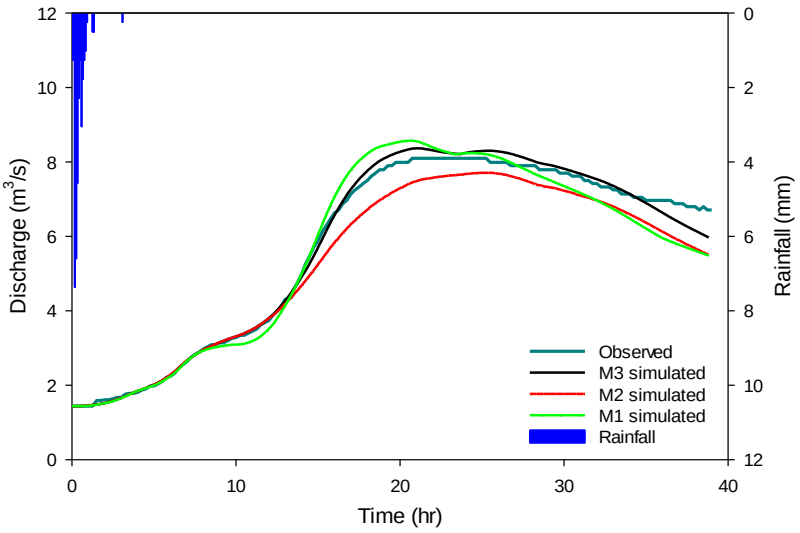

Figure 3.13. Comparisons of the observed and simulated hydrographs by three models M1–M3. M1 = HEC-HMS considering noncontributing areas; M2 = HYDROL-D with a single CT; and M3 = HYDROL-D with multiple CTs.

In the HYDROL-D modeling with a single CT (i.e., M2), a certain area of each subbasin contributed runoff water to its outlet before all depressions were fully filled (i.e., DS < TDS_h). M2 underestimated the streamflow (Figure 3.13), indicating that a single threshold control was not able to simulate the real depression filling and spilling dynamics. The discharges simulated by M2 and M3 are identical before t = 13.5 hr since the DS value of any subbasin did not reach its TDS at CT1. With an increase in the DS, the subbasins gradually released the ponded water in M3, while there was no water release before reaching TDS_h in M2. Hence, the discharges simulated by M2 were lower than those from M3 and the observed data. Overall, HYDROL-D with the new modeling structure and M3 with multiple CTs yielded improved simulations. The performances of the three models (M1, M2, and M3) were evaluated by using NSE and RMSE. Compared with the observed discharge data at the final outlet of the watershed, M3 provided

better simulations (NSE = 0.99, RMSE = 0.14) than M1 (NSE = 0.98 and RMSE = 0.28) and M2 (NSE = 0.97 and RMSE = 0.53).

To better understand how depressions influenced the hydrologic processes in the study area, the major mass balance terms (e.g., NDA outflow, NDA infiltration, DA outflow, DA infiltration and DA depression storage) simulated by M3 were analyzed for all subbasins. Figure 3.14 shows the ratio of each selected hydrologic variable to the total rainfall for each subbasin. Due to the small rainfall amount, DA infiltration and depression storage captured the most rainfall (0.76 and 0.14 in average, respectively). The ratio of NDA infiltration to the total rainfall was 0.08 because the NDA of each subbasin was small. The average outflow from the NDA and DA was approximately 0.02. Two subbasins (subbasins 5 and 6) reached their first CTs and released water from their DAs. The ratios of the DA outflow for subbasins 5 and 6 were 0.03 and 0.005, respectively. In addition, the water sources of depressions were quantified. For a subbasin, the water in depression storage came from the surface runoff generated in the CA of the subbasin. Another water source of depression storage was direct rainfall over the PA of the subbasin. The average ratios of the CA runoff and direct rainfall were 0.94 and 0.06.

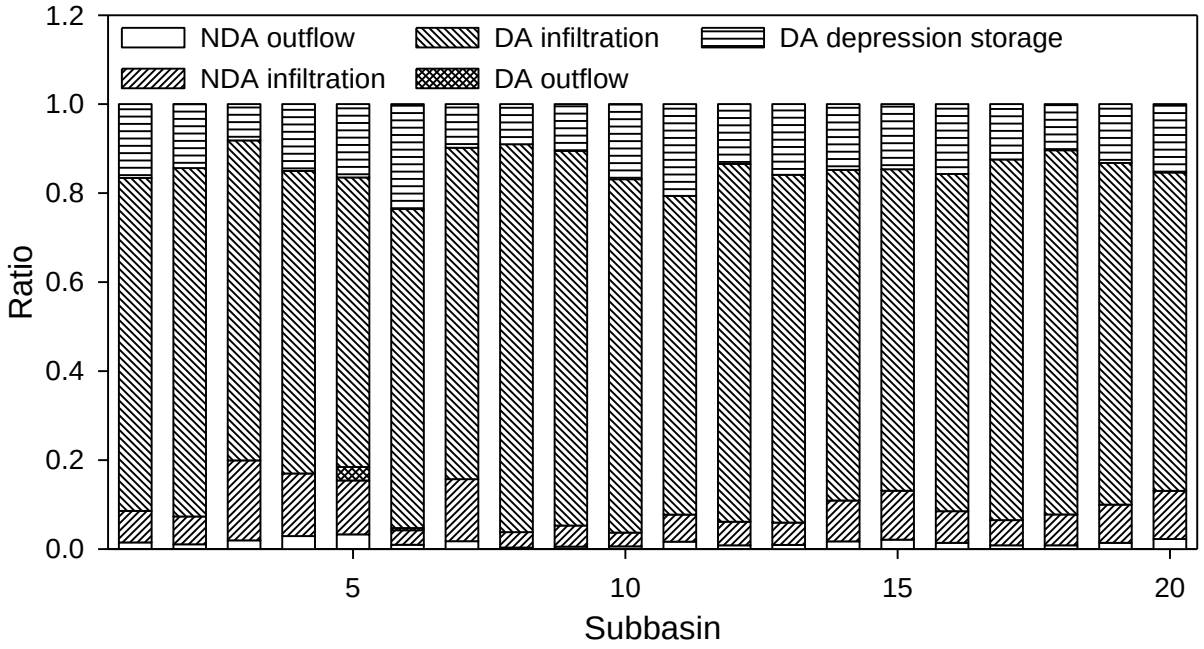

Figure 3.14. Ratios of five major hydrologic variables to the cumulative rainfall simulated by M3 for all subbasins

Because of the unique structure of HYDROL-D, a CA drains runoff water to its connected PA, instead of the outlet of its subbasin. Thus, the ratios of different characteristic areas to the entire subbasin area (i.e., r_{NDA}, r_{CA}, and r_{PA}) have significant influences on the modeling results. The ratios for the 20 subbasins at the final time step simulated by M3 in the real application are shown in Table 3.4. Among these ratios, the values of r_{CA} are the highest (ranging from 0.78 to 0.94), suggesting that most of the excess rainwater retained in the subbasins, instead of running off directly through the subbasin outlets. The ranges of r_{PA} and r_{NDA} for all subbasins are 0.02 - 0.10 and 0.04 - 0.20, respectively. Because the total amount of rainfall is relatively small and most of the rainwater infiltrates into the subsurface zone, r_{PA} is smaller than r_{NDA} for all subbasins, except for subbasin 10, at the final time step. For subbasin 10, its r_{NDA} is smaller than r_{PA}, which indicates that subbasin 10 has a better ability to retain water in depressions. This can be attributed to the high r_{DA} and its topographic characteristics.

Table 3.4. Ratios of different characteristic areas to the entire subbasin areas at the final time step simulated by M3 in the real application.

Subbasin	r_{NDA}	$r_{DA} = r_{CA} + r_{PA}$	
		r_{CA}	r_{PA}
1	0.09	0.87	0.04
2	0.07	0.88	0.05
3	0.20	0.78	0.02
4	0.17	0.79	0.04
5	0.15	0.78	0.07
6	0.04	0.86	0.10
7	0.16	0.82	0.02
8	0.04	0.94	0.02
9	0.05	0.91	0.04
10	0.04	0.91	0.05
11	0.08	0.86	0.06
12	0.06	0.90	0.04
13	0.06	0.89	0.05
14	0.11	0.86	0.03
15	0.13	0.84	0.03
16	0.08	0.89	0.03
17	0.06	0.91	0.03
18	0.08	0.89	0.03
19	0.10	0.87	0.03
20	0.13	0.84	0.02

Note: CA = contributing area in DA; DA = depressional area; M3 = HYDROL-D with multiple thresholds; NDA = non depressional area; PA = ponding area in DA; rCA = ratio of contributing area to entire subbasin area; rDA = ratio of depressional area to entire subbasin area; rNDA = ratio of non-depressional area to entire subbasin area; and rPA = ratio of ponding area to entire subbasin area.

3.5. Summary and Conclusions

The dynamic influences of surface depressions on hydrologic modeling are important, especially for depression-dominated areas. A new model, HYDROL-D, was developed in this study to quantify the hydrologic impacts of surface depressions. The unique features of HYDROL-D include: 1) it subdivided a subbasin into featured areas (i.e., DA, NDA, CA and PA) which revealed real topography characteristics and discontinuity caused by depressions in a watershed; 2) it revealed the depression filling process in a lumped way by using the variation function of PA and DS; 3) it simulated water release from puddles in depression dominated areas depending on hierarchical CTs. This study focused on demonstrating the unique features of HYDROL-D. The model was applied to a watershed in North Dakota under a 24-hour design storm and a real rainfall event. Based on the simulation results, the following conclusions were obtained:

Depressions did change water accumulations in a watershed significantly, and the entire subbasin area contributed surface runoff to its outlet only after reaching its highest CT. Because of the impact of depressions, only a small portion of the study area (3.72% to 19.91%) drained runoff water to subbasin outlets directly, while, as expected, most areas drained water to surface depressions in the beginning of the simulation. In addition, the variations in the PA and DS followed an increasing trend in the study area, but the relationships of the PA and DS varied for different subbasins due to the variations in surface topography.

The HYDROL-D modeling for the 24-hour design storm illustrated the intrinsic threshold behavior of surface runoff over a depression-dominated area and the unique modeling framework featured with threshold controls of water release from depressions. The HYDROL-D model with multiple CTs tended to yield more surface runoff, as well as smaller depression storage and

ponding area than the model with a single CT. The comparison of HEC-HMS (M1) with the two HYDROL-D models (M2 and M3) for the real application demonstrated the improved performance from the implementation of multiple CTs in HYDROL-D. This modeling study emphasized the necessity to introduce "non-contributing" areas to improve traditional hydrologic modeling for depression-dominated watersheds (e.g., HEC-HMS). In addition, such non-contributing areas may vary, depending upon the actual topographic, rainfall, and other conditions. The multiple CTs revealed the hierarchical water release mechanism of puddles in a lump way. The mass balance analysis for subbasins and the computation of different characteristic areas (e.g., r_{NDA}, r_{CA}, and r_{PA}) revealed that for the selected rainfall event only limited runoff was generated due to the significant impact of depressions on hydrologic processes (e.g., enhanced infiltration, and depression filling, spilling and storage).

Although the HYDROL-D model with multiple thresholds provides improved simulations of hydrologic processes for depression-dominated areas, there are some limitations. In the current HYDROL-D model, all depressions at the same level are lumped together and their detailed spatial distributions are not considered. In addition to the lag method used for channel routing in the current HYDROL-D model, more routing methods should be considered, depending on the real open channel flow conditions in a watershed.

3.6. References

Almendinger, J. E., Murphy, M. S., Ulrich, J. S., 2014. Use of the Soil and Water Assessment Tool to scale sediment delivery from field to watershed in an agricultural landscape with topographic depressions. J. Environ. Qual., 43(1), 9-17.

Amoah, J. K., Amatya, D. M., Nnaji, S., 2013. Quantifying watershed surface depression storage: determination and application in a hydrologic model. Hydrol. Process., 27(17), 2401-2413.

Chu, X., 2017. Delineation of pothole-dominated wetlands and modeling of their threshold behaviors. J. Hydrol. Eng., 22 (1), D5015003.

Chu, X., Yang, J., Chi, Y., Zhang, J., 2013. Dynamic puddle delineation and modeling of puddle-to-puddle filling-spilling-merging-splitting overland flow processes. Water Resour. Res., 49(6), 3825-3829.

Chu, X., Zhang, J., Chi, Y., Yang, J., 2010. An improved method for watershed delineation and computation of surface depression storage. In Proc., 2010 Watershed Management Conf., Innovations in Watershed Management under Land Use and Climate Change, edited by K. W. Potter and D. K. Frevert, 1113–1122. New York: ASCE.

Darboux, F., Davy, P., Gascuel-Odoux, C., Huang, C., 2002. Evolution of soil surface roughness and flowpath connectivity in overland flow experiments. Catena, 46(2), 125-139.

Gassman, P. W., Reyes, M. R., Green, C. H., Arnold, J. G., 2007. The soil and water assessment tool: historical development, applications, and future research directions. Trans. ASABE, 50(4), 1211-1250.

Hay, L., Norton, P., Viger, R., Markstrom, S., Regan, R. S., Vanderhoof, M., 2018. Modelling surface-water depression storage in a Prairie Pothole Region. Hydrol. Process., 32(4), 462-479.

Kreymborg, L. R., Forman, S. M., 2001. Modeling the hydrologic functions of wetland prairie potholes. In Proc., Wetlands Engineering and River Restoration Conf., 1–12. Reston, VA: ASCE.

Markstrom, S. L., Regan, R. S., Hay, L. E., Viger, R. J., Webb, R. M. T., Payn, R. A., LaFontaine, J. H., 2015. PRMS-IV, The precipitation-runoff modeling system, version 4. Chap. B7 in US Geological Survey techniques and methods, Book 6, 158. Reston, VA: US Geological Survey.

Martz, L. W., Garbrecht, J., 1993. Automated extraction of drainage network and watershed data from digital elevation models. J. Am. Water Resour. Assoc., 29(6), 901-908.

Mekonnen, B. A., Mazurek, K. A., Putz, G., 2016. Incorporating landscape depression heterogeneity into the Soil and Water Assessment Tool (SWAT) using a probability distribution. Hydrol. Process., 30(13), 2373-2389.

Nash, J. E., Sutcliffe, J. V., 1970. River flow forecasting through conceptual models part I – A discussion of principles. J. Hydrol., 10(3), 282-290.

Neitsch, S. L., Arnold, J. G., Kiniry, J. R., Williams, J. R., 2011. Soil and water assessment tool theoretical documentation version 2009. Texas Water Resources Institute.

Shaw, D. A., Pietroniro, A., Martz, L. W., 2013. Topographic analysis for the prairie pothole region of Western Canada. Hydrol. Process., 27(22), 3105-3114.

Skaggs, R. W., Youssef, M. A., Chescheir, G. M., 2012. DRAINMOD: Model use, calibration, and validation. Trans. ASABE, 55(4), 1509-1522.

Tahmasebi Nasab, M., Singh, V., Chu, X., 2017a. SWAT Modeling for Depression-Dominated Areas: How Do Depressions Manipulate Hydrologic Modeling? Water, 9(1), 58.

Tahmasebi Nasab, M., Zhang, J., Chu, X., 2017b. A new depression-dominated delineation (D-cubed) method for improved watershed modeling. Hydrol. Process., 31(19), 3364-3378.

USACE, HEC (Hydrologic Engineering Center). 2016. Hydrologic modeling system HEC-HMS, user's manual, version 4.2. Davis, CA: USACE-HEC.

USDA., 2017. WSS (Web Soil Survey) [WWW Document]. URL https://websoilsurvey.sc.egov.usda.gov/App/HomePage.htm (accessed 3.18.17).

USGS., 2017a. National water information system: Mapper [WWW Document]. URL https://maps.waterdata.usgs.gov/mapper/index.html (accessed 3.19.17).

USGS., 2017b. National water information system [WWW Document]. URL https://waterdata.usgs.gov/nwis/inventory?agency_code=USGS&site_no=05057200 (accessed 8.26.2017).

USGS., 2017c. The national map, TNM download, V1.0[WWW Document]. URL https://viewer.nationalmap.gov/basic (accessed 3.23.2017).

Yang, J., Chu, X., 2015. A new modeling approach for simulating microtopography-dominated, discontinuous overland flow on infiltrating surfaces. Adv. Water Resour., 78, 80-93.

4. FUNCTIONALITIES OF SURFACE DEPRESSIONS IN RUNOFF ROUTING AND HYDROLOGIC CONNECTIVITY MODELING

4.1. Abstract

Surface depression is one of the most significant topographic characteristics in a depression-dominated area. Hydrologic processes in depression-dominated areas are controlled by the spatial distribution of the depressions and their dynamic hydrologic connectivity. The objective of this research is to examine and quantify the watershed-scale functionalities of depressions in runoff processes and hydrologic connectivity. A depression-oriented hydrologic model with accounting for dynamic hydrologic connectivity (HYDROL-DC) is developed for continuous simulations of hydrologic processes in depression-dominated areas. Unlike traditional semi-distributed models, HYDROL-DC uses a unique modeling framework to facilitate separate modeling for puddle-based units, as well as off-stream and on-stream channel-based units in each subbasin. The HYDROL-DC was applied to the Edmore Coulee watershed in North Dakota and was calibrated and validated by using the observed discharge data. A surface delineation algorithm, HUD-DC, and the hydrology toolset in ArcGIS were used to analyze the topographic characteristics of the selected watershed to provide input data for HYDROL-DC. The simulation results demonstrated that the new modeling framework was able to effectively account for the depression-controlled variations in hydrologic processes. Depressions had not only retention but also acceleration capabilities in surface runoff generation. In addition, depressions exhibited dynamic influences on hydrologic connectivity and such influences became more significant as more highest-level depressions were fully filled.

4.2. Introduction

Surface depressions increase the complexity of hydrologic connectivity across land surfaces (Yang et al. 2010; Golden et al. 2014; Grimm and Chu 2018) and retain runoff water, which leads to reduced peak flow during a rainfall event (Philips et al. 2011; Chen et al. 2013). In traditional semi-distributed hydrologic models, the entire area of a watershed is assumed to be well connected to its associated outlet, and surface depressions are often lumped as a single depth to retain runoff from the entire watershed and control runoff water release (Kim et al., 2012; Amoah et al., 2013; Shaw et al., 2013). In reality, however, the contributing areas of depressions are determined by the spatial distribution of depressions and the generation of runoff is influenced by the dynamic connectivity between depressions. Therefore, hydrologic processes may not be accurately simulated if a model fails to account for such topographic characteristics of depressions and their impacts.

To consider the retention effect of surface depressions on surface runoff generation, some hydrologic models, such as the Precipitation-Runoff Modeling System (PRMS) and the Soil and Water Assessment Tool (SWAT) (Markstrom et al., 2015; Gassman et al., 2007), have been developed to specify the contributing areas for depressions. Such models have been applied to quantify the impacts of depressions on hydrologic processes (e.g., Vining, 2002; Wang et al., 2008; Hay et al., 2018). Some tools or algorithms have also been developed to determine the storage, ponding area, and contributing areas of depressions based on digital elevation models (DEMs) (e.g., Temme et al., 2006; Arnold, 2010; Chu et al., 2010; Tahmasebi Nasab et al., 2017a; Wang and Chu 2020). Furthermore, some researchers incorporated the geographic information extracted from DEMs into hydrologic models to simulate hydrologic processes

under the influence of depressions (e.g., Arnold, 2010; Mekonnen et al., 2016; Tahmasebi Nasab et al., 2017b; Wang et al., 2019).

Surface depressions are disconnected in most conditions and the connections between depressions occur only when there is sufficient rainfall or snowmelt (Van and Hayashi 2009; Hayashi et al. 2016). Thereofere, although specifying the contributing areas for lumped depressions can improve the hydrologic simulations in depression-dominated areas, the aforementioned models still fail to account for the spatial distribution of depressions and their hydrologic connectivity, as well as the real dynamic hydrologic processes in depression-dominated areas. In recent decades, many studies have been implemented to reveal the dynamic connectivity in depression-dominated areas and the significant influences of hydrologic connectivity on hydrologic processes (e.g., Leibowitz and Vining 2003; Yang and Chu 2013; Grimm and Chu 2018). Therefore, instead of a lumping depression in a region, considering individual depressions is more appropriate for hydrologic simulation in depression-dominated areas. For example, Chu et al. (2013) developed a physically-based puddle-to-puddle (P2P) model to simulate the depression-dominated filling, merging, spilling, and splitting overland flow processes and the dynamic hydrologic connectivity. In the P2P model, depressions were classified into a number of levels, and lower-level depressions that sharing the same thresholds can merge and generate a higher-level depression during the filling process (Chu et al. 2013). Puddle-based unit (PBU), which consists of a highest-level depression and its associated contributing area, was utilized as the basic component to calculate cell-to-cell and P2P processes on a surface (Chu 2017; Grimm and Chu 2018). Although P2P model can simulate the hydrologic processes and connectivity related to the hierarchical depression structure, it requires intensive computation resources, especially for large watershed-scale problems. Since there is no

outflow from a PBU to its downstream unit until the highest-level depressions in the PBU is fully filled, considering highest-level depressions is an efficient way to simulate hydrologic processes in depression-dominated watersheds.

The objective of this research is to examine the watershed-scale functionalities of surface depressions in runoff generation processes and hydrologic connectivity. A new watershed-scale and depression-oriented hydrologic model (i.e., HYDROL-DC) is developed for continuous simulation of hydrologic processes and connectivity, and it is further tested using the Edmore watershed in North Dakota. Based on the calibrated HYDROL-DC, a depression impact coefficient (C_d) is proposed to quantify the impacts of both the storage and spatial distribution of depressions on hydrologic processes. HYDROL-DC model is also applied for hydrologic simulation without considering depressions. The comparison between the two simulations highlights the influences of depressions on specific hydrologic processes. In addition, the normalized connected area is compared with the normalized activated area to quantify the dynamic influences of depressions on hydrologic connectivity.

4.3. Materials and Methods

4.3.1. Overview of the HYDROL-DC Framework

HYDROL-DC is a semi-distributed, physically-based model for continuously simulating hydrologic processes and accounting for the dynamic hydrologic connectivity within subbasins in depression-dominated areas. As illustrated in Figure 4.1, HYDROL-DC delineates a watershed into subbasins, each of which is further divided into one main channel and a number of PBUs and channel-based units (CBUs). CBUs are further classified into off-stream CBUs for those that have no direct interactions with the main channel and on-stream CBUs for those that have direct interactions with the main channel. Following the definitions proposed by Chu et al.

(2010, 2013), a PBU is composed of a ponding area (PA) and its contributing area (CA), while a CBU includes a channel segment (a main channel or a tributary channel) and its CA. Moreover, each PBU has at least one downstream unit (note that multiple thresholds are considered for PBUs in HYDROL-DC), while a CBU has only one downstream unit (Figure 4.1). In a PBU, surface runoff transfers from CA to PA, and then to its downstream unit(s) after the depression storage of the PBU reaches a threshold value (i.e., the maximum storage of the highest-level depression of the PBU). However, surface runoff in a CBU runs directly into its tributary channel or the main channel. In the vertical direction (Figure 4.2), each unit is divided into four zones, including canopy zone, snow zone, surface zone, and soil zone. The soil zone is further divided into upper and lower soil zones, and the upper soil zone consists of a number of soil cells. In addition, all units in a subbasin share the same shallow groundwater zone (Figure 4.2). Water is tracked zone-by-zone and unit-by-unit, and finally converted into deep groundwater and streamflow.

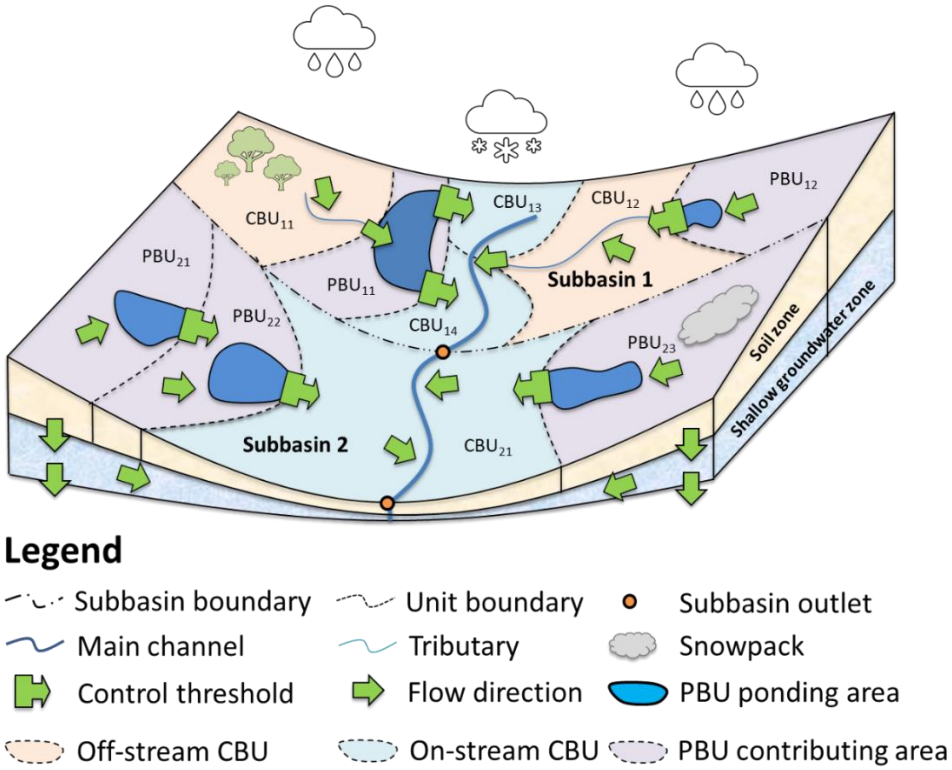

Figure 4.1. Conceptual model of HYDROL-DC in the horizontal direction (PBU: puddle-based unit; On-stream CBU: channel-based unit that has interaction with the main channel; Off-stream CBU: channel-based unit that has no interaction with the main channel; CA: Contributing area; PA: Ponding area).

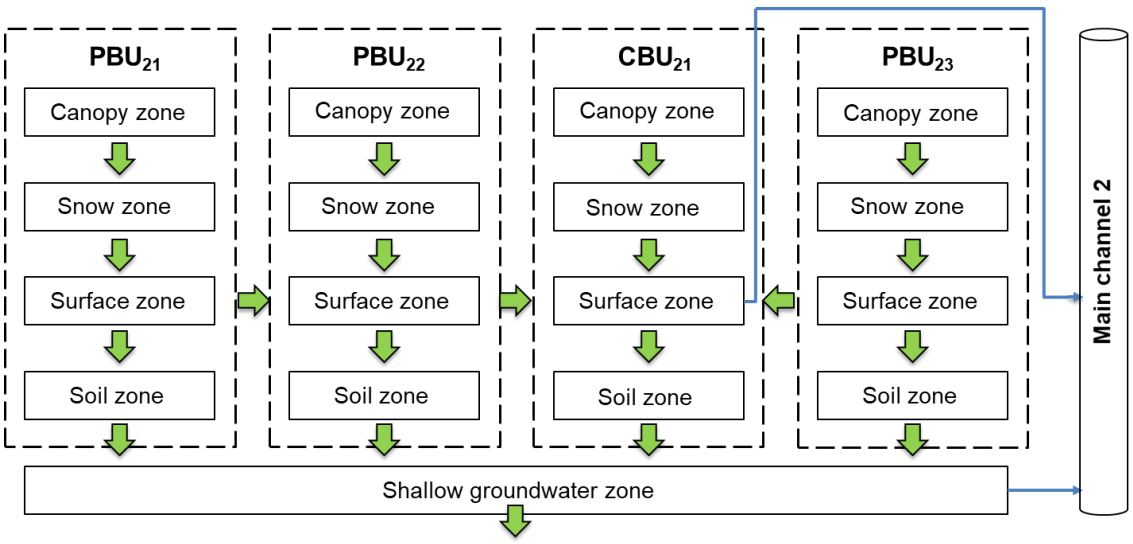

Figure 4.2. Conceptual model of HYDROL-DC in the vertical direction for a subbasin.

There are three nested loops in HYDROL-DC, including subbasin loop, unit loop, and time loop (Figure 4.3). The time loop is implemented from the most upstream units in the most upstream subbasins to the most downstream units in the most downstream subbasins. In the time loop of a unit in a subbasin, the mass balance is calculated following the order of canopy zone, snow zone, and surface zone. For a PBU, the evaporation from its PA and its depression storage is calculated. If the depression storage is greater than the maximum depression storage (MDS), puddle routing is implemented for the calculation of water released from the PA to its associated unit outlet(s). Otherwise, the CA and PA are updated based on the current depression storage. For an off-stream CBU, its outflow to the associated unit outlet is determined by tributary channel routing. After the tributary channel or puddle routing, the mass balance of the soil zone of the unit is calculated. The percolation from all units in a subbasin is considered as the source of the shallow groundwater zone of the subbasin in the mass balance computation. Main channel routing is implemented after the main channel in a subbasin receives water from the surface zone of all on-stream CBUs and the shallow groundwater zone of the subbasin (baseflow).

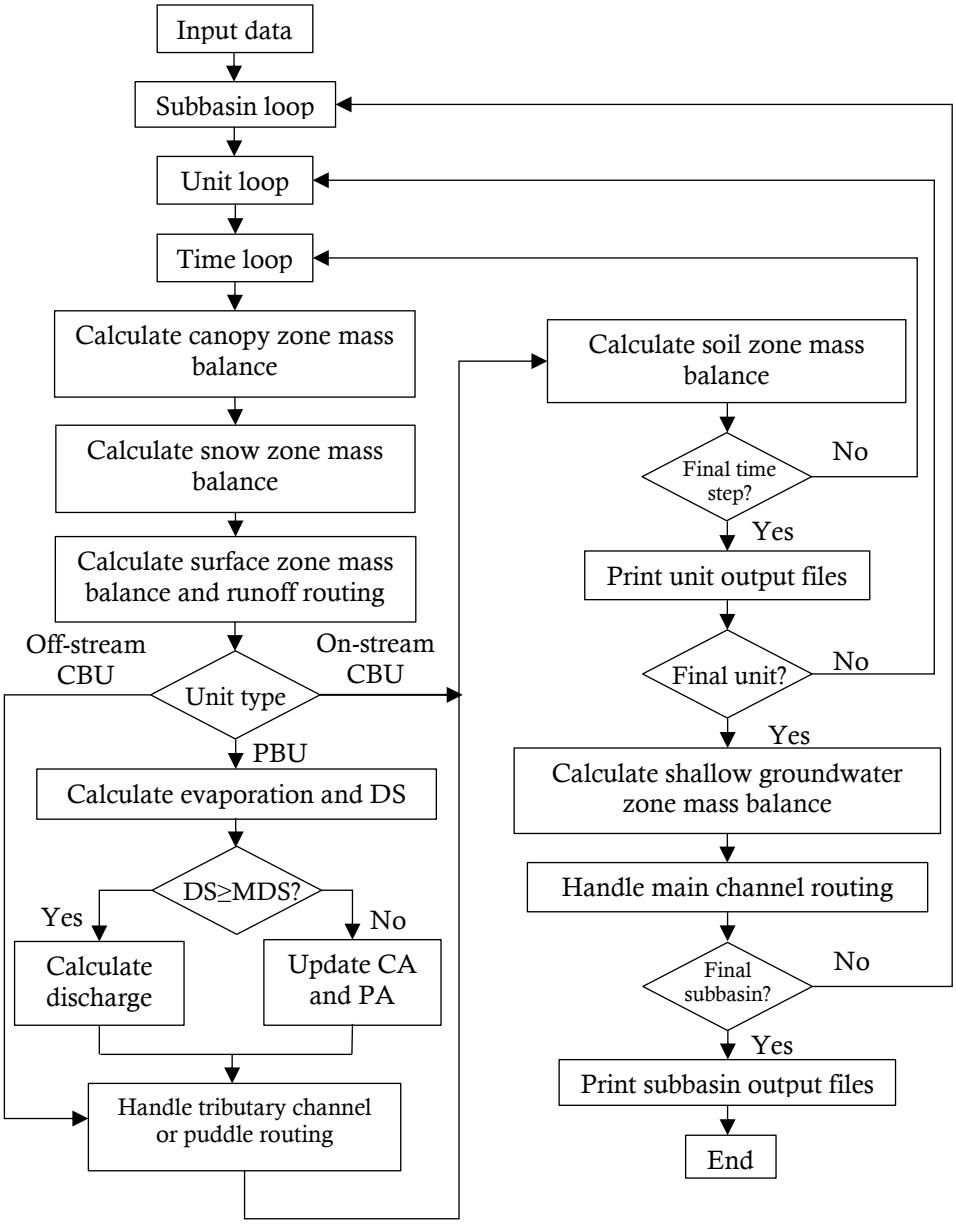

Figure 4.3. Flowchart of HYDROL-DC (DS: depression storage; MDS: maximum depression storage).

4.3.2. Descriptions of HYDROL-DC

4.3.2.1. Canopy zone simulation

The water mass balance for the canopy zone of a unit (PBU or CBU) can be expressed as:

$$M_{cnp}(t) = M_{cnp}(t-1) + P_{cnp}(t) - E_{cnp}(t) - P_{cano}(t) \quad (4.1)$$

where M_{cnp} is the canopy storage (L); P_{cnp} is the precipitation received by the canopy zone (L); $E_{cnp,t}$ is the evaporation from the canopy zone (L); P_{cano} is the precipitation exceeding the canopy zone capacity (L); and *t* is the time step.

The canopy capacity and the ratio of precipitation falling into the canopy zone are respectively determined by (DHI 2007):

$$MC_{cnp}(t) = LAI(t) \times MC_{cnp,max} \tag{4.2}$$

$$P_{cnp}(t) = C_{cnp} \times P_{total}(t) \tag{4.3}$$

where MC_{cnp} is the canopy capacity (L); LAI is the leaf area index; $MC_{cnp,max}$ is the maximum canopy capacity (L); C_{cnp} is the ratio of precipitation falling into the canopy zone; and P_{total} is the total precipitation (L).

The evaporation from the canopy zone is calculated based on the canopy storage and reference evapotranspiration (RET) by using Equation 4.4 and the residual RET is calculated after the calculation of the canopy zone evaporation by using Equation 4.5.

$$E_{cnp}(t) = min\,[RET(t),\ M_{cnp}(t-1) + P_{cnp}(t)] \tag{4.4}$$

$$RET_{cnp}(t) = \begin{cases} 0 & for\ RET(t) < M_{cnp}(t-1) + P_{cnp}(t) \\ RET(t) - E_{cnp}(t) & for\ RET(t) \geq M_{cnp}(t-1) + P_{cnp}(t) \end{cases} \tag{4.5}$$

where RET is the reference evapotranspiration (L); $E_{cnp,t}$ is the evaporation from the canopy zone (L); and RET_{cnp} is the residual RET after the calculation of canopy zone evaporation (L).

The precipitation exceeding the canopy zone capacity is calculated by:

if $M_{cnp}(t-1) + P_{cnp}(t) - E_{cnp}(t) < MC_{cnp}(t)$:

$$P_{cano}(t) = 0 \tag{4.6}$$

otherwise:

$$P_{cano}(t) = M_{cnp}(t-1) + P_{cnp}(t) - E_{cnp}(t) - MC_{cnp}(t) \tag{4.7}$$

4.3.2.2. Snow zone simulation

For the snow zone of a unit, the source term is the precipitation falling on the snow zone and the sink terms include snowmelt, sublimation, and precipitation falling into the surface zone. The water mass balance of this zone is given by:

$$M_{sno}(t) = M_{sno}(t-1) + P_{sno}(t) - P_{sur}(t) - SM(t) - E_{sno}(t) \quad (4.8)$$

where M_{sno} is the snow zone storage (L); P_{sno} is the precipitation falling into the snow zone (L); E_{sno} is the sublimation from the snow zone (L); P_{sur} is the precipitation falling into the surface zone (L); and SM is the snowmelt (L).

In Equation 4.8, P_{sno} equals the sum of the precipitation falling directly into the snow zone and the precipitation exceeding the canopy zone capacity as follows:

$$P_{sno}(t) = (1 - C_{cnp}) \times P_{total}(t) + P_{cano}(t) \quad (4.9)$$

When the average air temperature ($T_{air,ave}$) at a time step is greater than the temperature for snowfall (T_{sf}), the precipitation is rainfall; otherwise, the precipitation is snowfall. The precipitation falling into the surface zone is calculated by:

$$P_{sur}(t) = \begin{cases} 0 & for\ T_{air,ave}(t) < T_{sf} \\ P_{sno}(t) & for\ T_{air,ave}(t) \geq T_{sf} \end{cases} \quad (4.10)$$

The temperature index method (Neitsch et al. 2011) is used in HYDROL-DC to simulate the snowmelt of the snow zone of each unit. For a unit, snowmelt occurs when the snow zone storage is greater than zero and the maximum air temperature is higher than the temperature for snowmelt, as quantified by Equation 4.11:

$$SM(t) = min\left[c_{sm} \times r_{SC}(t) \times \left[\frac{T_{sz}(t)+T_{air,max}(t)}{2} - T_{sm}\right],\ M_{sno}(t-1) + P_{sno}(t) - P_{sur}(t)\right] \quad (4.11)$$

where c_{sm} is a snowmelt factor (L/T -C); r_{SC} is the ratio of area covered by snow; T_{sz} is the temperature of the snow zone (ºC); $T_{air,max}$ is the maximum air temperature in a unit (ºC); and T_{sm} is the temperature for snowmelt (ºC).

The sublimation from the snow zone is calculated by using Equation 4.12 based on RET_{cnp} (DHI 2007) and the residual RET after the calculation of the sublimation is determined by using Equation 4.13.

$$E_{sno}(t) = min\left[c_{se} \times RET_{cnp}(t),\ M_{sno}(t-1) + P_{sno}(t) - P_{sur}(t) - SM(t)\right] \quad (4.12)$$

$$RET_{sno}(t) = RET_{cnp}(t) - E_{sno}(t) \quad (4.13)$$

where E_{sno} is the sublimation from the snow zone (L); c_{se} is a coefficient that controls sublimation; and RET_{sno} is the residual RET after the calculation of sublimation (L).

4.3.2.3. Surface zone simulation

As aforementioned, a PBU consists of a PA and its associated CA, and a CBU consists of a channel and its associated CA. For the CA of a PBU, the source terms include precipitation falling into the surface zone of the CA and the outflow of its upstream unit(s) (including PBUs and CBUs), and the sink terms are the infiltration into the soil zone and the discharge to its associated PA. Different from the CA in a PBU, if the upstream of a CBU is an off-stream CBU, the outflow of the upstream off-stream CBU flows directly to the channel of the current CBU. Therefore, the source terms of a CBU are the precipitation falling into the surface zone and the outflow of its upstream PBU, and the sink terms are the infiltration into the soil zone and the discharge to its associated channel. The mass balance equation for the CA of a PBU/CBU can be expressed as:

$$M_{ca}(t) = M_{ca}(t-1) + [P_{sur}(t) + SM(t)] \times r_{ca}(t) - D_{ca}(t) + Q_{ca,in}(t) - Q_{ca,out}(t) \quad (4.14)$$

where M_{ca} is the CA storage (L); r_{ca} is the ratio of CA to the entire area of a unit; D_{ca} is the infiltration into the soil zone in the CA (L); $Q_{ca,in}$ is the CA inflow from its associated upstream unit(s) (L); and $Q_{ca,out}$ is the water from the CA to the PA or channel in a unit (L).

The PA in a PBU receives water from rainfall, snowmelt, and its associated CA, and loses water through evaporation, infiltration/percolation, and outflow to its downstream unit(s). The mass balance equation can be expressed as:

$$M_{pa}(t) = M_{pa}(t-1) + Q_{pa,in}(t) + [P_{sur}(t) + SM(t)] \times r_{pa}(t) - E_{pa}(t) - D_{pa}(t) - Q_{pa,out}(t) \quad (4.15)$$

where M_{pa} is the PA storage (L); r_{pa} is the ratio of PA to the entire area of a unit; E_{pa} is the evaporation from the PA (L); D_{pa} is the infiltration/percolation from the PA to the soil zone (L); $Q_{pa,in}$ is the water from the CA to the PA (L) [$Q_{pa,in} = Q_{ca,out}$]; and $Q_{pa,out}$ is the water from the PA to its downstream unit (L).

For a tributary or main channel, the mass balance can be calculated by using Equation 4.16. Additionally, the inflows of a tributary channel include the outflows from its associated CA and its upstream off-stream CBU(s). However, the main channel in a subbasin receives water from the CAs of all on-stream CBUs, its upstream off-stream CBUs, and the main channel of its upstream subbasin(s).

$$M_{ch}(t) = M_{ch}(t-1) + Q_{ch,in}(t) - Q_{tc,out}(t) \quad (4.16)$$

where M_{ch} is the channel storage (L); $Q_{ch,in}$ is the water flowing into the channel (L); and $Q_{ch,out}$ is the water flowing out of the channel (L).

The surface runoff from the CA of a unit is calculated by (Mishra and Singh 2003):

$$R_{ca}(t) = \begin{cases} 0 & for\ I_a < \alpha S(t) \\ \frac{[P_{sur}(t) + SM(t) - I_a]^2}{P_{sur}(t) + SM(t) + S(t) - I_a} \times r_{ca} & for\ I_a \geq \alpha S(t) \end{cases} \quad (4.17)$$

$$S(t) = C\left[\frac{1000}{CN(t)} - 10\right] \quad (4.18)$$

$$D_{ca}(t) = [P_{sur}(t) + SM(t)] \times r_{ca} - R_{ca}(t) \quad (4.19)$$

where R_{ca} is the surface runoff generated from the CA (L); S is the potential maximum retention of the CA (L); r_{ca} is the ratio of the CA to the entire area of a unit ($r_{ca} = 1 - r_{pa}$); I_a is the initial abstraction (L); CN is the curve number; α is a calibration coefficient; and C is a unit conversion factor.

In the continuous simulation, $CN(t)$ of a unit is updated by using Equations 4.20 - 4.23 based on the soil water content of the first soil cell in the upper soil zone (Chu and Marino 2007).

if $WC_{us,1}(t) < WP_{us,1}$:

$$CN(t) = CN_I \quad (4.20)$$

else if $WP_{us,1} \leq WC_{us,1}(t) < 0.6FC_{us,1} + 0.4WP_{us,1}$:

$$CN(t) = CN_I + (CN_{II} - CN_I)\frac{WC_{us,1}(t) - WP_{us,1}}{0.6(FC_{us,1} - WP_{us,1})} \quad (4.21)$$

else if $0.6FC_{us,1} + 0.4WP_{us,1} \leq WC_{us,1}(t) < 0.5(FC_{us,1} + WS_{us,1})$:

$$CN(t) = CN_{II} + (CN_{III} - CN_{II})\frac{WC_{us,1}(t) - 0.6FC_{us,1} - 0.4WP_{us,1}}{0.5WS_{us,1} - 0.1FC_{us,1} - 0.4WP_{us,1}} \quad (4.22)$$

else:

$$CN(t) = CN_{III} \quad (4.23)$$

where $WC_{us,1}$, $WP_{us,1}$, $FC_{us,1}$, and $WS_{us,1}$ are respectively the soil water content, wilting point, field capacity, and saturated water content of the first soil cell; and CN_I, CN_{II}, and CN_{III} are the curve numbers for the dry, normal, and wet antecedent soil moisture conditions, respectively.

The identification of frozen soil is critical for hydrologic simulation in cold regions. In a unit, if the temperature of a soil cell is lower than zero, this cell is assumed to be frozen, vice versa. Additionally, CN is updated by using Equation 4.24 if the first soil cell is frozen (Mohammed et al., 2013):

$$CN_{fz}(t) = CN(t) \times \left[1 + c_{fz} \frac{WC_{us,1}(t)}{WS_{us,1}}\right] \quad (4.24)$$

where CN_{fz} is the curve number under a frozen condition; and c_{fz} is a shape parameter used to control the variation of curve number with soil water content.

After the surface runoff in the CA of a unit is calculated, Equation 4.25 is used to determine the outflow from the CA to the PA or the channel in the unit (Neitsch et al., 2011).

$$Q_{ca,out}(t) = [R_{ca}(t) + M_{ca}(t-1)] \times [1 - exp\,(-lag_{sur}/TC)] \quad (4.25)$$

where lag_{sur} is a parameter that controls water release from the CA to its associated PA or channel (T); and TC is the time of concentration of the unit (T).

The percolation/infiltration from the PA of a PBU is assumed to be added to the first cell in the upper soil zone and is controlled by the water content of the first soil cell by using Equation 4.26 (Neitsch et al. 2011):

$$D_{pa}(t) = \begin{cases} KS_{us,1} \times r_{pa}(t) \times \Delta t & for\ WC_{us,1}(t) < 0.5FC_{us,1} \\ KS_{us,1} \frac{WC_{us,1}(t)}{FC_{us,1}} \times r_{pa}(t) \times \Delta t & for\ 0.5FC_{us,1} \le WC_{us,1}(t) < FC_{us,1} \\ 0 & for\ WC_{us,1}(t) \ge FC_{us,1} \end{cases} \quad (4.26)$$

where D_{pa} is the percolation/infiltration from the PA of the surface zone to the soil zone (L); $KS_{us,1}$ is the saturated hydraulic conductivity of the first upper soil cell (L/T); and Δt is the time interval used in the simulation (T).

If the storage of the snow zone of a PBU is zero and the residual RET after the calculation of sublimation (RET_{sno}) is greater than zero, the evaporation from the PA of the PBU is calculated based on the RET_{sno} by using Equation 4.27 (Allen et al. 1998):

$$E_{pa}(t) = min\,(c_{epa} \times RET_{sno}\,(t) \times r_{pa}(t), M_{pa}(t-1) + Q_{pa,in}(t) + [P_{sur}(t) + SM(t)] \times r_{pa}(t) - D_{pa}(t)) \quad (4.27)$$

where E_{pa} is the evaporation from the PA (L); and c_{epa} is the crop coefficient of the PA.

For the tributary channel in an off-stream CBU or the main channel in a subbasin, the variable storage method (Williams 1969) is used for channel routing as follows:

$$Q_{ch,out}(t) = c_{ch} \times \left[Q_{ch,in}(t) + M_{ch}(t-1)\right] \tag{4.28}$$

where M_{ch} is the channel storage (L); $Q_{ch,in}$ is the channel inflow (L); $Q_{ch,out}$ is the channel outflow (L); and c_{ch} is the storage coefficient.

For a PBU, if its depression is fully filled, two methods are used to handle depression routing, and their selection is based on a user-defined depression storage ($M_{pa,rt}$). When the MDS of the PBU is less than $M_{pa,rt}$, all water exceeding the MDS flows out of the PA immediately. Otherwise, a linear reservoir equation is used to handle the depression routing:

$$Q_{pa,out}(t) = \beta_1 \times Q_{pa,in}(t) + \beta_1 \times Q_{pa,in}(t-1) + \beta_2 \times Q_{pa,out}(t-1) \tag{4.29}$$

where β_1 and β_2 are two coefficients used to control the water from the PA of a PBU to its downstream unit(s).

Variable PA and depression storage of a PBU are simulated in HYDROL-DC and are respectively given by (Liu and Schwartz 2011):

$$A_{pa}(t) = \pi r(t)^2 = \pi \left[\frac{r_{max}}{2\pi} arccos\left(1 - \frac{2h(t)}{h_{max}}\right)\right]^2 \tag{4.30}$$

$$M_{pa}(t) = \int_0^{h(t)} \pi \left[\frac{r_{max}}{2\pi} arccos\left(1 - \frac{2h'}{h_{max}}\right)\right]^2 dh' \tag{4.31}$$

where A_{pa} is the area of the PA in a PBU (L^2); M_{pa} is the storage of the PA in a PBU (L^3); $r(t)$ and $h(t)$ are the radius and the depth of the PA (L); and r_{max} and h_{max} are the maximum radius and depth of the PA (L).

4.3.2.4. Soil zone simulation

As aforementioned, the soil zone of a unit is divided into an upper soil zone and a lower soil zone, and the upper soil zone is further divided into different cells. The source terms of the

upper soil zone in a PBU are the infiltration/percolation from the CA and PA of the PBU. The percolation from a channel into the soil zone is not considered in the current HYDROL-DC. Therefore, the source term of the upper soil zone in a CBU is the infiltration from the CA of a CBU. The sink terms of the upper soil zone include evaporation, transpiration, and percolation to the lower soil cell or zone. The soil water storage and water content of a cell in the upper soil zone can be respectively expressed as:

$$M_{us,i}(t) = M_{us,i}(t-1) + D_{us,i-1}(t) - E_{us,i}(t) - TR_{us,i}(t) - D_{us,i}(t) \tag{4.32}$$

$$WC_{us,i}(t) = M_{us,i}(t)/TK_{us,i} \tag{4.33}$$

where $M_{us,i}$ is the water storage of the i^{th} soil cell (L); $D_{us,i-1}$ and $D_{us,i}$ are the percolation from the i-1^{th} and i^{th} soil cells (L) [if i=1, $D_{us,i-1}(t) = D_{ca}(t) + D_{pa}(t)$]; $TR_{us,i}$ and $E_{us,i}$ are the transpiration and evaporation of the i^{th} soil cell (L); and $TK_{us,i}$ is the thickness of the i^{th} soil cell (L).

In HYDROL-DC, it is assumed that evapotranspiration occurs only in the upper soil zone within a user-defined depth. The transpiration and evaporation from a soil cell in the upper soil zone are respectively given by (Kristensen and Jensen, 1975):

$$TR_{us,i}(t) = F1(t) \times F2(t) \frac{RET_{sno}(t)}{N_s} \times r_{ca} \tag{4.34}$$

$$E_{us,i}(t) = F3(t) \frac{RET_{sno}(t)}{N_s} + F4(t) \left[\left(1 - F3(t)\right) \frac{RET_{sno}(t)}{N_s} - TR_{us}(t) \right] \times [1 - F1(t)] \times r_{ca} \tag{4.35}$$

in which

$$F1(t) = C2 + C1 \times LAI(t) \tag{4.36}$$

$$F2(t) = 1 - \left(\frac{FC_{us,i} - WC_{us,i}(t)}{FC_{us,i} - WP_{us,i}}\right)^{\frac{C3}{RET_{sno}(t)}} \tag{4.37}$$

$$F3(t) = \begin{cases} C2 & for\ WC_{us,i}(t) \geq WP_{us,i} \\ C2 \times \frac{WC_i(t)}{WP_i} & for\ WR_{us,i} \leq WC_{us,i}(t) < WP_{us,i} \\ 0 & for\ WC_{us,i}(t) < WR_{us,i} \end{cases} \tag{4.38}$$

$$F4(t) = \begin{cases} \frac{WC_{us,i}(t) - \frac{WP_{us,i}+FC_{us,i}}{2}}{FC_{us,i} - \frac{WP_{us,i}+FC_{us,i}}{2}} & for\ WC_{us,i}(t) \geq \frac{WP_{us,i}+FC_{us,i}}{2} \\ 0 & for\ WC_{us,i}(t) < \frac{WP_{us,i}+FC_{us,i}}{2} \end{cases} \quad (4.39)$$

where $TR_{us,i}$ and $E_{us,i}$ are the transpiration and evaporation of the i^{th} soil cell (L); $C1$, $C2$, and $C3$ are empirical parameters that are specified by users; $F1(t)$, $F2(t)$, $F3(t)$, and $F4(t)$ are the parameters calculated based on the leaf area index of the unit and the water content of the i^{th} soil cell; $FC_{us,i}$, $WC_{us,i}$, $WP_{us,i}$, and $WR_{us,i}$ are the field capacity, water content, wilting point, and residual water content of the i^{th} soil cell; and N_s is the number of soil cells within the evapotranspiration depth.

Without considering the suction head of a soil cell in the upper soil zone of a unit, the percolation rate of the soil cell is estimated by (Van Genuchten 1980):

$$D_{us,i}(t) = K_i\left[WC_{us,i}(t)\right] \times \Delta t \quad (4.40)$$

where $D_{us,i}(t)$ is the percolation from the i^{th} soil cell (L); K_i is the unsaturated hydraulic conductivity of the i^{th} soil cell for water content of $WC_{us,i}(t)$ (L/T).

In HYDROL-DC, it is assumed that there is no percolation when an upper soil cell is frozen (i.e., the temperature of the cell is below zero). To determine the soil condition and control the percolation in different soil cells, the temperature of a soil cell is calculated by (Klein, 2018):

$$T_{us,i}(t) = T_{us,i}(t-1) + 0.346\left[T_{air,ave}(t) - T_{us,i}(t-1)\right] \times exp(-0.027028 d_i) \times \Delta t \quad (4.41)$$

where $T_{us,i}$ is the temperature of the i^{th} soil cell (ºC); $T_{air,ave}$ is the average air temperature of the unit; and d_i is the depth from the land surface to the center of the i^{th} soil cell (L). For the lower soil zone of a unit, the entire zone is assumed homogeneous and its water content is assumed

invariant. The percolation from this zone to the shallow groundwater zone is estimated by (Neitsch et al. 2011):

$$D_{ls}(t) = \left[1 - exp\left(-\frac{1}{lag_{ls}}\right)\right] \times D_{us,j}(t) + exp\left(-\frac{1}{lag_{ls}}\right) \times D_{us,j}(t-1) \quad (4.42)$$

where D_{ls} is the percolation of the lower soil zone (L); lag_{ls} is the delay time of soil water flow through the entire lower soil zone (T); and j is the last soil cell in the upper soil zone.

4.3.2.5. Groundwater zone simulation

In a subbasin, the shallow groundwater zone receives water from the lower soil zones of all units and drains water to the main channel and the deep groundwater zone. The mass balance of the shallow groundwater zone can be expressed as:

$$M_{sgw}(t) = M_{swg}(t-1) + Q_{sgw,in}(t) - D_{sgw}(t) - Q_{sgw,out}(t) \quad (4.43)$$

where M_{sgw} is the shallow groundwater storage (L); $Q_{sgw,in}$ is the inflow of the shallow groundwater zone (L); D_{sgw} is the percolation from the shallow groundwater zone to the deep groundwater zone; and $Q_{sgw,out}$ is the outflow from the shallow groundwater zone to the main channel (L).

Since all units in a subbasin share the same shallow groundwater zone, the inflow of the shallow groundwater zone equals the total percolating water from the lower soil zones of all units (Equation 4.44). In addition, the percolation from the shallow groundwater zone to the deep groundwater zone is calculated by using Equation 4.45.

$$Q_{sgw,in}(t) = \sum_{i=1}^{N_u} D_{ls,i}(t) \quad (4.44)$$

$$D_{sgw}(t) = c_{pco} \times Q_{sgw,in}(t) \quad (4.45)$$

where N_u is the number of units in the subbasin; $D_{ls,i}$ is the percolation from the lower soil zone of the i^{th} unit to the shallow groundwater zone (L); and c_{pco} is a parameter that controls the percolation.

In a subbasin, if the storage of the shallow groundwater zone is greater than a water release threshold, an exponential recession function is used to calculate the outflow from the shallow groundwater zone to its associated main channel (Nielsen and Hansen, 1973):

$$Q_{sgw,out}(t) = Q_{sgw,out}(t-1) \times e^{\frac{-1}{c_{sgw}}} + \left[Q_{sgw,in}(t) - D_{sgw}(t)\right] \times (1 - e^{\frac{-1}{c_{sgw}}}) \quad (4.46)$$

where c_{sgw} is a parameter that controls the outflow.

4.3.3. Introduction to ArcGIS Hydrology Toolset and HUD-DC

The hydrology toolset in ArcGIS consists of a number of spatial analyst tools, and is widely used to calculate flow directions, identify stream networks, delineate a watershed, and analyze topographic characteristics based on DEMs (Eris 2012). The ArcGIS-based surface delineation algorithm, HUD-DC (Wang and Chu 2020) is used in this study to identify PBUs and CBUs and reveal the connectivity between the units using two modules, the depression identification module and the channel and unit identification module. HUD-DC has its unique ability to identify contributing areas for both depressions and channels and calculate connectivity between units. The delineation processes of HUD-DC are shown in Figure 4.4. Based on the input DEM, the depression identification module is used to delineate all highest-level depressions and their overflow thresholds, and calculate the property parameters of the depressions and thresholds (e.g., MDS, maximum ponding area, and the slope of each threshold to its downstream cell with the steepest descent). After all depressions and thresholds are identified, the channel and unit identification module is implemented to search all channel segments and channel ending nodes based on user-specified flow accumulation and channel

length. Furthermore, PBUs and CBUs are determined by searching for contributing areas for all depressions and channels.

In this study, HUD-DC and the hydrology toolset in ArcGIS were used to prepare topographic parameters for HYDROL-DC. Specifically, HUD-DC was utilized to identify depressions, channels, units, and the connectivity between units. The toolset in ArcGIS was used to delineate subbasins, classify main channels and tributary channels, and further assort CBUs into on-stream CBUs and off-stream CBUs according to the spatial relationships between the CBUs and the main channels or tributary channels.

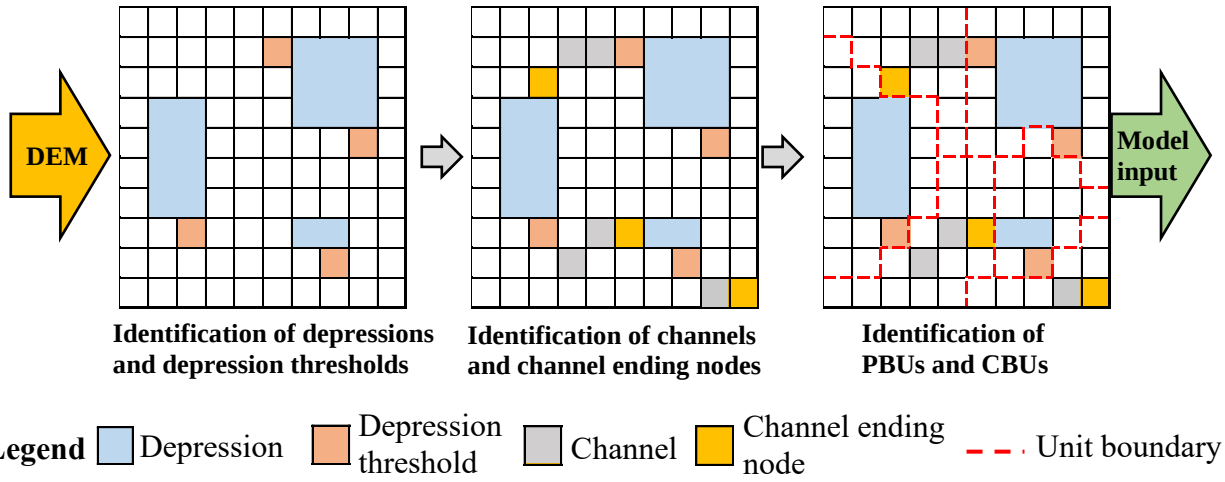

Figure 4.4. Schematic diagram of the hydrologic unit delineation algorithm for depressions and channels (HUD-DC).

4.3.4. Study Area and Input Data

The Edmore Coulee watershed (Figure 4.5), which covers 995.58 km^2 in the middle of the Prairie Pothole Region (PPR), was selected to test the performance of HYDROL-DC. The Edmore Coulee watershed drains runoff water into Sweetwater Lake, and the final outlet of the watershed is located at the United States Geological Survey (USGS) 05056200 Edmore Coulee gauge station (latitude: 48°20’12’’ N; longitude: 98°39’36’’ W) in Ramsey County. Based on the

2011 NLCD (National Land Cover Database), the watershed is mostly covered by cultivated crops (63.97%), pasture (15.04%), and open water and wetlands (13.33 %).

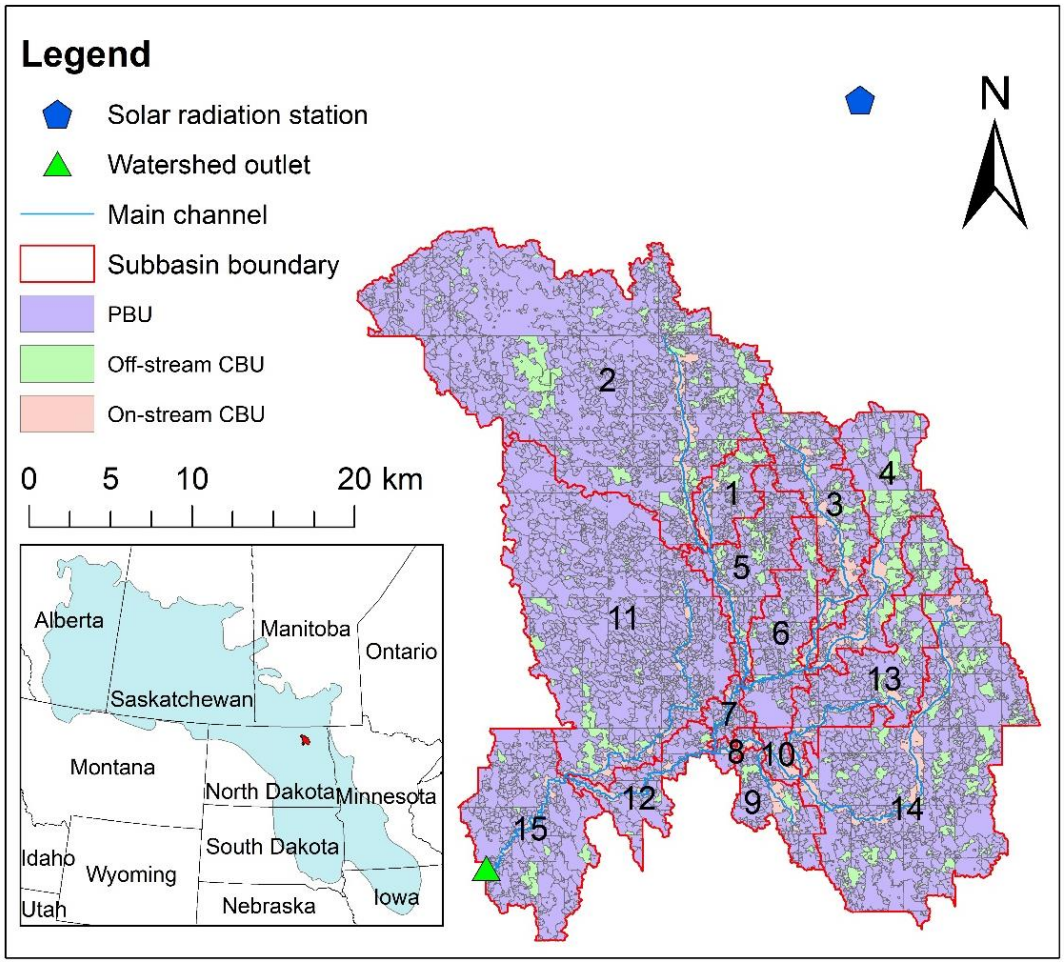

Figure 4.5. Location of the Edmore Coulee watershed and surface delineation results.

The input data of HYDROL-DC can be classified into subbasin-level and unit-level data (Table 4.1). The 10-m DEM of the watershed was downloaded from the USGS National Map Viewer and used for delineation of depressions, channels, units, and subbasins. During the delineation, the DEM was pre-filled by 10-cm water to eliminate any artifacts, and the delineation errors caused by buildings, roads, and other structures were corrected based on the USGS Watershed Boundary Dataset and National Hydrography Dataset (NHD). In addition, the

topographic property parameters, such as MDS and maximum ponding area (MPA), were also calculated based on the DEM in HUD-DC.

Table 4.1. Input data of HYDROL-DC for the hydrologic simulation in the Edmore Coulee watershed.

Input data	**Source**	**Type**	**Level**
Precipitation	http://www.prism.oregonstate.edu/ (PRISM Climate Data)	Raster (4km)	Subbasin
Temperature	http://www.prism.oregonstate.edu/ (PRISM Climate Data)	Raster (4km)	Subbasin
Leaf area index	https://lpdaac.usgs.gov/node/863 (MOD15A2H, Combined Fraction of Photosynthetically Active Radiation (FPAR), and Leaf Area Index (LAI) product)	Raster (500m)	Subbasin
Solar radiation	https://ndawn.ndsu.nodak.edu/ (North Dakota Agricultural Weather Network)	Gauge station	Subbasin
Digital Elevation Model	https://viewer.nationalmap.gov/basic/ (USGS TNW download)	Raster (10m)	Unit
Soil data	https://websoilsurvey.sc.egov.usda.gov/App/HomePage.htm (Web Soil Survey Home)	Polygon	Unit
Land use and land cover	https://viewer.nationalmap.gov/basic/ (USGS TNW download)	Raster (30m)	Unit

The 2011 NLCD and STATSGO2 (State Soil Geographic Dataset) soil type data were obtained for the computation of curve numbers under the average antecedent moisture condition. In this study, the upper soil zone of each unit was divided into 4 soil cells, and the thickness of each soil cell was 40 cm. The parameters of each soil cell were estimated based on the STATSGO2 data, Rawls and Brakensiek (1983), Carsel and Parrish (1988), and Maidment (1993). The daily precipitation and temperature were downloaded from the Parameter-elevation

Regressions on Independent Slopes Model (PRISM) (Daly et al., 2008). The leaf area index data with a 500-m resolution and an 8-day time step were obtained from the MOD15A2H Version 6 Moderate Resolution Imaging Spectroradiometer (MODIS) (USGS 2019). The solar radiation data were downloaded from the North Dakota Agricultural Weather Network (NDAWN) website and further were used to calculate RET (NDAWN 2019). Moreover, the daily discharge data at the Edmore Coulee gauge station were downloaded from the USGS National Water Information System and used for the calibration and validation of HYDROL-DC.

4.3.5. Model Evaluation and Criteria

Based on the delineation results from HUD-DC, the topographic characteristics of all subbasins were analyzed to highlight the distribution and connectivity of depressions in the subbasins. For HYDROL-DC modeling, a one-year warming-up period was selected to set initial parameters and the calibration and validation periods were 1/1/2005 – 12/31/2010 and 1/1/2011 – 12/31/2016, respectively. The Nash-Sutcliffe efficiency (NSE) coefficient (Nash and Sutcliffe, 1970) and the percent bias (PBIAS; Gupta et al., 1999) were used to evaluate the performance of HYDROL-DC. The NSE and PBIAS can respectively be expressed as:

$$NSE = 1 - \frac{\sum_{i=1}^{N}(O_i - S_i)^2}{\sum_{i=1}^{N}(O_i - \bar{O})^2} \tag{4.47}$$

$$PBIAS = \frac{\sum_{i=1}^{N}(O_i - S_i)}{\sum_{i=1}^{N} O_i} \times 100 \tag{4.48}$$

where O_i is the observed value at time step i, S_i is the simulated value at time step i, $\bar{O}$ is the mean observed value, and N is the total number of time steps.

4.3.6. Analyses of the Depression Functionalities in Hydrologic Processes

In a subbasin, rainfall and snowmelt entering the surface zone (i.e., P_{sur} and SM) are eventually converted to the following: (1) infiltration in the CA of a subbasin (D_{ca}); (2) storage

of the CA (M_{ca}); (3) storage of tributary channels (M_{tr}); (4) storage of the PA (M_{pa}); (5) percolation in the PA (D_{pa}); (6) evaporation from the PA (E_{pa}); and (7) inflow of the main channel ($Q_{mc,in}$). In this study, a depression impact coefficient (C_d) was proposed to quantify the subbasin-level influence capacity of depressions on hydrologic processes during the entire simulation period (Equation 4.49).

$$C_d = \frac{\overline{M_{pa}}+\overline{D_{pa}}+\overline{E_{pa}}}{\overline{P_{sur}}+\overline{SM}} \tag{4.49}$$

where $\overline{P_{sur}}$, $\overline{SM}$, $\overline{M_{pa}}$, $\overline{D_{pa}}$, and $\overline{E_{pa}}$ respectively are the average daily values of P_{sur}, SM, M_{pa}, D_{pa}, and E_{pa} during the entire simulation period.

The storages of depressions and their spatial distribution in subbasins with dissimilar topographic characteristics were compared to analyze the differences in their C_d values. Moreover, HYDROL-DC was also used to simulate hydrologic processes without considering depressions by setting the MDSs of all depressions in the selected watershed to zero. The average daily mass balance terms for the entire simulation period, simulated by the HYDROL-DC with and without considering depressions, were compared to quantify the influences of depressions on different hydrologic processes (e.g., infiltration in CA and channel inflow) within each subbasin. In addition, the daily channel inflow reduced by depressions was calculated and analyzed to highlight the dynamic functionalities of depressions in the generation of surface runoff.

4.3.7. Analyses of the Influences of Depressions on Hydrologic Connectivity

Since only the highest-level depressions are considered in HYDROL-DC, this study focuses on the influences of the highest-level depressions on hydrologic connectivity. Two concepts, activated area (A_{act}) and connected area (A_{con}), are introduced to analyze the influences. The A_{act} of a subbasin is defined as the total area of all off-stream CBUs, on-stream

CBUs, and fully filled PBUs in the subbasin, while the A_{con} of a subbasin excludes the off-stream CBUs and the fully-filled PBUs that have no direct connection to the main channel in the subbasin. That is, the A_{con} of a subbasin is defined as the total area of all on-stream CBUs, off-stream CBUs, and PBUs that are directly connected to their associated main channel in the subbasin. Therefore, A_{act} and A_{con} of a subbasin are respectively the maximum area (potential area) and the actual area that contributes runoff water to the subbasin outlet.

For each subbasin, the differences between the normalized A_{act} and the normalized A_{con} at different ponding conditions are utilized to reveal the dynamic variation of hydrologic connectivity, and the range of the differences is used to highlight the diversity of the distribution of the fully filled highest-level depressions. Moreover, to quantify the variation of the range in each subbasin, the range of A_{con} (0-1) is divided into 10 intervals. For each A_{con} interval, the standard deviation (STD) of the differences between A_{act} and $A_{con,}$ and the related coefficient of determination (R^2) are respectively calculated by:

$$STD = \sqrt{\frac{\sum_{i=1}^{N}(z_i-\bar{z})^2}{N}} \tag{4.50}$$

$$R^2 = \frac{\left[\sum_{i=1}^{N}(x_i-\bar{x})(y_i-\bar{y})\right]^2}{\sum_{i=1}^{N}(x_i-\bar{x})^2 \sum_{i=1}^{N}(y_i-\bar{y})^2} \tag{4.51}$$

where x_i, y_i, and z_i are respectively the normalized A_{act}, normalized A_{con}, and the difference between the normalized A_{act} and A_{con} of the i^{th} data point in an A_{con} interval; $\bar{x}$, $\bar{y}$, and $\bar{z}$ are respectively the average values of the normalized A_{act}, A_{con}, and the difference between the normalized A_{act} and A_{con} in an A_{con} interval; and N is the total number of data points in an A_{con} interval. A greater STD and a smaller R^2 indicate a narrower range of the difference between A_{act} and A_{con}, implying that the depression distribution has a less influence on the hydrologic connectivity.

4.4. Results and Discussion

4.4.1. Topographic Characteristics

In this study, the Edmore Coulee watershed was delineated into 15 subbasins by using the ArcGIS hydrology toolset, which were further divided into 12,250 units (PBUs and CBUs) by using HUD-DC (Figure 4.5). Table 4.2 lists the topographic parameters for all subbasins. The low ratio of on-stream CBUs (0.02 to 0.34) indicated that depressions dominated all subbasins, and only a limited area directly contributed surface runoff to its associated subbasin outlet in each subbasin. Numerous depressions were identified in the study area and the ratio of the total maximum storage of all depressions in a subbasin to the entire subbasin area (TMDS) ranged from 21.77 mm to 130.89 mm. To characterize their spatial distribution, the depressions in each subbasin were classified into three categories based on the ratio of their MDS to the subbasin area (RMDS): (1) small depressions (0 mm < RMDS ≤ 0.01 mm); medium depressions (0.01 mm < RMDS ≤ 1 mm); and large depressions (RMDS > 1 mm). Unlike small and medium depressions, large depressions had limited numbers but greater storage percentages in all subbasins except subbasin 3 (Table 4.2). In addition, small and medium depressions were randomly distributed in all subbasins (Figures. 4.6a and 4.6b), while large depressions tended to show certain distribution patterns (e.g., the large depressions in subbasin 8 were located near the subbasin boundary) (Figure 4.6c). Therefore, the locations of large depressions were critical to surface runoff generation and hydrologic connectivity in all subbasins. In the selected watershed, the percentage of the control area of large depressions in the entire area of a subbasin (PCA_l) ranged from 12.26% to 84.35%.

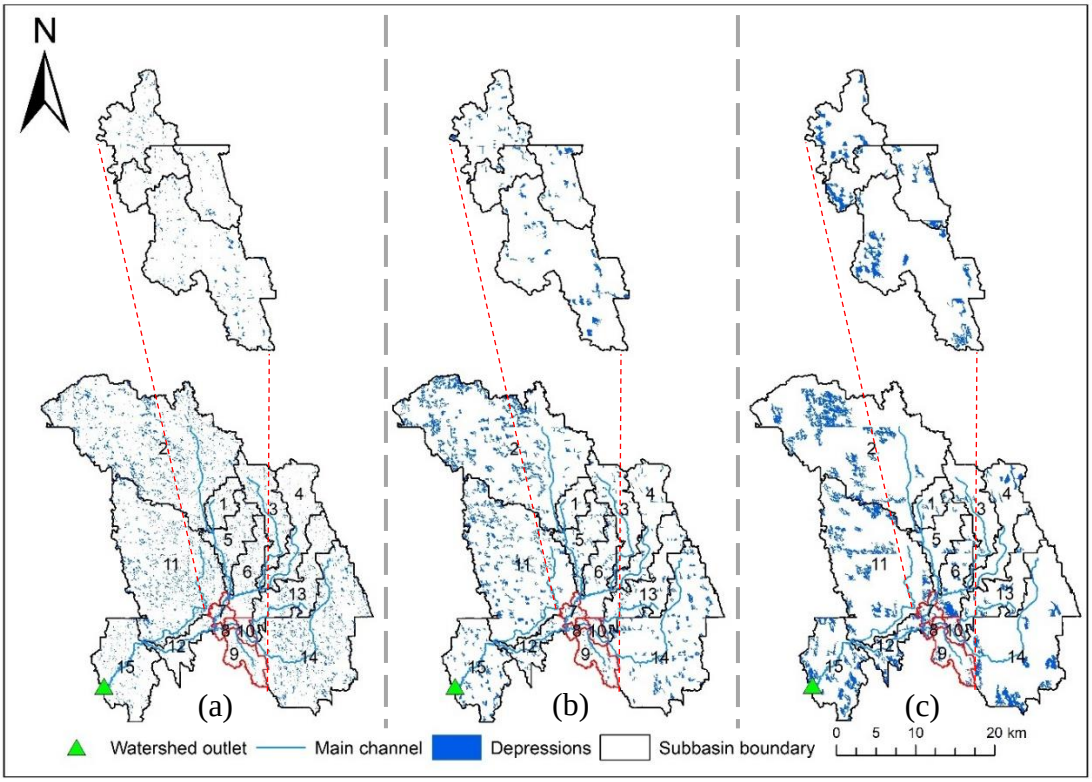

Figure 4.6. Spatial distribution of (a) small depressions, (b) medium depressions and (c) large depressions in all subbasins of the Edmore Coulee watershed.

Table 4.2. Topographic characteristics of all subbasins (On-stream CBU: channel-based unit that has interaction with the main channel; Off-stream CBU: channel-based unit that has no interaction with the main channel; PBU: puddle-based unit; TMDS: ratio of the summation of the maximum storages of all depressions in a subbasin to the subbasin area; PCA_l: percentage of the control area of large depressions in the entire area of a subbasin).

Subbasin ID	**Area (km^2)**	**Off-stream CBU (Ratio)**	**On-stream CBU (Ratio)**	**PBU (Ratio)**	**TMDS (mm)**	**Depression types**						**PCA_l (%)**
						Small		Medium		Large		
						Number	Storage (%)	Number	Storage (%)	Number	Storage (%)	
1	18.98	0.12	0.11	0.77	25.32	299	16.45	17	21.04	6	62.50	31.97
2	258.57	0.08	0.02	0.90	113.41	2404	14.50	174	37.06	19	48.43	62.53
3	48.93	0.10	0.18	0.72	21.77	607	25.38	37	49.06	3	25.57	12.26
4	54.79	0.21	0.11	0.68	50.95	478	8.25	36	21.03	11	70.73	34.55
5	36.37	0.09	0.09	0.82	38.05	518	16.85	53	49.95	7	33.19	57.86
6	35.72	0.08	0.03	0.89	71.54	438	6.90	41	19.57	12	73.54	84.35
7	7.49	0.01	0.18	0.81	47.67	134	5.88	41	23.88	11	70.25	49.09
8	4.38	0.00	0.34	0.66	63.98	37	1.80	11	5.61	7	92.59	34.46
9	20.46	0.08	0.13	0.79	35.74	258	9.61	27	29.05	7	61.34	52.72
10	6.04	0.02	0.24	0.74	27.44	66	5.63	15	19.08	6	75.28	44.74
11	185.27	0.04	0.04	0.92	130.89	1879	12.22	157	34.56	28	53.22	67.33
12	24.07	0.03	0.14	0.83	104.50	179	2.11	43	13.11	16	84.78	55.29
13	57.44	0.14	0.08	0.78	40.62	604	15.06	46	28.93	8	56.01	79.04
14	166.36	0.11	0.06	0.83	61.26	1664	19.38	81	33.22	12	47.39	61.43
15	70.73	0.04	0.04	0.92	104.23	617	6.35	62	19.68	21	73.97	83.34

4.4.2. Model Calibration and Validation

Because the selected watershed is located in a cold region and surface runoff mainly occurs in early spring, snow zone and surface zone are the major zones that influence the hydrologic simulation in the watershed. Table 4.3 shows the parameter ranges for calibration and the calibrated parameters for the two zones. Figure 4.7 shows the comparisons of the simulated and the observed discharges at the USGS gauge station during the calibration and validation periods at both daily and monthly time scales. Because of snowmelt, it was found that most of the peak flows occurred in the early spring of each year (from the end of March to the end of April). The overall performance of HYDROL-DC was very good in the simulations of both daily and monthly discharges during the calibration and the validation periods (Table 4.4). From the simulation results for the calibration and validation periods at both daily and monthly time scales, it was found that the NSE values of the calibration period were similar to those of the validation period, but the PBIAS values of the calibration period were much better than those of the validation period. According to the PBIAS values, HYDROL-DC overestimated the discharge on average, but underestimated some peak flows due to the limitations of the methods used for the snow zone and the frozen soil in HYDROL-DC.

Table 4.3. Calibrated parameters for the snow zone and surface zone.

Parameter	Description	Calibration ranges	Calibrated values
lag_{sno}	Snow temperature lag factor	0 to 1	0.25
T_{sf}	Mean air temperature for snow (ºC)	-5 to 5	-1
T_{sm}	Threshold temperature for snowmelt (ºC)	-5 to 5	0
$c_{sm,6}$	Melt factor for snow on June 21 (cm H2O/day -ºC)	0 to 1	1
$c_{sm,12}$	Melt factor for snow on December 21 (cm H2O/ºC-day)	0 to 1	0.24
I_a	Initial abstraction	0 to 0.2	0.15
lag_{sur}	Surface runoff lag coefficient (hr)	0 to 24	0.6
c_{fz}	Frozen soil factor	0 to 1	0.5

Table 4.4. Calibration and validation results in the simulation of discharge at the USGS gauge station in the Edmore Coulee watershed.

Time scale	Calibration (2005-2010)		Validation (2011-2016)	
	NSE	PBIAS (%)	NSE	PBIAS (%)
Daily	0.80[a]	-9.66[a]	0.77[a]	-18.66[c]
Monthly	0.84[a]	-9.67[a]	0.90[a]	-18.66[c]

[a]Very good: 0.75 < NSE ≤ 1.0, PBIAS ≤ ±10%
[b]Good: 0.65 < NSE ≤ 0.75, ±10% < PBIAS ≤ ±15%
[c]Satisfactory: 0.50 < NSE ≤ 0.65, ±15% < PBIAS ≤ ±25%
[d]Unsatisfactory: NSE ≤ 0.50, PBIAS > ±25% (Moriasi et al., 2007)

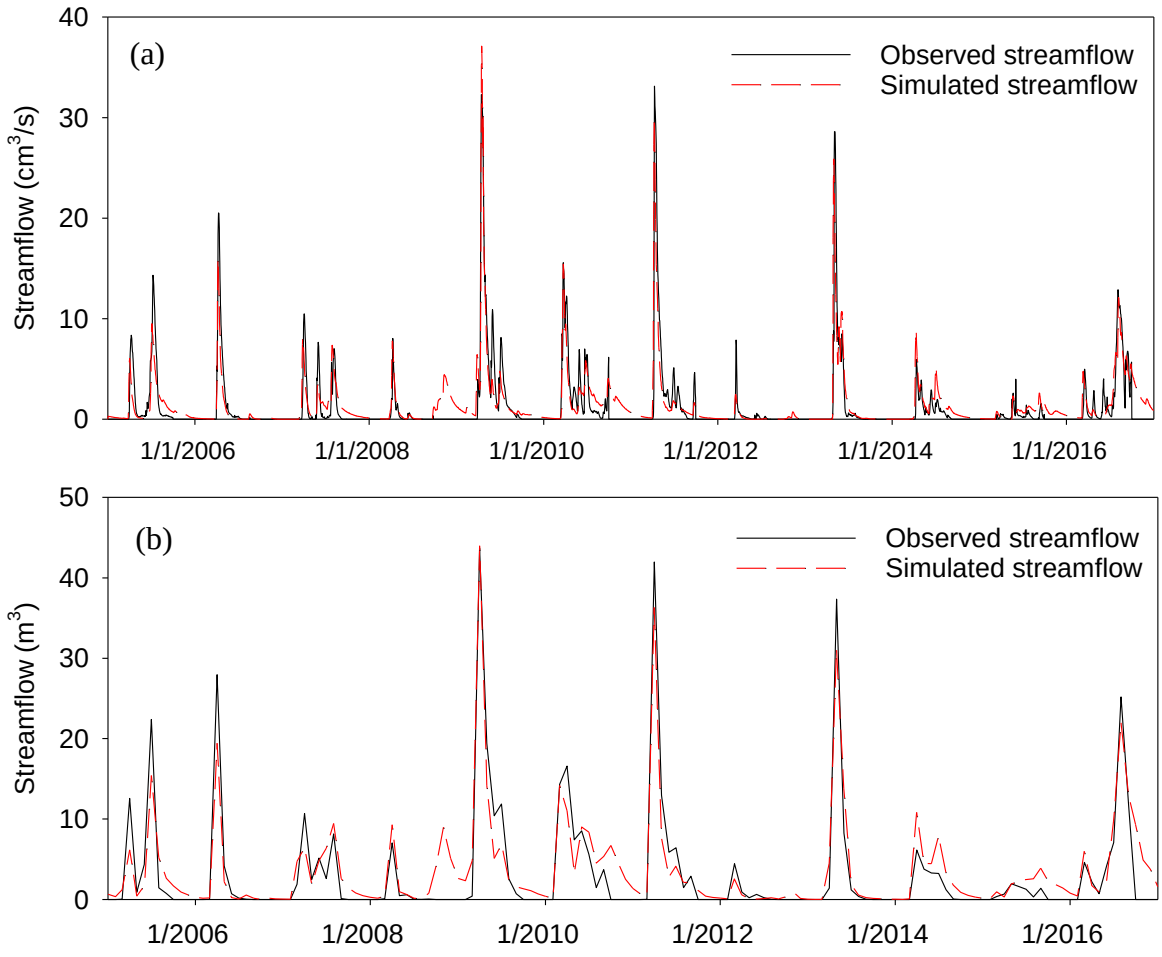

Figure 4.7. Comparison of the simulated and the observed (a) daily discharge and (b) monthly discharge in the calibration and validation periods.

4.4.3. Depression Functionalities in Hydrologic Processes

There were two source terms and seven sink terms for the surface zone of each subbasin. Figure 4.8 shows the ratios of five other sink terms (i.e., infiltration in the CA, percolation in the PA, evaporation from the PA, storage of the PA, and inflow of the main channel) to the total source water of the surface zone. Note that the ratios of CA storage and tributary channel storage to the total source water of the surface zone (i.e., the sum of rainfall and snowmelt entering the surface zone) were negligible (smaller than 10^{-4}). Additionally, subbasins were sorted according to their TMDS values from small to large (Figure 4.8). For the surface zone of each subbasin, most of the total source water was converted to the infiltration in the CA, and the ratio ranged from 0.72 to 0.81 (Figure 4.8). The ratio of the channel inflow to the total source water ranged from 0.03 to 0.11, and the remaining source water was finally transferred into sink terms related to depressions. The depression impact coefficients (i.e., C_d) of all subbasins are also shown in Figure 4.8. According to Figure 4.8, it can be observed that C_d increased with the TMDS in general. Certain disagreements with the increasing trend were mainly due to the influences of the distribution of depressions (especially large depressions). For example, large depressions were concentrated in the north part of subbasin 4, while the distribution of large depressions in subbasin 7 was relatively scattered (Figure 4.6c). In addition, the PCA_l values of subbasins 4 and 7 were 34.55% and 49.09 %, respectively. Therefore, although the TMDS of subbasins 4 was greater than that of subbasin 7 (Table 4.2), the C_d value of subbasin 4 was smaller than that of subbasin 7 (Figure 4.8).

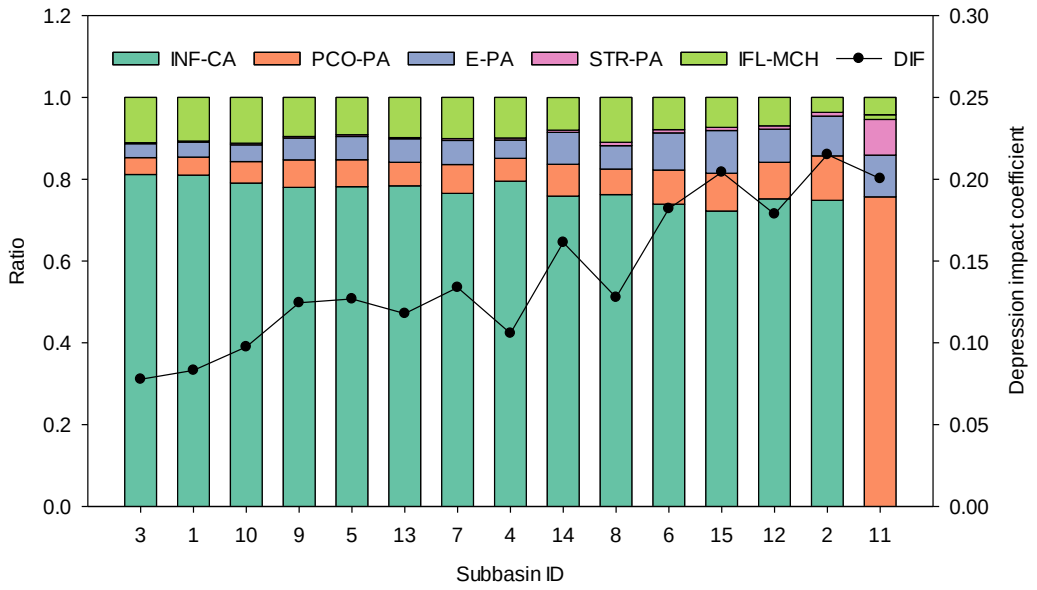

Figure 4.8. Ratios of five major hydrologic variables to the total source water of the surface zone and the depression impact factors of all subbasins (INF-CA = infiltration in the contributing area; PCO-PA = percolation in the ponding area; E-PA = evaporation in the ponding area; STR-PA = storage of ponding area; IFL-MCH = inflow of the main channel; and DIF = depression impact factor).

Figure 4.9 shows the ratios of the daily average CA infiltration and channel inflow to the daily average source water reduced by depressions in all subbasins. Because of the existence of depressions, the ratios of daily average CA infiltration and channel inflow decreased by 0.08 and 0.06 on average, respectively (Figure 4.9). In addition, the daily channel inflow reduced by depressions was calculated by comparing the channel inflows simulated by HYDROL-DC with and without considering depressions. Negative values were observed for the reduced channel inflow, indicating that the existence of depressions increased surface runoff. Therefore, depressions not only retained runoff water but also showed an acceleration capability in the generation of surface runoff (e.g., Figure 4.10). In a subbasin, the acceleration capability of depressions can be attributed to the low percolation rate in the ponding area of the subbasin. For example, the average infiltration rate in the non-ponding area (i.e., the summation of CBUs and the CAs of PBUs) of subbasin 12 was 0.44 cm/d. However, the average percolation rate in the

PA of the subbasin was 0.02 cm/d. Therefore, if there were some fully filled depressions in the A_{ca} of a subbasin, depressions may accelerate the generation of surface runoff.

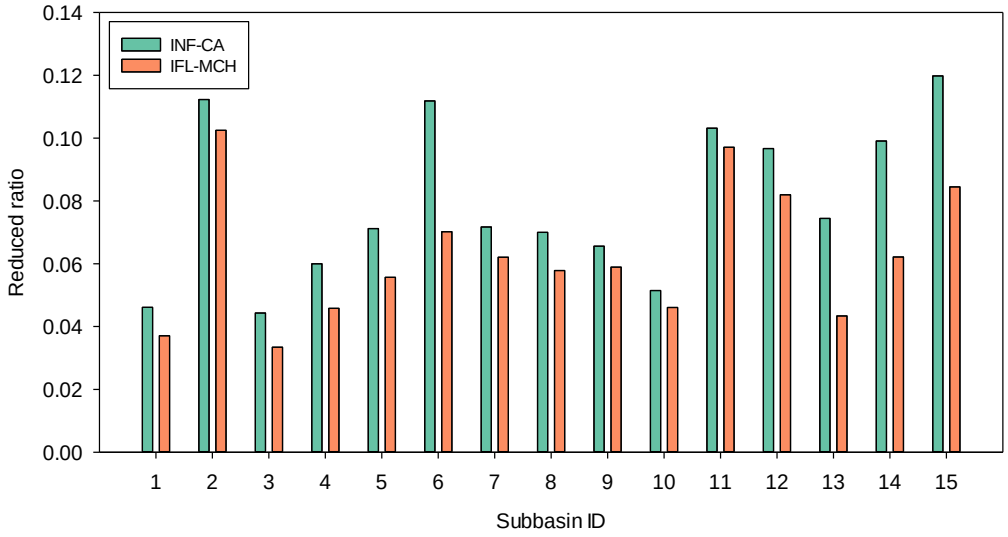

Figure 4.9. Ratios of the daily average CA infiltration and channel inflow to the daily average source water reduced by depressions in all subbasins.

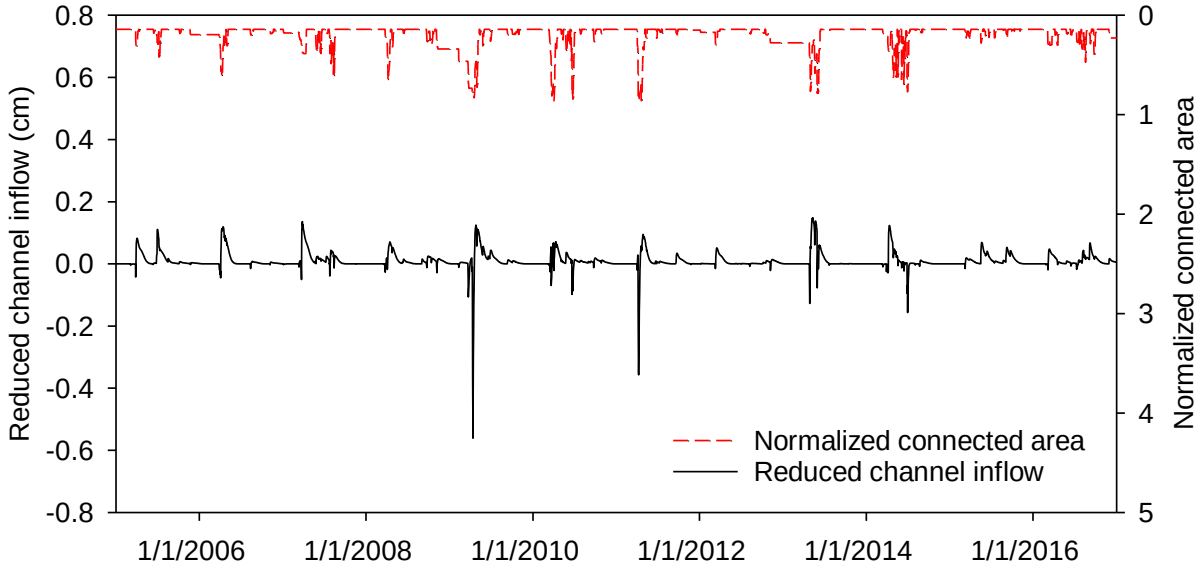

Figure 4.10. Daily channel inflow reduced by depressions and normalized connected area in subbasin 12.

4.4.4. Influence of Depressions on Hydrologic Connectivity

Figure 4.11 shows the comparisons of the normalized A_{act} and Ac_{on} during the entire simulation period for all subbasins. For each subbasin, when A_{con} was small, the limited differences were due to the fact that most depressions were not fully filled at this early stage. In addition, most of the fully filled depressions were small depressions, which had a very limited influence on the difference. For example, the normalized A_{act} and A_{con} of subbasin 12 on 6/4/2015 were 0.18 and 0.16, respectively. The difference between A_{act} and A_{con} of subbasin 12 at this time was caused by one fully filled PBU and the off-stream CBUs that were not connected to their associated main channel (Figures 4.12a and 4.12d). With the increase of A_{con} over time, more depressions were fully filled. However, the runoff from some fully filled PBUs and off-stream CBUs might be "blocked" by their downstream units that were not connected to the outlet yet. Thus, great difference occurred due to the distribution of the fully filled highest-level depressions (Figure 4.11). For example, the normalized A_{act} and A_{con} of subbasin 12 on 3/21/2010 were 0.40 and 0.62, respectively. Fully filled PBUs and off-stream CBUs, which were "blocked" by their downstream units, were found in the north, northeast, and south parts of subbasin 12 (Figures 4.12b and 4.12e). After most depressions were fully filled, most areas were connected to the subbasin outlet and the differences decreased (Figure 4.11). For example, the normalized A_{act} and A_{con} of subbasin 12 were very close on 6/25/2010 (the normalized A_{act} = 0.84 and the normalized A_{con} = 0.86), and their small difference was due to some small units that drained runoff water to the PBUs with partially-filled large depressions (Figures 4.12c and 4.12f).

For an A_{con} interval, the range of the differences between the normalized A_{act} and A_{con} revealed the diversity of the distributions of fully filled highest-level depressions. A greater

range indicated more distribution types of the fully filled highest-level depressions. For all subbasins, as the normalized A_{con} increased, the range increased first and then decreased (Figure 4.11). Figure 4.13 shows the STD and R^2 curves for four typical subbasins in the selected watershed, and the curves of other subbasins had similar trends. The STD and R^2 values of subbasin 12 perfectly matched the variation of the range of the differences between the normalized A_{act} and A_{con} in Figure 4.11 (Figure 4.13c). Although the STD and R^2 of subbasin 11 had certain fluctuations, their curves still reflected the general variation of the ranges (Figure 4.13b). In addition, in subbasins 7 and 15 (Figures 4.13a and 4.13d), the STD and R^2 values were found to be inconsistent with the variation of the ranges, which was mainly due to the division of the range of the normalized A_{con}. When the normalized A_{con} was in an interval with small values (e.g., 0.1-0.2 for subbasin 12), the diversity of the distribution of the fully filled highest-level depressions was limited since only a few small depressions were fully filled at this status. In addition, because most depressions were fully filled, limited diversities were found in the A_{con} intervals with a great value (e.g., 0.7-0.8 for subbasin 12). For other A_{con} intervals, the depressions exhibited significant diversity, which could further influence the hydrologic connectivity.

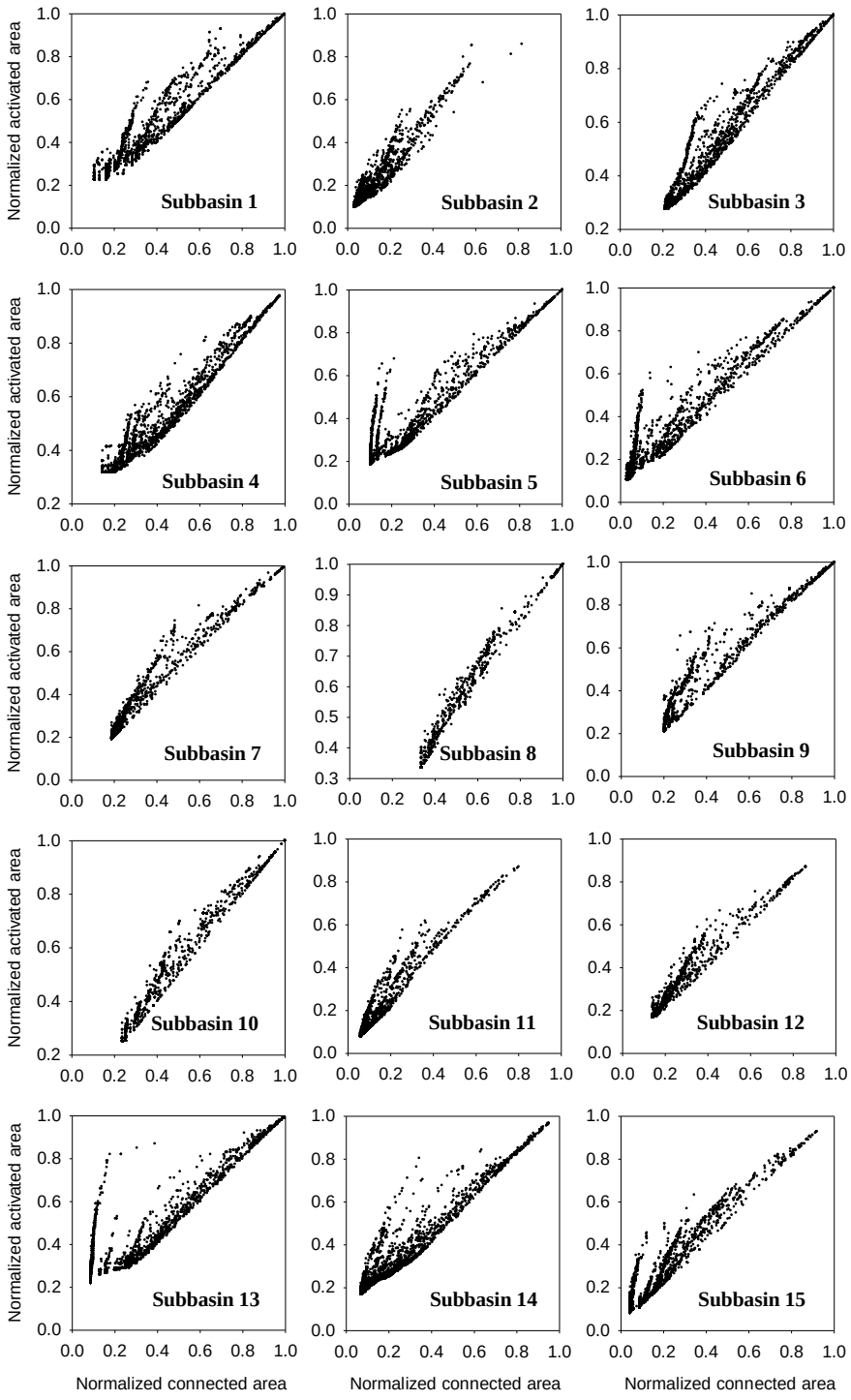

Figure 4.11. Comparison of the normalized connected area and the normalized activated area for all subbasins.

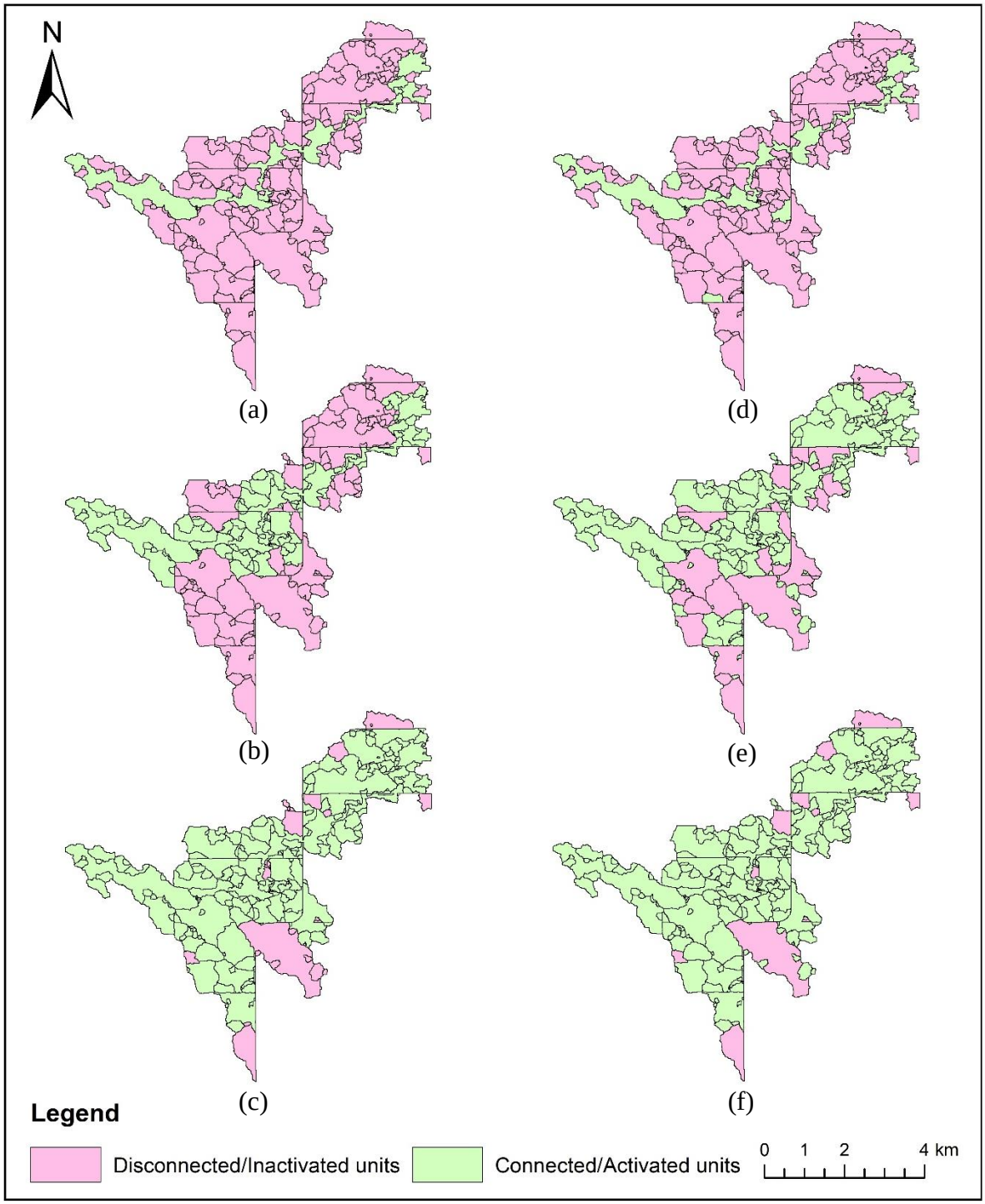

Figure 4.12. Spatial distribution of the connected area in subbasin 12 on (a) 6/4/2015, (b) 3/21/2010, and (c) 6/25/2010; spatial distribution of the activated area in subbasin 12 on (d) 6/4/2015, (e) 3/21/2010, and (f) 6/25/2010.

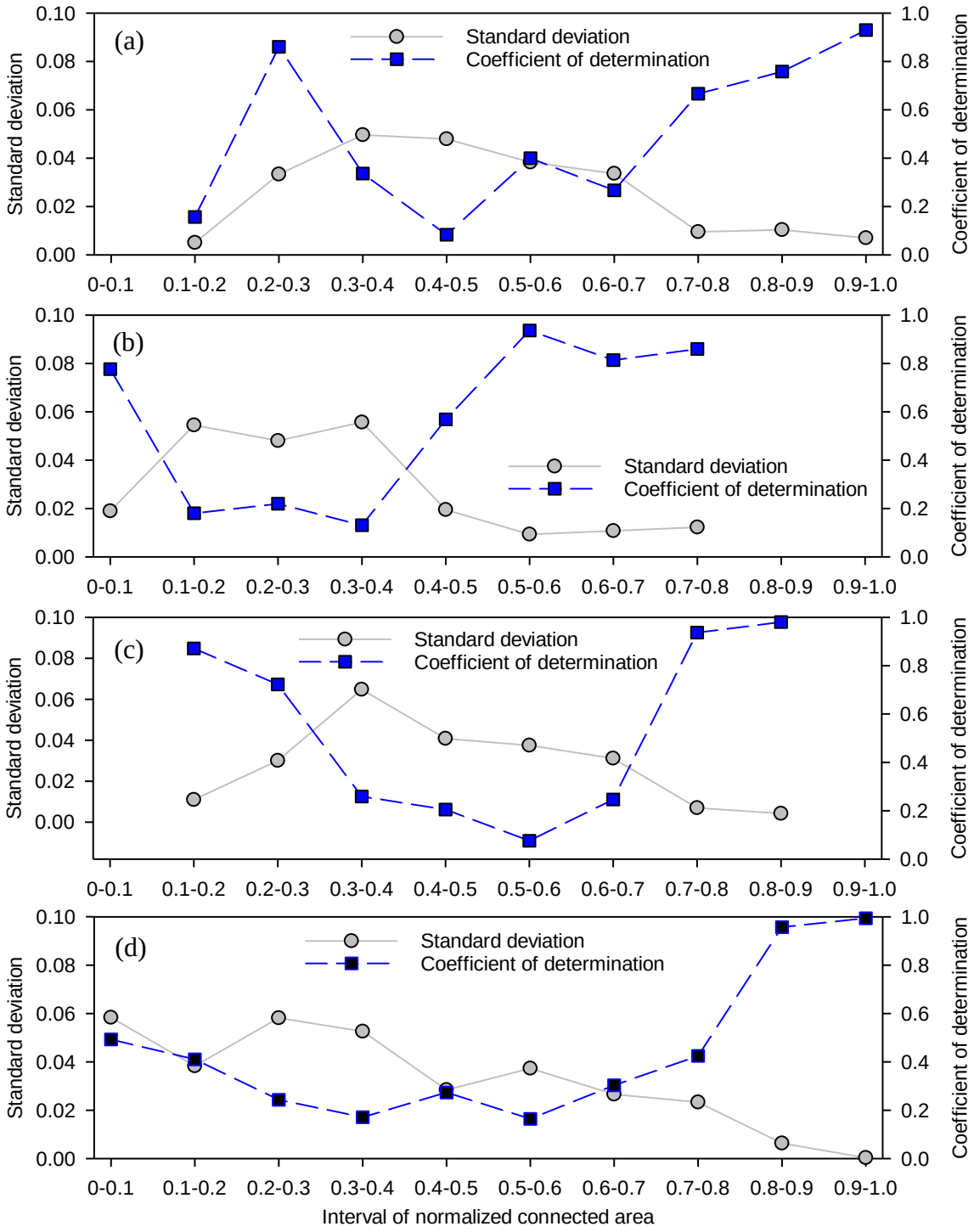

Figure 4.13. Standard deviation and coefficient of determination of the difference between the normalized connected area and the normalized activated area for (a) subbasin 7, (b) subbasin 11, (c) subbasin 12, and (d) subbasin 15.

4.5. Summary and Conclusion

In this study, a new depression-oriented hydrologic model, HYDROL-DC, was developed for hydrologic simulation in depression-dominated watersheds with considering both the storage and spatial distribution of depressions. In HYDROL-DC, a unique structure was proposed to handle specific modeling for a number of units based on their connectivity and functionalities. With the unique model structure, HYDROL-DC was able to track runoff unit by unit and simulate the dynamic hydrologic connectivity within subbasins.

HYDROL-DC was applied to the Edmore Coulee watershed. The delineation results demonstrated the complexity of surface connectivity in the selected watershed. Because of the existence of depressions, only a small portion of the area of each subbasin (2% - 34%) was directly connected to its associated main channel. The influences of depressions on hydrologic processes were quantified by using an impact coefficient (i.e., C_d), and the comparison of the C_d values of different subbasins indicated that both depression storage and distribution influenced the impact capacities of depressions in hydrologic processes. The comparison of the simulated hydrologic processes with and without considering depressions revealed that the existence of depressions decreased the infiltration in CA and channel inflow. Generally, depressions mainly exhibited the retention capability in surface runoff generation within each subbasin. However, they also could accelerate the generation of surface runoff. The variation of the differences between A_{con} and A_{act} indicated that depressions had dynamic influences on hydrologic connectivity. In addition, due to the diverse distributions of the fully filled highest-level depressions, significant influences were found when a portion of highest-level depressions were fully filled.

Since the interactions between surface water and groundwater were simplified and the groundwater discharge to depressions was not considered in HYDROL-DC, this research focused on investigating the functionalities of depressions in the surface water system. In the future research, HYDROL-DC can be combined with groundwater models to investigate the influences of depressions on the entire hydrologic system.

4.6. References

Allen, R. G., Pereira, L. S., Raes, D., Smith, M., 1998. Crop evapotranspiration: Guidelines for computing crop water requirements, FAO Irrigation and Drainage Paper 56. Food and Agriculture Organization of the United Nations, Rome, 300(9), D05109.

Amoah, J. K., Amatya, D. M., Nnaji, S., 2013. Quantifying watershed surface depression storage: determination and application in a hydrologic model. Hydrol. Process., 27(17), 2401-2413.

Arnold, N., 2010. A new approach for dealing with depressions in digital elevation models when calculating flow accumulation values. Prog. Phys. Geogr., 34(6), 781-809.

Carsel, R.F., Parrish, R.S., 1988. Developing joint probability distributions of soil water retention characteristics. Water Resour. Res., 24, 755-769.

Chen, L., Sela, S., Svoray, T., Assouline, S., 2013. The role of soil-surface sealing, microtopography, and vegetation patches in rainfall–runoff processes in semiarid areas. Water Resour. Res., 49(9), 5585–99.

Chu, X., Marino, M. A., 2007. IPTM-CS: A Windows-based integrated pesticide transport model for a canopy-soil system. Environ. Modell. Softw., 22(9), 1316-1327.

Chu, X., Zhang, J., Chi, Y., Yang, J., 2010. An improved method for watershed delineation and computation of surface depression storage. 1113-1122. In: Watershed Management 2010:

Innovations in Watershed Management Under Land Use and Climate Change, 1113-1122. Proceedings of the 2010 Watershed Management Conference, edited by K. W. Potter and D. K. Frevert. American Society of Civil Engineers.

Chu, X., Yang, J., Chi, Y., Zhang, J., 2013. Dynamic puddle delineation and modeling of puddle-to-puddle filling-spilling-merging-splitting overland flow processes. Water Resour. Res., 49(6), 3825-3829.

Chu, X., 2017. Delineation of pothole-dominated wetlands and modeling of their threshold behaviors. J. Hydrol. Eng., 22, D5015003.

Daly, C., Halbleib, M., Smith, J.I., Gibson, W.P., Doggett, M.K., Taylor, G.H., Curtis, J., Pasteris, P.P., 2008. Physiographically sensitive mapping of climatological temperature and precipitation across the conterminous United States. Int. J. Climatol., 28, 2031–2064.

DHI., 2007. MIKE SHE user manual, volume 2: reference guide. DHI Water and Environment, Horsholm, Denmark.

Esri. (2012) GIS for water resources [WWW Document]. URL https://www.esri.com/en-us/industries/water/segments/water-resources (accessed 06.24.20).

Gassman, P. W., Reyes, M. R., Green, C. H., Arnold, J. G., 2007. The soil and water assessment tool: historical development, applications, and future research directions. Trans. ASABE 50(4), 1211-1250.

Golden, H. E., Lane, C. R., Amatya, D. M., Bandilla, K. W., Kiperwas, H. R., Knightes, C. D., Ssegane, H., 2014. Hydrologic connectivity between geographically isolated wetlands and surface water systems: a review of select modeling methods. Environ. Modell. Softw., 53, 190-206.

Grimm, K., Chu, X., 2018. Modeling of spatiotemporal variations in runoff contribution areas and analysis of hydrologic connectivity. Land Degrad. Dev., 29(8), 2629-2643.

Gupta, H. V., Sorooshian, S., Yapo, P. O., 1999. Status of automatic calibration for hydrologic models: Comparison with multilevel expert calibration. J. Hydrol. Eng., 4(2), 135-143.

Hay, L., Norton, P., Viger, R., Markstrom, S., Regan, R. S., Vanderhoof, M., 2018. Modelling surface-water depression storage in a Prairie Depression Region. Hydrol. Process., 32(4), 462-479.

Hayashi, M., van der Kamp, G., Rosenberry, D. O., 2016. Hydrology of prairie wetlands: understanding the integrated surface-water and groundwater processes. Wetlands, 36(2), 237-254.

Kim H, Amatya DM, Broome SW, Hesterberg DL, Choi M., 2012. Sensitivity analysis of the DRAINWAT model applied to an agricultural watershed in the lower coastal plain, North Carolina, U.S.A. Water Environ. J., 26(1), 130–145.

Klein, M., 2018. User Manual PELMO (Pesticide Leaching Model) Version 5.0. Fraunhofer Institute: Schmallenberg, Germany.

Kristensen, K. J., Jensen, S. E., 1975. A model for estimating actual evapotranspiration from potential evapotranspiration. Hydrol. Res., 6(3), 170-188.

Leibowitz, S. G., Vining, K. C., 2003. Temporal connectivity in a prairie pothole complex. Wetlands, 23(1), 13-25.

Liu, G., Schwartz, F. W., 2011. An integrated observational and model-based analysis of the hydrologic response of prairie pothole systems to variability in climate. Water Resour. Res., 47(2).

Maidment, D. R., 1993. Handbook of Hydrology. McGraw-Hill, Inc.

Markstrom, S. L., Regan, R. S., Hay, L. E., Viger, R. J., Webb, R. M., Payn, R. A., LaFontaine, J. H., 2015. PRMS-IV, the precipitation-runoff modeling system, version 4. US Geological Survey Techniques and Methods (6-B7).

Mekonnen, B. A., Mazurek, K. A., Putz, G., 2016. Incorporating landscape depression heterogeneity into the Soil and Water Assessment Tool (SWAT) using a probability distribution. Hydrol. Process., 30(13), 2373-2389.

Mishra, S. K., Singh, V. P., 2003. SCS-CN Method. In Soil conservation service curve number (SCS-CN) methodology. Springer, Dordrecht.

Mohammed, G. A., Hayashi, M., Farrow, C. R., Takano, Y., 2013. Improved characterization of frozen soil processes in the Versatile Soil Moisture Budget model. Can. J. Soil Sci., 93(4), 511-531.

Moriasi, D. N., Arnold, J. G., Van Liew, M. W., Bingner, R. L., Harmel, R. D., Veith, T. L., 2007. Model evaluation guidelines for systematic quantification of accuracy in watershed simulations. Trans. ASABE., 50(3), 885-900.

Nash, J. E., Sutcliffe, J. V., 1970. River flow forecasting through conceptual models part I – A discussion of principles. J. Hydrol., 10 (3), 282-290.

NDAWN, 2019. North Dakota Agricultural Weather Network [WWW Document]. URL https://ndawn.ndsu.nodak.edu/ (accessed 7.18.19).

Neitsch, S. L., Arnold, J. G., Kiniry, J. R., Williams, J. R., 2011. Soil and water assessment tool theoretical documentation version 2009. Texas Water Resources Institute.

Nielsen, S. A., Hansen, E. 1973. Numerical simulation of the rainfall-runoff process on a daily basis. Hydrol. Res., 4(3), 171-190.

Philips, R. W., Spence, C., Pomeroy, J. W., 2011. Connectivity and runoff dynamics in heterogeneous basins. Hydrol. Process., 25, 3061–3075.

Rawls, W. J., Brakensiek, D. L., 1983. A procedure to predict Green and Ampt infiltration parameters. Adv. Infil., 102-112.

Shaw, D. A., Pietroniro, A., Martz, L. W., 2013. Topographic analysis for the prairie depression region of Western Canada. Hydrol. Process., 27(22), 3105-3114.

Tahmasebi Nasab, M., Zhang, J., Chu, X., 2017a. A new depression-dominated delineation (D-cubed) method for improved watershed modeling. Hydrol. Process., 31(19), 3364-3378.

Tahmasebi Nasab, M., Singh, V., Chu, X., 2017b. SWAT Modeling for Depression-Dominated Areas: How Do Depressions Manipulate Hydrologic Modeling? Water, 9(1), 58.

Temme, A. J., Schoorl, J. M., Veldkamp, A., 2006. Algorithm for dealing with depressions in dynamic landscape evolution models. Comput. Geosci., 32(4), 452-461.

USGS, 2019. MOD15A2H v006 [WWW Document]. URL https://lpdaac.usgs.gov/products/mod15a2hv006 (accessed 7.18.19).

Van Genuchten, M. T., 1980. A closed-form equation for predicting the hydraulic conductivity of unsaturated soils 1. Soil sci. soc. Am. J., 44(5), 892-898.

Van der Kamp, G., Hayashi, M., 2009. Groundwater-wetland ecosystem interaction in the semiarid glaciated plains of North America. Hydrogeol. J., 17(1), 203-214.

Vining, K. C., 2002. Simulation of streamflow and wetland storage, Starkweather Coulee subbasin, North Dakota, water years 1981-98 (No. 2002-4113).

Wang, X., Yang, W., Melesse, A. M., 2008. Using hydrologic equivalent wetland concept within SWAT to estimate streamflow in watersheds with numerous wetlands. Trans. ASABE., 51(1), 55-72.

Wang, N., Zhang, X., Chu, X., 2019. New model for simulating hydrologic processes under influence of surface depressions. J. Hydrol. Eng., 24(5), 04019008.

Wang, N., Chu, X., 2020. A new algorithm for delineation of surface depressions and channels. Water, 12(1), 7.

Williams, J. R., 1969. Flood routing with variable travel time or variable storage coefficients. Trans. ASAE, 12(1), 100-0103.

Yang, W., Wang, X., Liu, Y., Gabor, S., Boychuk, L., Badiou, P., 2010. Simulated environmental effects of wetland restoration scenarios in a typical Canadian prairie watershed. Wetl. Ecol. Manag., 18(3), 269-279.

Yang, J., Chu X., 2013. Quantification of the spatio-temporal variations in hydrologic connectivity of small-scale topographic surfaces under various rainfall conditions. J. Hydrol., 505:65-77.

5. OVERALL CONCLUSIONS

Surface depressions, which increase the complexity of surface connectivity and break the continuity of hydrologic processes, are nonnegligible for both surface delineation and hydrologic simulation in depression-dominated areas. Due to some simplified assumptions related to depressions, traditional watershed-scale surface delineation algorithms and hydrologic models cannot be directly applied to those areas. This dissertation research focuses on analyzing and quantifying the topographic characteristics of surface depressions and their impacts on hydrologic processes in depression-dominated areas. Specifically, one surface delineation algorithm for depressions and channels (HUD-DC), and two depression-oriented hydrologic models (HYDROL-D and HYDROL-DC) were developed to enhance our understanding of topographic features and hydrologic processes under the influence of surface depressions.

HUD-DC is a surface delineation algorithm designed for quantifying the depression filling and spilling processes and revealing the internal hydrologic connectivity within subbasins. A unique method is proposed and utilized in the HUD-DC to identify all highest-level depressions and their overflow thresholds, as well as channels. Furthermore, puddle-based units (PBUs) and channel-based units (CBUs) are identified based on the highest-level depressions and channels and the detailed hydrologic connectivity between units is determined. In this study, the accuracy of HUD-DC in surface delineation was evaluated by comparing the delineation results of HUD-DC with those of Arc Hydro. In addition, complex hydrologic connectivity caused by surface depressions was quantified based on the delineation results of HUD-DC. It was found that the hydrologic connectivity of a depression-dominated watershed exhibited a dynamic and hierarchical variation pattern during the filling of depressions. Moreover, the

topographic characteristics under different filling conditions were evaluated. HUD-DC can also be used to remove the artifacts in DEMs.

A semi-distributed, depression-oriented hydrologic model, HYDROL-D, was developed to analyze the impacts of depressions on runoff processes during rainfall events and the mechanism of water release from depressions. In HYDROL-D, the influences of depressions on runoff routing were accounted for by using a novel model structure, in which each subbasin of a watershed was divided into a non-depressional area (NDA) and a depression area (DA), and the DA was further divided into a time-varying contributing area (CA) and a ponding area (PA). Additionally, multiple control thresholds were considered in HYDROL-DD to control runoff water release from depressions. In this study, two rainfall events and three models (HEC-HMS, HYDROL-D with a single threshold, and HYDROL-D with multiple thresholds) were developed to evaluate the performances of HYDROL-D in the simulation of hydrologic processes. The comparisons of the simulation results from two models (HYDROL-D with single threshold and HYDROL-D with multiple thresholds) for a hypothetical rainfall event highlighted the intrinsic threshold behaviors in the generation of surface runoff and the runoff water release from depressions. Because of the multiple control thresholds, HYDROL-D with multiple thresholds exhibited improved performance in comparison with the two other models in the simulation of hydrologic processes under real rainfall events. The simulation results of HYDROL-D with multiple thresholds revealed that only a limited amount of runoff was generated in each subbasin due to the existence of depressions.

To analyze the watershed-scale functionalities of depressions in the continuous simulation of hydrologic processes and connectivity, a depression-oriented hydrologic model, HYDROL-DC, was developed with considering both storage and spatial distribution of

depressions. Based on the unique characteristics and connections of depressions and channels, the entire area of each subbasin was divided into one main channel, PBUs, off-stream CBUs, and on-stream CBUs and separate modeling was implemented for each unit to track runoff and simulate the dynamic hydrologic connectivity within subbasins. A depression impact factor (C_d) was proposed in this study to quantify the subbasin-level influence capacity of depressions. The comparison of the C_d values between subbasins with dissimilar topographic characteristics revealed that C_d increased with an increase in the total maximum depression storage in general, and certain disagreements occurred due to the diverse distributions of depressions in different subbasins. To analyze the influences of depressions on surface runoff generation, HYDROL-DC was used to simulate the channel inflow with and without considering depressions, indicating that the daily average channel inflow reduced due to depressions. It was found that depressions mainly exhibited a retention capability in a subbasin, while their acceleration capability was also observed due to the low percolation rate in the ponding area of the subbasin. Two concepts, activated area (A_{act}) and normalized connected area (A_{con}), were proposed, and the variations of the difference between the normalized A_{act} and normalized A_{con} highlighted the dynamic impacts of the fully filled highest-level depressions on hydrologic connectivity. Moreover, because of the diverse distributions of the fully filled highest-level depressions, significant influences between the normalized A_{act} and A_{con} were found when the A_{con} was in middle intervals.

Since depressions significantly influence hydrologic processes and the fate and transport of sediments, nutrients, and other contaminants, it is essential to analyze the complex topographic characteristics of depressions, the runoff release mechanisms and other hydrologic processes associated with surface depressions in depression-dominated areas. Overall, this dissertation research improved the understanding of the relevant hydrologic processes, and the

new modeling approached developed in this research can be used for water resources management and water quality modeling and assessment. According to the unique characteristics of the proposed algorithm and models, the following applications can be considered in the future:

- The delineation results of the HUD-DC algorithm can be used to quantify the structural and functional hydrologic connectivity for depression-dominated watersheds.
- The HYDROL-D and HYDROL-DC models can be used to assess the impacts of climate change and land use and land cover change on the simulations of hydrologic processes in depression-dominated areas.

Although this research makes unique contributions to hydrologic modeling, especially for depression-dominated areas, the following improvements can be made to enhance the performances of the proposed algorithm and models:

- The delineation algorithm and hydrologic models proposed in this study were only applied to the selected watersheds, and more tests would be helpful to verify their applicability.
- The HYDROL-D and HYDROL-DC models were calibrated and validated by using the observed hydrographs at the watershed outlets. More observed data (e.g., hydrographs within watersheds and remote sensing images) would be helpful for model calibration and validation.
- The subsurface system was simplified in the HYDROL-D and HYDROL-DC models and more efforts can be made to improve the modeling of the interactions between surface water and groundwater.

- The models developed in this research can also be further extended for water quality modeling.